UNIVERSITY *of* TASMANIA | AMC Australian Maritime College

AN EXPERIMENTAL INVESTIGATION INTO WEC OPERATION IN REALISTIC SEA STATES USING PIV

by

Thomas Mitchell Ferguson, B.E (Hons)

National Centre for Maritime Engineering and Hydrodynamics
Australian Maritime College

Submitted in fulfillment of the requirements
for the Degree of Doctor of Philosophy

Supervisors:
Assoc. Prof. Irene Penesis
Assoc. Prof. Gregor Macfarlane
Dr. Alan Fleming
Prof. Neil Bose

University of Tasmania
October, 2015

Declarations

I declare that this thesis contains no material which has been accepted for a degree or diploma by the University or any other institution, except by way of background information and duly acknowledged in the thesis, and that, to the best of my knowledge and belief, this thesis contains no material previously published or written by another person, except where due acknowledgement is made in the text of the thesis.

This thesis may be made available for loan and limited copying in accordance with the *Copyright Act 1968*

Signed: _____
Thomas Mitchell Ferguson

Date: 23/10/2015

Statement of Published Work Contained in Thesis

The publishers of the papers comprising Chapters 2, 4, Appendix A and B hold the copyright for that content, and access to the material should be sought from the respective journals and conference proceedings. The remaining non published content of the thesis and Chapters 3 are submitted and under review, and may be made available for loan and limited copying and communication in accordance with the Copyright Act 1968.

Statement of Co-Authorship

The following people and institutions contributed to the publication of work undertaken as part of this thesis:

- Thomas Mitchell Ferguson, University of Tasmania (Candidate)
- Associate Professor Irene Penesis, University of Tasmania (Co-Author 1)
- Associate Professor Gregor Macfarlane, University of Tasmania (Co-Author 2)
- Doctor Alan Fleming, University of Tasmania (Co-Author 3)

For all works the Candidate was the primary author. Co-Author 1, Co-Author 2, and Co-Author 3 assisted with research direction, advice, and presentation. [Candidate: 85%, Author 1: 5%, Author 2: 5%, Author 3: 5%]

We the undersigned agree with the above stated proportion of work undertaken for each of the published (or submitted) peer-reviewed manuscripts contributing to this thesis

Signed:

Associate Professor Irene Penesis
Primary Supervisor
National Centre for Maritime Engineering and Hydrodynamics
Australian Maritime College
University of Tasmania

Associate Professor Gregor Macfarlane
Co-Supervisor
National Centre for Maritime Engineering and Hydrodynamics
Australian Maritime College
University of Tasmania

Doctor Alan Fleming
Co-Supervisor
National Centre for Maritime Engineering and Hydrodynamics
Australian Maritime College
University of Tasmania

Acknowledgements

Firstly I thank my supervisory team Irene Penesis, Gregor Macfarlane and Alan Fleming. The support, guidance and encouragement provided during the last few years has made working on this project a fantastic experience. The development of this research would not have been possible without your help.

I also thank all the staff at NCMEH, in particular Roberto Ojeda, for initially sparking my interest in research and allowing me to develop my skills not only as a researcher but also as an academic. The environment created by the staff within the centre has given me opportunities I will be forever grateful for.

I thank the team at the Towing Tank for their work in what was a challenging build. Your assistance made my time in the Towing Tank run as smoothly as could possibly be hoped for.

Most of all, I thank Kim, without your patience and support I would not be where I am today.

This research was conducted as part of an Australian Research Council Linkage Project (LP110200129) in association with Oceanlinx Ltd and Bombora Wave Power.

Abstract

The focus of this study is on two key aspects of model scale experimentation when investigating the operation of ocean wave energy converters: the type of wave in which the device is exposed to; and the presence of three dimensional effects within and around the device. Scale model experiments were performed on an oscillating water column (OWC) in different conditions utilising particle image velocimetry (PIV). PIV is an advanced experimental technique which captures full velocity fields without interference with the flow and can be used to provide both qualitative and quantitative flow visualisation.

To investigate the impact of wave type on the operation of an OWC, experiments were performed in three wave types: regular, polychromatic and irregular waves. While regular and irregular waves are often used, polychromatic waves offer an intermediate option which has properties of both. When investigating polychromatic waves phase averaging was shown to be a useful tool to generate averaged results for both PIV velocity fields and other more conventional data sources with a reduction in uncertainty. It was seen that testing in regular waves results in unrealistic harmonic effects which impact on device performance, in particular the formation and size of vortices. For experiments in irregular waves, a linear relationship was identified between the energy within vortices and the total energy within the velocity field.

Identifying the presence of three dimensional effects was achieved by capturing two dimensional (2D) flow velocities at four transverse planes. This showed the transition between inflow and outflow conditions occurs at different times across the device. Velocity field divergence was calculated and large vortices were identified at the inside lip of the sidewall during inflow. It also indicated the device utilises the volume outside of its sidewalls during outflow, allowing an effective width greater than the extents of its sidewalls. This results in the potential for more power to be generated during outflow than inflow.

This study has revealed the importance of performing experiments in realistic sea states and has highlighted the value of experiments in polychromatic and/or irregular waves early in the design process. The use of PIV provided a vast amount of information on the operation and performance of wave energy converters and should be strongly considered when performing quantitative flow visualisation, comparative studies and validation of numerical models.

Table of Contents

List of Figures

List of Tables

Nomenclature

Dimensionless Numbers

Symbol	Description	Definition
CW	Capture width	$\frac{P_{PTO}}{EF}$
W	Non-dimensional chamber width	$\frac{y}{w}$

Greek Symbols

Symbol	Description	Units
∇	Chamber volume flux per unit width	$m^3/s/m$
ω	Vorticity	rads/s
ϕ	Wave phase shift	rads
ρ	Water density	kg/m^3

Roman Symbols

Symbol	Description	Units
Δp	Chamber pressure differential	Pa
dx	Pixel width	m
dy	Pixel height	m
EF	Wave energy flux	J/m^2
E_{k_T}	Total kinetic energy	J/m
E_{k_ω}	Total kinetic energy in vortices	J/m
f	Wave frequency	Hz

$H_{chamber}$	Average chamber water elevation	m
l	Chamber length	m
n	Wave component	-
P_{PTO}	Power at PTO per unit width	W/m
t	Time	s
T_{data}	Data recorded time	s
T_{end}	Phase end time	s
T_{start}	Phase start time	s
V	Velocity field	m/s
V_x	Water velocity in x	m/s
V_y	Water velocity in y	m/s
w	Chamber width	m
x	Displacement from front of chamber	m
y	Displacement from centreline	m
z	Displacement from static waterline	m

Abbreviations

2D	Two Dimensional
3D	Three Dimensional
ITTC	International Towing Tank Conference
LCOE	Levelised Cost of Electricity
OWC	Oscillating Water Column
PIV	Particle Image Velocimetry
PTO	Power Take-Off
TRL	Technology Readiness Level
WEC	Wave Energy Converter

Chapter 1

Thesis Introduction

1.1 Introduction

To combat global warming, man-made carbon and greenhouse gas emissions must be reduced. Currently energy production methods utilising the burning of fossil fuels such as coal, gas and oil generate 26% of the worlds carbon emissions (Intergovernmental Panel on Climate Change, 2012). As we attempt to reduce our reliance on these traditional energy production methods new renewable sources of energy must be developed. Thus far, solar and wind energy have made rapid progress towards becoming an economical alternative. Each of these has disadvantages, for example; solar energy not being available at night, and wind energy being difficult to predict and therefore difficult to rely upon for production. Ultimately diversity in energy sources will be required for a stable energy base (Geoscience Australia *et al.*, 2010).

Ocean wave energy is one resource which has been underutilised. As a concentrated form of solar energy, ocean waves are generated by wind which travels over large distances of water unimpeded. As they lose little energy as they travel the average energy density (2-3 kW/m^2) of waves far exceed that of solar (0.5 kW/m^2) and wind (0.1-0.3 kW/m^2) (Falnes, 2007). In addition, ocean waves can be accurately predicted at up to 3 days in advance (Behrens *et al.*, 2012), a highly desirable trait when connected to a power grid.

Australia has one of the best ocean wave energy resources in the world, with a total of 1300 TWh each year, the equivalent of five times of the country's energy requirements (CSIRO, 2012). With an efficient and importantly economical method for capturing this energy it is estimated that ocean wave energy could provide 11% of the country's energy needs (Behrens *et al.*, 2012; Gunn *et al.*, 2012).

Wave energy converters (WECs) are devices which are designed to capture wave energy and are in the early stages of research and development. Therefore a wide variety of WEC concepts exist. Common designs include attenuators, point absorbers, wave surge converters, oscillating water columns and overtopping devices (Clément *et al.*, 2002; Cruz (ed.), 2008; Falcão, 2010; Falnes, 2007). Notable examples of WECs which have been tested at full scale are shown in Figure 1.1. While there have been many devices which have progressed to large scale prototype testing no commercial devices are currently in operation.

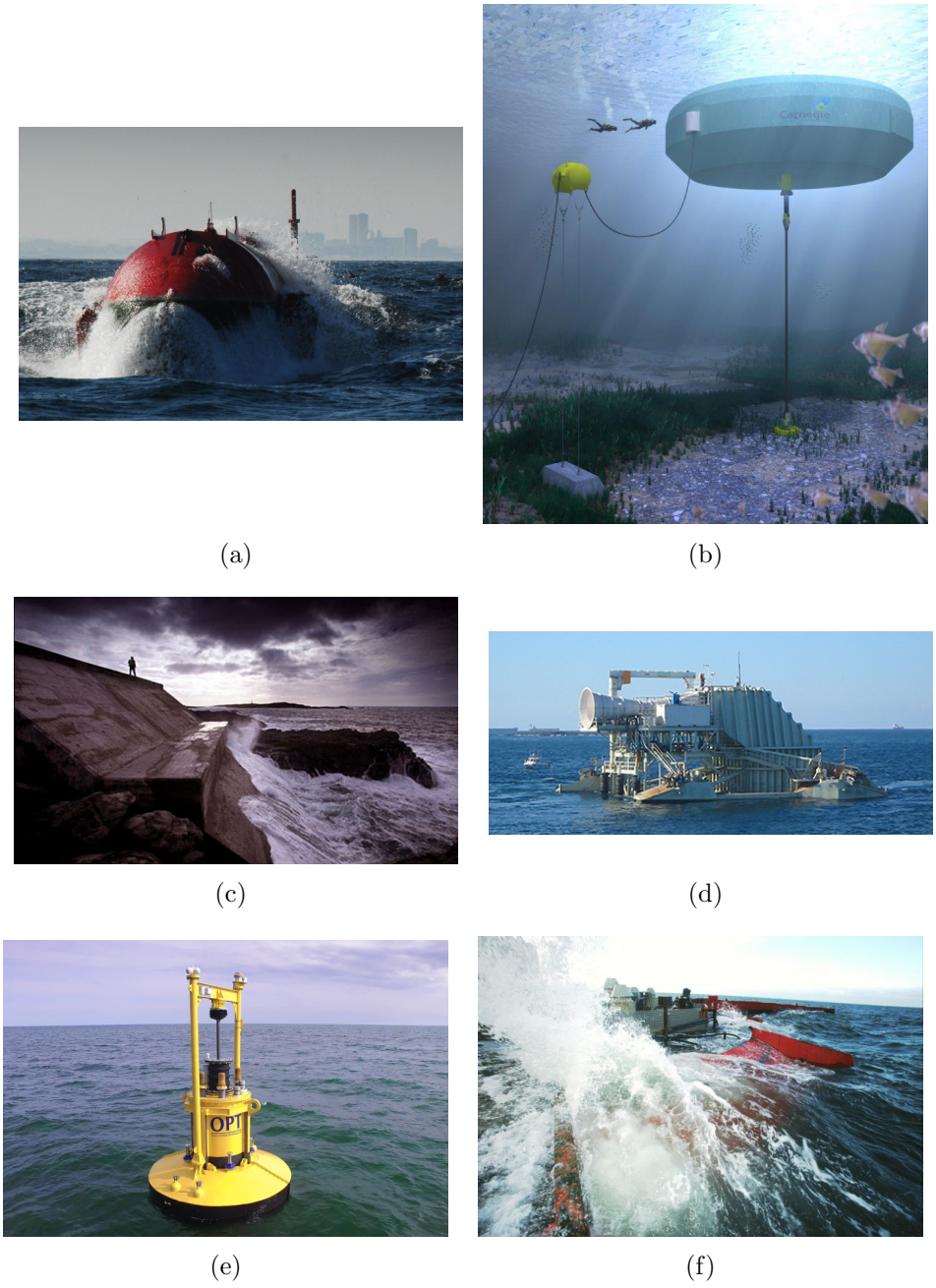

Figure 1.1: (a) Surface following attenuator Pelamis Wave Energy Converter (Pelamis Wave Energy Converter, 2015), (b) submerged point absorber Carnegie Wave Energy CETO 6 (Carnegie Wave Energy, 2015), (c) shore mounted oscillating water column Islay LIMPET (The Guardian, 2008), (d) floating oscillating water column Oceanlinx MK1 (Oceanlinx Ltd, 2013a), (e) floating point absorber Ocean Power Technologies Powerbouy (Ocean Power Technologies, 2015) and , (f) overtopping device Wave Dragon (Wavedragon, 2015)

One design concept which shows great promise and has been trialled at full scale is the oscillating water column (OWC). The device utilises a semi enclosed chamber of air and water and operates on similar principles as a blowhole; as the wave enters and leaves the chamber the free surface of the water rises and falls creating a pressure

change within the chamber as shown in Figure 1.2. The difference in air pressure between the chamber and the atmosphere is used to drive a unidirectional turbine (Cruz (ed.), 2008). When correctly configured, resonance between the water column and the incoming wave can occur resulting in improved energy output (Dizadji *et al.*, 2011; Olvera *et al.*, 2007).

This design has the potential to be used in a wide variety of applications, including floating (Forestier *et al.*, 2007; Washio *et al.*, 2001), shallow water (Folley *et al.*, 2005), shore based (Müller *et al.*, 1995; Wang *et al.*, 2002) or as part of a breakwater (Takahashi *et al.*, 2011). This concept has also been put into practice with a number of working prototypes such as the Pico plant in Portugal (Brito-Melo *et al.*, 2008), the Mighty Whale in Japan (Washio *et al.*, 2001) and various Oceanlinx projects (Oceanlinx Ltd, 2013a) in Australia.

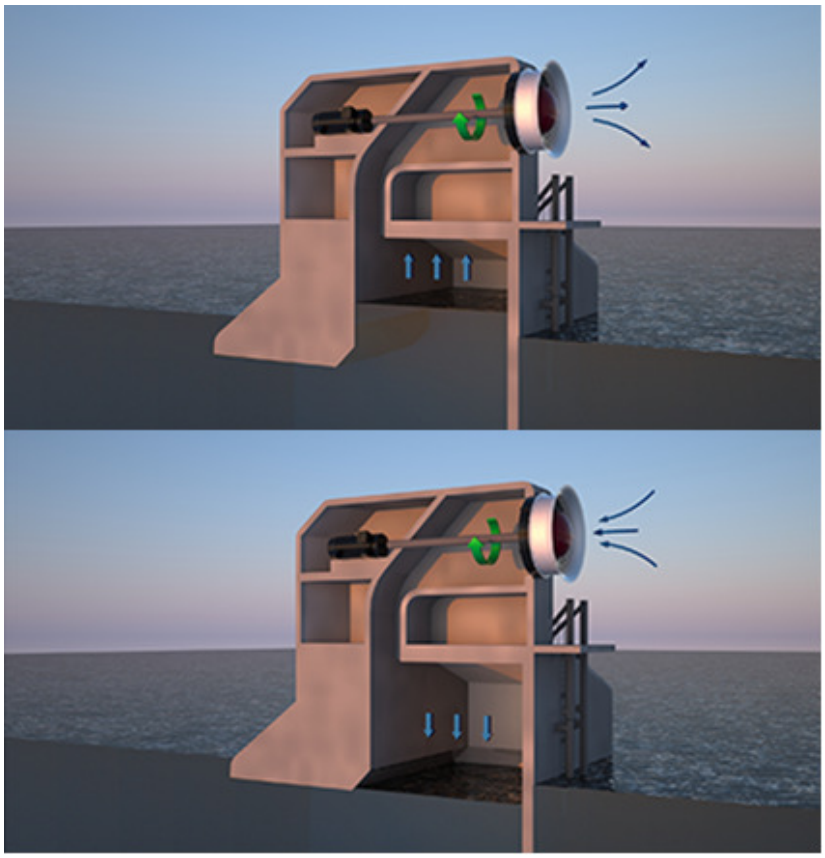

Figure 1.2: OWC operation showing the inflow (top) and outflow (bottom) conditions and the unidirectional turbine (Oceanlinx Ltd, 2012)

1.2 Problem Definition

The key challenge facing the development of wave energy as a major source of energy is reaching economic viability when compared with not only traditional emissions based energy sources but other renewable sources (Behrens *et al.*, 2012). The levelised cost of electricity (LCOE) is used to compare different energy sources by estimating output and the total cost required including capital, maintenance and fuel and is given in $AUD per MWh. Behrens *et al.* (2012) compared the LCOE for various energy sources based on predicted technology levels in 2030 (Figure 1.3) showing that much progress has to be made for ocean energy to become a viable energy source. In favourable conditions such as the presence of a carbon pricing or trading scheme, wave energy would need to reduce its LCOE to at least 109 $AUD/MWh.

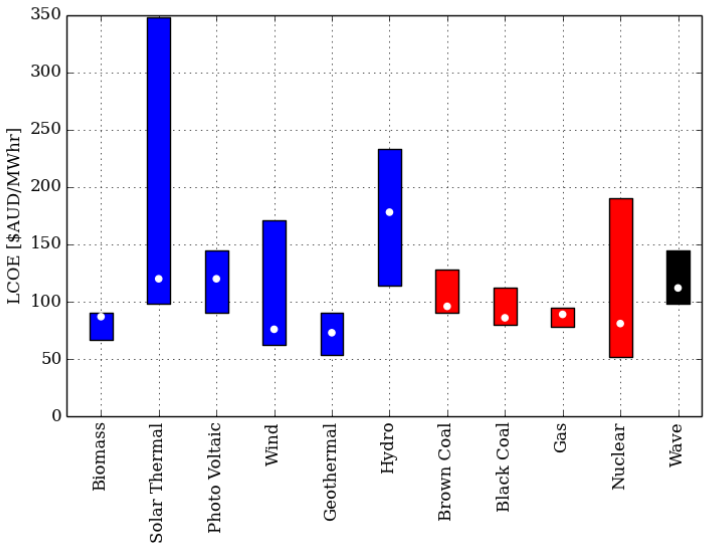

Figure 1.3: Projected LCOE of various renewable (blue) and non-renewable (red) sources in 2030 compared with ocean wave energy (black) (Data sourced: Behrens *et al.* (2012))

The path from device conception to commercial installation can be summarised into nine stages or Technology Readiness Levels (TRL) (Mankins, 1995). When applied to wave energy converters, TRL stages 1-3 refer to the research stage up to and including proof of concept, design optimisation and preliminary performance prediction and is usually undertaken using model scale experimentation. TRL stages 4-5 includes validation of advanced models, mooring design and advanced performance prediction using site specific wave spectrum. TRL stages 6-9 typically adopt full scale testing to investigate full system validation (ITTC, 2014).

When simplified, improvement in economic viability can be achieved in two ways, reducing costs and/or increasing output. Capital and maintenance costs will be reduced on a per device basis as commercial scale arrays are introduced and economies of scale can be introduced but basic costs such as materials and construction will remain high. Therefore a major source of improvement must come from increasing the efficiency and therefore output of the device (Webb *et al.*, 2005).

To successfully increase device efficiency it is important to be able to understand and model device behaviour. Experimental studies provide quality data which can be used to evaluate and investigate the devices operation. While full scale testing can be performed, model scale testing provides a number of advantages including cost, controlled conditions and available instrumentation. Due to this, experimental model scale testing has been widely used to evaluate the performance of OWCs (Folley *et al.*, 2013; Morris-Thomas *et al.*, 2007; Morrison, 1995; Morrison *et al.*, 1992; Wang *et al.*, 2002). Experimental studies can be performed with a number of objectives such as concept validation, performance prediction, optimisation and numerical model validation. Depending on the required outcomes of the testing, different procedures should be applied. These can include the models scale, types of waves tested in, power take-off (PTO) simulation and instrumentation (Holmes, 2009).

Traditionally model scale experimentation has been performed in two different wave types: a regular and/or an irregular wave (Cruz (ed.), 2008). Regular waves are discrete single frequency sinusoidal waves and provide a highly repeatable flow for experimentation, however due to this simplification these waves cannot capture some nonlinear effects (Folley *et al.*, 2002). An irregular wave is a continuous spectrum of waves designed to replicate the more random sea state these devices will operate in and therefore much more realistic than a regular wave. The use of irregular waves allow non-linearities to be incorporated into the performance prediction of the WEC (Gervelas *et al.*, 2011). The International Towing Tank Conference (ITTC) recommend testing in irregular waves during the validation stage of design at TRL stages 4-5 (ITTC, 2014).

The required outcomes also impact the level of instrumentation used during testing. Simple outcomes such as power output can often be determined using instruments such as wave probes, pressure transducers, displacement sensors and load cells. For a more detailed investigation of the water flow particle image velocimetry (PIV) can be utilised. PIV is a technique which is used to quantitatively capture flow velocity fields (Raffel *et al.*, 2007) and has been used in a variety of maritime engineering applications including flow around an escort tug (Molyneux *et al.*, 2007), study of wave impacts (Muthanna *et al.*, 2009) and wake from a ducted propeller (El Lababidy *et al.*, 2005).

PIV has also been applied to the study of the flow within and around OWCs (Fleming *et al.*, 2011, 2012b; Graw *et al.*, 2000; Morrison *et al.*, 1992). Velocity fields provide a wealth of information about the devices operation and can be used both qualitatively to visualise the flow and identify inefficiencies in the design of the underwater geometry and also to quantify various flow properties. Initial studies performed by Morrison *et al.* (1992) identified a number of flow features including large vortices being created at the leading edge of the chamber. Graw *et al.* (2000) subsequently quantified the amount of energy contained within these vortices.

Thus far, PIV velocity fields of OWC operation have only been gathered in regular waves. As instrumentation limits often result in low sampling rates for PIV, phase averaging is applied Fleming *et al.*, 2011, 2012b. Phase averaging is a data processing technique which can be applied to data which is cyclical to reduce data to an averaged result over a single period with a reduction in uncertainty. Importantly this technique can only be applied to data which is cyclical or repeating such as that generated by the response of an OWC in regular waves.

Fleming *et al.* (2012a) subsequently used the phase averaged velocity fields to generate an energy balance for an oscillating water column. An energy balance is used to examine the operation of a system by tracking the flow of energy into, through and out of a system. The identification of sources (wave potential and kinetic energy) and sinks (PTO, outgoing waves, viscous losses, turbulence losses and vortex transport) showed that energy contained within vortices was not able to reach the PTO and therefore was indicative of inefficiency in the design of the underwater geometry.

PIV can be used to provide valuable information on the operation of OWCs and utilised to improve device efficiency. But it is important that this knowledge is applicable not only in highly controlled model scale testing conditions, but also when applied in more random sea states that devices will experience in their operating environment.

1.2.1 Objectives

This study investigates two aspects of model scale testing which are key to achieving applicable results; the wave in which the device is tested and the presence of three dimensional effects. The focus of this study is on the operation of an OWC device, however many of the findings are likely to be applicable to other types of WECs. In particular this work will focus on the following questions:

- Can model scale testing in regular waves be used to provide an accurate representation of the expected flow when compared to tests performed in an irregular or polychromatic sea?

  Ideally experimental testing should be performed in a sea state which is as simple as possible while still gathering data which is relevant to the required outcomes. This question will attempt to answer how complex a wave type must be to give an accurate understanding of device performance in a realistic sea state.

- Are there significant changes in flow across an OWC and if so what impact will these have on the performance?

  The flow within the device mostly occurs within the longitudinal plane. However the presence of sidewalls means the device will experience some changes in flow across the device. This question will investigate how large these changes are and if the changes should be considered when designing the devices geometry.

The answers to these questions will provide researchers with information to enable them to design scale model testing programs which provide accurate and detailed information on a WECs operation in a realistic sea state with the minimal required complexity.

1.3 Key Considerations

When comparing WEC performance and operation in different conditions it is important to have a set of parameters to make clear comparisons.

1.3.1 Device Power Output

The primary concern of designers is the power output of the device as this has a direct impact on the devices profitability. The power output for an OWC device is determined by a number of factors but a major component relates to how efficiently the device can convert energy from the wave to heave within the chamber. The design of the underwater geometry plays a large role in this process.

The power dissipated by the by the PTO is calculated using the pressure in the chamber and the flow rate through the orifice. The flow rate through the orifice is determined using wave probes to determine the rate of change of the mean water surface within the chamber and is calculated using Equation 1.1, where P_{PTO} is the PTO output per unit width, Δp is the pressure differential between the chamber and the atmosphere, ∇ is the volumetric flow rate, $H_{chamber}$ is the mean water elevation within the chamber and l is the chamber length. This model assumes the air is incompressible.

$$\begin{aligned} \nabla &= \frac{dH_{chamber}}{dt} \times l \\ P_{PTO} &= \Delta p \times \nabla \end{aligned} \tag{1.1}$$

1.3.2 Energy Balance

An energy balance captures energy sources, stores and sinks that occur during the operation of a device. Fleming *et al.* (2012a) developed an energy balance for an OWC which can be used to provide further information for the analysis of velocity fields (Figure 1.4). A key finding of the energy balance was that energy contained within vortices cannot be transferred to the devices power take off and therefore represents and inefficiency in the design of the geometry. This study uses the proportion of energy contained within vortices to be a key component to compare the operation of an OWC in differing wave conditions.

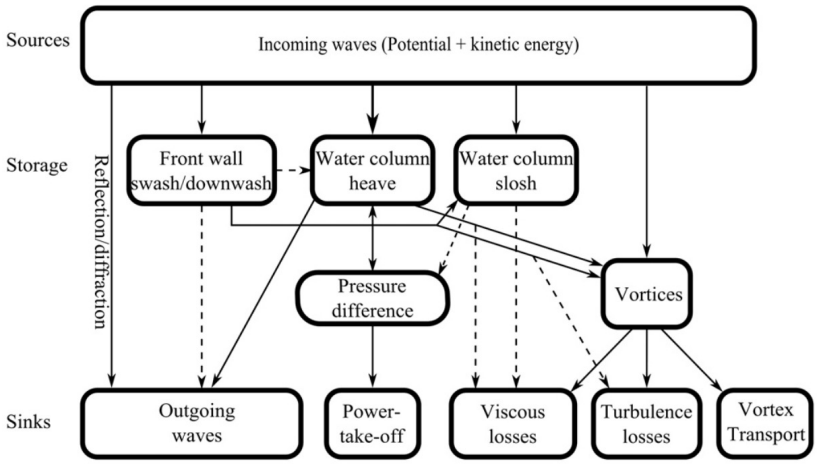

Figure 1.4: Energy balance for an OWC (Fleming *et al.*, 2012a)

1.4 Novel Aspects

This study provides a significant contribution through the application of PIV in a range of complex sea states - including regular, polychromatic and irregular waves - to investigate the operation and performance of an OWC. The novel aspects of this work include the following:

- The application of phase averaging to polychromatic waves. While phase averaging is a well-established method, previous work has limited its application to the analysis of experimental data in regular waves (Fleming *et al.*, 2011; Longo *et al.*, 2007).
- The measurement of sloshing within an OWC chamber in the transverse direction. Sloshing has been identified as a store of energy within the device but previous works have limited their investigation of sloshing to only the longitudinal direction (Fleming *et al.*, 2012b; Müller *et al.*, 1995).
- The application of PIV to investigate the flow and performance of a WEC in polychromatic waves. Polychromatic waves have been used to investigate the performance of an OWC water pump using more conventional measurement techniques (Godoy-Diana *et al.*, 2007), while PIV has been used to measure velocity fields in and around an OWC in regular waves (Fleming *et al.*, 2011; Graw *et al.*, 2000; Morrison *et al.*, 1992).
- The use of PIV to investigate the flows within and around a WEC in irregular waves. Irregular waves are widely used when testing and evaluating the perfor-

mance of WECs during model scale experiments (Gervelas *et al.*, 2011; Korde, 1999) but PIV has never been applied to investigate the devices operation.

- The application of histograms as an analysis method of time series data from an OWC. Time series data is usually presented using a time history plot (Gervelas *et al.*, 2011) which can be difficult to interpret and evaluate.

- The measurement and investigation of the change in flow that occurs across the device utilising PIV to investigate several longitudinal planes. PIV has previously only be used to study the flow at the centreline of the device (Fleming, 2012; Graw *et al.*, 2000; Morrison *et al.*, 1992).

- A detailed study of the flow in the vicinity of the sidewall of an OWC using divergence to identify vortices. Previous works have shown that an OWC can have a capture width of greater than unity (Cruz (ed.), 2008). This work demonstrates how an OWC can utilise the volume of water outside of its sidewalls to generate power.

1.5 Thesis Outline

This work has been completed as a series of peer-reviewed journal papers and are collated and presented as chapters within this thesis. Where the chapter has been published it is clearly indicated on the first page of the chapter. The chapter body is then the most recent version provided for publication. The structure of the thesis is as follows:

The opening chapter, Chapter 1, commences with an introduction to the subject area before providing more specific information about the project undertaken, including the problem definition, objectives, key considerations and novel aspects.

Chapter 2 introduces the concept of polychromatic waves, a wave with multiple frequency components yet still a finite period. Phase averaging methodology previously applied to analyse experimental data in regular waves is adapted to polychromatic waves. Wave probes within the chamber are used to identify non-linearity in the device operation. Sloshing within the chamber is identified and the importance of using an array of sensors to capture the surface highlighted. The phase averaging methodology developed for polychromatic waves is subsequently applied to PIV velocity fields. The uncertainty in the velocity field is calculated and compared with that of regular waves. Prominent features in the flow are identified and the proportion of kinetic energy contained within vortices compared between regular and polychromatic waves.

Chapter 3 expands on the work presented in the second chapter by comparing PIV data from regular, polychromatic and irregular waves. As the irregular wave does not have finite period, a time domain data processing method for the PIV data is developed and velocity fields determined. Histograms are used to compare various properties quantifying the devices operation such as the power generated and the kinetic energy within the velocity field. Recommendations for the selection of wave types for the analysis of wave energy converters are provided.

Chapter 4 investigates the change in flow that occurs across the transverse plane of the device by using PIV to measure the flow at four longitudinal planes both within and outside of the device. Changes in the flow are observed and the total kinetic energy within each plane is used to identify the transition between inflow and outflow at different planes, which can be used to identify the transverse location which provides the best approximation of the flow across the device. Divergence is used to detect out of plane flows and identify a number of features of the flow such as vortices and jets.

The final chapter, Chapter 5, provides an overall summary of results and conclusions. Key findings are presented and their implication for further work in the area of model scale testing of wave energy devices is discussed.

Work related to this thesis was presented by the author at the 2nd Asian Wave and Tidal Energy Conference in Tokyo, Japan (Mitchell Ferguson *et al.*, 2014a,b). These two non-refereed conference papers are included as Appendix A and B. A majority of the content of these conference papers appears in similar form within Chapter 2. The remaining content is additional work not appearing elsewhere in the thesis.

Some selected photographs of the model have been presented in Appendix C and examples of raw data and unprocessed PIV images can be found in Appendix D.

Chapter 2

Improving OWC performance prediction using polychromatic waves

The work presented in this chapter has been accepted for publication in *Energy*. The citation for the research article is:

Mitchell Ferguson, T., Fleming, A., Penesis, I. and Macfarlane, G.,(2015) "Improving OWC performance prediction using polychromatic waves", *Energy*, [*In Press*].

Abstract

The performance of wave energy converters using model scale experiments has been assessed primarily using regular waves with limited testing in irregular waves. A viable alternative is the use of polychromatic waves, superposition of discrete regular waves with a definite period. Polychromatic waves allow well proven phase-averaging techniques to be applied to a wave which is more random and therefore representing a more realistic sea-state than regular waves. This paper presents results from model experiments on a generic forward-facing bent-duct oscillating water column in polychromatic waves using a wave probe array within the device and particle image velocimetry. By adapting phase averaging methodology the results show that more reliable predictions of the devices operation are obtained in polychromatic waves. Results from the wave probe array show that a longitudinal array is required to capture sloshing within the chamber. Velocity fields reveal a reduction in the proportion of kinetic energy within vortices in polychromatic waves compared with regular waves. This study highlights the importance of performing experiments in sea-states that are more realistic than simple regular waves to ensure an accurate representation of the devices performance and operation.

2.1 Introduction

The ability to successfully capture wave energy and efficiently convert it into usable energy could play a key role in reducing our reliance on fossil fuels as an energy source. One wave energy converter (WEC) that has demonstrated this ability is the oscillating water column (OWC). To further develop and improve the design of these devices research must be undertaken to provide designers with a detailed understanding of the devices operation to maximise its efficiency.

Scale model testing is one of the methods that is commonly used to further this understanding by providing controlled experimental conditions at a substantially reduced cost compared with full scale prototyping. When performing scale model experiments, a number of options are available depending on the desired outcomes including: scale, instrumentation and the use of flow visualisation. These decisions often require compromise between testing in the most realistic, and therefore accurate, scenario possible and the additional complexity, and therefore cost and time to perform and analyse the data, required for a more realistic test.

One of the key decisions when testing a wave energy device is the type of waves to simulate. Experiments are generally performed in either regular (Morris-Thomas *et al.*, 2007; Wang *et al.*, 2002) or irregular waves (Folley *et al.*, 2010; Gervelas *et al.*, 2011). Regular waves consist of a single frequency wave which results in a highly repeatable, if unrealistic, test. The repeatable nature of the regular wave allows analysis techniques such as phase averaging (Fleming *et al.*, 2011) and model validation (Liu *et al.*, 2010; Wang *et al.*, 2002) to be applied. Irregular waves utilise a spectrum of frequencies designed to represent a realistic sea state, however use of this wave type requires extended testing and more advanced data analysis techniques (Cruz (ed.), 2008).

An alternative to regular or irregular wave is a polychromatic wave (Godoy-Diana *et al.*, 2007). This features two or more discrete regular waves superimposed to create a wave which has a variety of peak and trough heights and periods, similar to an irregular wave and closer to a real world sea state than a regular wave. With careful selection of the frequency of each component of the polychromatic wave the sequence of peaks and troughs will repeat, resulting in a defined period. This means many of the analysis methods which have been developed for regular waves can be readily applied to the polychromatic (pseudo-irregular) waves.

The calculation of power output in a model scale test often requires the accurate calculation of the flow rate through an orifice (Morris-Thomas *et al.*, 2007; Morrison *et al.*, 1992; Wang *et al.*, 2002). In most cases, this requires the accurate calculation of the average surface elevation within the chamber. Generally wave probes are used to measure this however as wave probes only measure the elevation at a single location this can be complicated if sloshing is present within the chamber.

Particle image velocimetry (PIV) is an experimental methodology used to capture the velocity fields (Graw *et al.*, 2000). It is performed by seeding the fluid with particles and utilising a light sheet generated by a high powered laser to capture two images of the flow within a small time interval. Each image pair is subsequently compared by subdividing each image into a number of interrogation windows. The fluid velocity at each interrogation window is determined by finding the displacement of particles within the window using cross-correlation (LaVision GmbH, 2010). This allows the measurement of the velocity field without any interference with the flow. However, a current limitation of the method is the low sampling rate which is available with current technology levels.

To overcome this limitation, phase-averaging can be applied. This is a data analysis methodology which can be applied to cyclical or repeating data such as that produced by waves. Phase-averaging aligns all data over a common time period to determine

the most likely result at any point within the period. This methodology is particularly useful for the investigation of data sources which have low sampling rates such as that produced by PIV. This technique has previously been applied to PIV velocity fields of propeller wake fields (Longo *et al.*, 2007) and OWCs (Fleming *et al.*, 2011, 2012b).

An energy balance can be used to analyse the performance of a wave energy device and aims to map the transport of energy that occurs during the devices operation. Fleming *et al.* (2012a) developed an energy balance for an OWC which highlighted that energy contained within vortices cannot be transferred to the power take off (PTO) and is instead lost through viscous effects, turbulence and vortex transport. As this energy does not contribute to the devices output it is an inefficiency and therefore should be minimised if possible.

This paper presents the application of phase-averaging methodology to two series of model scale experiments using polychromatic waves. The first series utilises an array of wave probes within the model to investigate the applicability of polychromatic waves and compare results with those generated using regular waves. The array was used to investigate the presence of sloshing and the selection of an appropriate array to sufficiently capture the water surface elevation within the chamber. The second series of experiments utilises PIV to capture velocity fields. As an indication of inefficiency in design, the proportion of kinetic energy contained within vortices are compared between regular and irregular waves.

2.2 Methodology

2.2.1 Experimental Setup

Two series of experiments were performed, one with PIV and one without. Both were performed in the Australian Maritime College towing tank, which has a length of 100 m, a width of 3.55 m and a depth of 1.5 m (Australian Maritime College, 2015). Waves were generated using a single hydraulically powered paddle-type wave maker. A sloped beach at the end of the tank reduced the magnitude of reflected waves.

Experiments were performed on a 1:30 scale model of a generic forward facing bent duct OWC constructed of 6 mm thick transparent acrylic and a constant cross-section as shown in Figure 2.3. The selection of scale is important when performing experiments with OWCs as many effects such as air compressibility, viscosity and turbulence must all be considered. Ideally the largest practical scale should be used for the facility

available. Cruz suggests a 1:30 scale model is suitable for the validation of numerical models and optimisation studies (Cruz (ed.), 2008).

The model was placed centrally within the tank with the inlet facing towards the wave maker to generate a head seas condition and was rigidly secured to the carriage above. The positioning of the model provided a separation of 1060 mm between the lower lip and the tank bottom. The power take off (PTO) was modelled by a 50.8 mm diameter orifice due to its simplicity and ability to represent the pressure-flow relationship of an impulse turbine (Cruz (ed.), 2008; Folley *et al.*, 2002). The sizing of the orifice gave a ratio between the chamber surface area and orifice area of 65:1. A majority of the damping associated with the operation of an OWC is provided by the turbine, represented by an orifice in this study. By altering the size of the orifice the natural frequency of the device can be altered. An earlier study (Fleming *et al.*, 2011) utilising this geometry determined that an orifice diameter of 50.8 mm gave the device the desired natural frequency of approximately 0.55 Hz (wave period of 10 seconds at full scale).

The water elevation was measured using an array of capacitance-type wave probes, placed within and around the OWC and monitored using Churchill wave probe monitors. The approximate locations of each wave probe in the arrays used in the first and second series of experiments are shown in Figure 2.1. An additional wave probe, the incident wave probe, measured the incoming wave and was placed adjacent and offset to the front wall of the chamber, approximately 150 mm from the side of the tank to minimise interference from the device. Two Endevco Model 8510B-2 (2PSI) pressure transducers were placed in the chamber roof approximately half way between the orifice and the chamber sides and measured the chamber pressure differential. These were conditioned using a three channel Endevco 136 voltage amplifier. Both the pressure and wave probe data was captured at a rate of 1000 Hz. An uncertainty analysis was performed for both the wave probe and pressure transducer data and incorporated the uncertainty in both measurement and in the averaging process. Uncertainty in wave probe elevation was determined using data gathered during calibration, while the manufacturers stated uncertainty was used for the pressure transducer. The uncertainty in the averaging methodology was determined using standard deviation of measurements from the phase averaged mean value. The greatest uncertainty measured with a 95% confidence interval for the water elevation at each of the wave probes indicated a maximum uncertainty of 2.14 mm, whilst the pressure transducers have an uncertainty of 10.9 Pa.

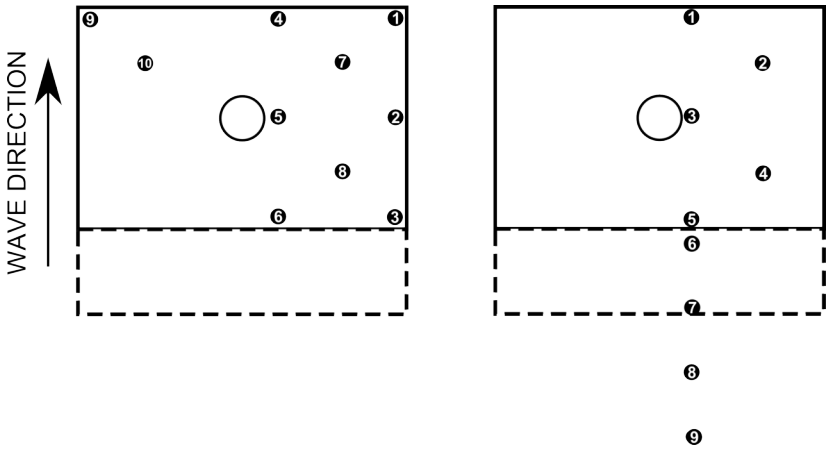

Figure 2.1: Plan view of the geometry showing the placement of wave probes for the first series (left) and second series (right) of experiments. The solid line indicates the boundary of the chamber, while the dashed line indicates the underwater upper lip of the bent duct OWC (refer Figure 2.3).

In addition to the wave probes and pressure transducers the second series of experiments utilised PIV to capture velocity fields in a longitudinal plane. A dual cavity 120 mJ Nd-Yag laser in addition to underwater optics directed a longitudinal light sheet along the centreline of the model (Figure 2.2). The water was seeded with neutrally buoyant fluorescing particles sized between 36 and 75 μm. A single sCMOS camera (16 bit, 2560x2150 pixels) was positioned outside a window in the side of the tank. Image pairs were captured at a rate of 15 Hz with an inter-frame time of 10 ms. To capture the field of interest with the desired resolution, adequate lighting from the light sheet and viewing angles for the camera, three separate fields of views were required (Figure 2.3).

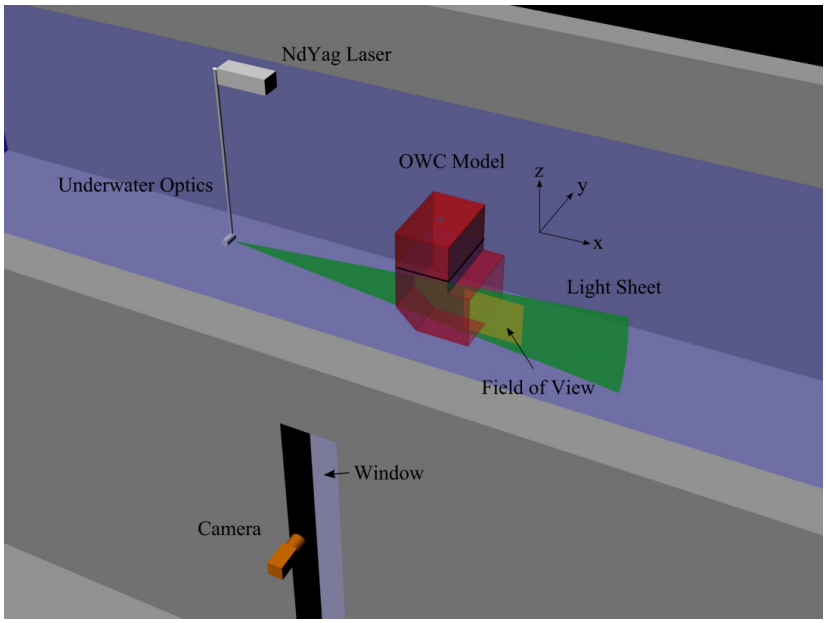

Figure 2.2: PIV setup for the second series of experiments

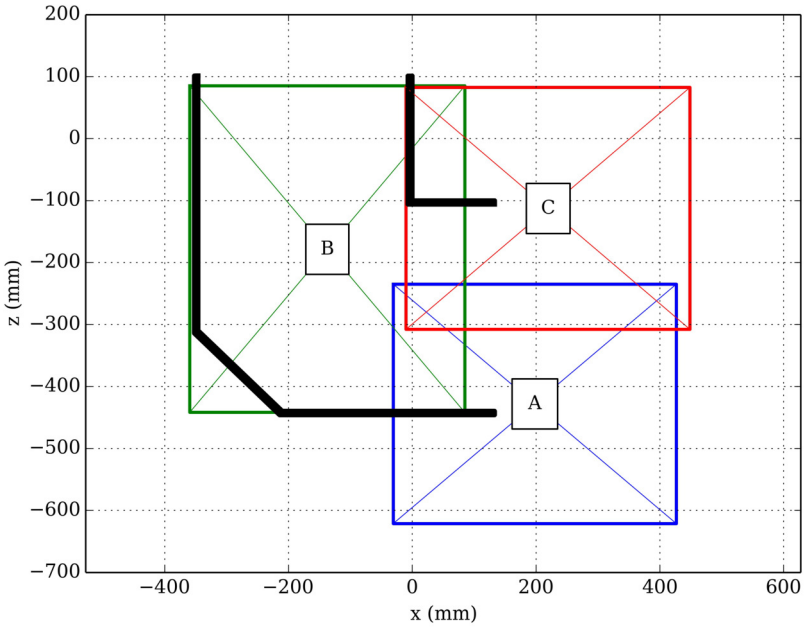

Figure 2.3: Cross section of the OWC used in the model scale experiments (black, solid) and the three fields of view (A,B,C) captured when performing PIV experiments. Images were captured at the device centreline (y = 0 mm).

Images were captured and post-processed using LaVision GmbH software package DaVis 8 (LaVision GmbH, 2010). Prior to post-processing images were masked above the waterline to eliminate the possibilities of reflections and improve the accuracy of the software. This was achieved by fitting a spline at the water surface using the data captured by the wave probe array. Areas above the estimated waterline were removed.

Velocity fields were created using a multi-pass method, initially using a 64x64 pixel square interrogation window before two passes using a 32x32 pixel square window. Vector post-processing was performed to remove spurious vectors and perform minor smoothing.

Polychromatic Waves

The model was exposed to both regular and polychromatic waves of frequencies between 0.45 and 0.60 Hz. This corresponds to a full scale period of between approximately 12.2 and 9.1 seconds respectively. Three component polychromatic waves were generated by the summation of three regular waves of equal height. Minor inaccuracies in the transfer function and losses between the wave maker and the device required the wave to be measured at the device. Regular waves can be defined using two properties: height and frequency, while polychromatic waves at a single location require each component of the wave to be defined by three properties: height, frequency and phase. The component heights and frequency is common for all locations however the phase will vary depending on the distance from the wave maker due to the differing phase velocities of the wave components. As it is impractical to tune the wave maker to give each component a defined phase at the testing location this must be determined.

A polychromatic wave with a defined period requires that all component frequencies satisfy Equation 2.1, where n_i is an integer ≥ 1, f_i is the component frequency and T is the desired period of the polychromatic wave. For example, a polychromatic wave with a period of 20 seconds could have component frequencies of 0.05, 0.1, 0.15 ... Hz. A longer period allows greater resolution in the frequencies available to be selected. For polychromatic waves of shorter periods it would be prudent to ensure the devices steady state response has the same period of the polychromatic wave, as some harmonic responses may have a significant response of greater than a single period.

$$f_i = \frac{n_i}{T} \tag{2.1}$$

To determine these properties the phase-averaged (see Section 2.2.2) wave elevation measured at the incident wave probe was fitted to Equation 2.2:

$$\sum_{i=0}^{n} \frac{h_i}{2} \cos 2\pi f_i t + \phi_i \tag{2.2}$$

where n is the number of components, h_i is the component height, f_i is the component frequency and ϕ_i is the component phase.

The desired and measured components of the polychromatic wave for each series of experiments are shown in Table 2.1. The resulting polychromatic wave with component frequencies of 0.45, 0.50 and 0.60 Hz has a period of 20 seconds and as shown in Figure 2.4. It is clear that the result provides a much more random sea state than a regular wave that is repeated every 20 seconds.

Table 2.1: Constants required for Equation 2.2 to describe the three component polychromatic waves in the first and second series of experiments

		Series 1			Series 2		
n_i	f_i [Hz]	Desired Height [mm]	h_i [mm]	ϕ_i [rads]	Desired Height [mm]	h_i [mm]	ϕ_i [rads]
0	0.45	30	31	-0.50	23	19	0.08
1	0.50	30	30	0.38	23	24	-0.51
2	0.50	30	30	0.35	23	23	0.44

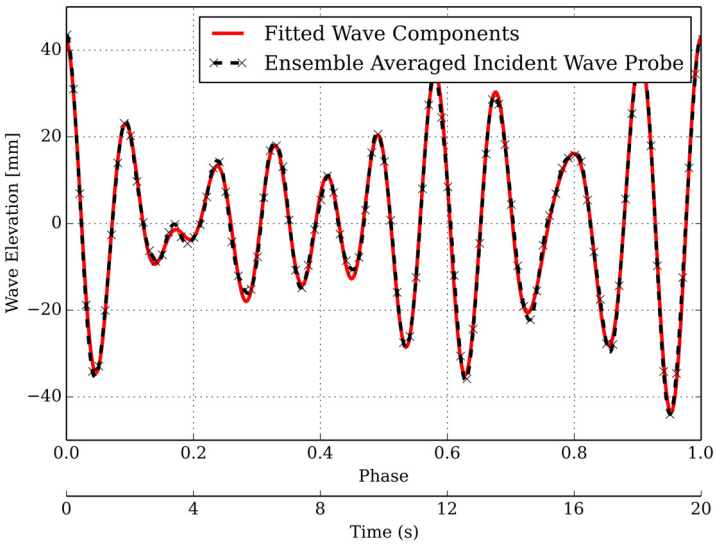

Figure 2.4: The phase-averaged elevation of the polychromatic wave in the first series of experiments (black, dashed) and the fitted sinusoidal function (red, solid)

To prevent interference of reflected waves from the end of the tank the recorded length of each run was limited to a maximum of 120 seconds. Multiple runs for each combination tested were required to ensure an adequate sample was obtained. For the first series of experiments three runs were completed for each regular wave and ten runs were completed for the polychromatic wave. For each field of view of the second series of experiments four repeat runs were performed for the polychromatic wave and

two runs for the regular waves resulting in approximately 7200 image pairs for the polychromatic wave and 1800 for regular waves.

2.2.2 Data Processing

Phase-averaging is a data analysis technique which can be applied to cyclical data, such as waves. To be effective it requires all phenomena being investigated to occur with a common period. Successful application of phase-averaging results in an averaged result over a single period and which can both reduce uncertainty and quantify the level of uncertainty. Phase-averaging is performed in two stages; phase assignment and data fitting. The aim of phase assignment is to locate each data point within the period being investigated by assigning phase value between zero and one, where zero is the start of the period and one is the end and each data point investigated will fall between the two values. This value is determined using Equation 2.3:

$$Phase\left[\frac{T}{t}\right] = \frac{T_{data} - T_{start}}{T_{end} - T_{start}} \tag{2.3}$$

where T_{data} is the time for the data point, T_{start} is the time at the start of the period and T_{end} is the time at the end of the period.

Accurately identifying the start and finish of each period is of great importance to ensure phase averaging is performed successfully. As it is independent of the device, the incident wave probe provides the best data source to determine these points. Previous applications to regular wave data have used points such as the zero crossing or peaks however a different approach is required for a polychromatic wave. A sinusoidal function (Equation 2.2) with a period equal to the period of the polychromatic wave was fitted to the time-series data using a Nelder-Mead simplex minimisation algorithm (Jones *et al.*, 2001-) to minimise the difference between the measured elevation and the theoretical sinusoidal function and the point of greatest elevation identified as the start/finish of each period. This method can be applied to both regular and polychromatic waves and provides other advantages as it takes into account all data points within the run not only those at the zero-crossing or the peak. Figure 2.5 shows the result after 42 periods of the wave elevation is sorted by its assigned phase.

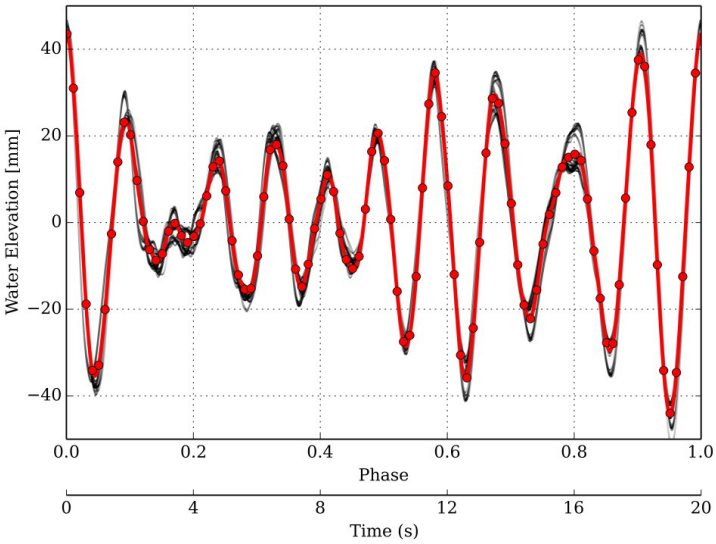

Figure 2.5: Phase assigned wave elevation at the incident wave probe (black) and the ensemble averaged result (red) from the first series of experiments. Markers indicate every 5^{th} bin

The second stage in phase-averaging requires fitting a curve to the data to find the most likely result for each phase. Due to the differing sampling rates between the pressure transducer and wave probe data and the PIV velocity fields two methods were used, ensemble averaging and spline fitting. For the first series of experiments ensemble averaging was used to divide the phase assigned data into 600 equally spaced bins. The second series utilised ensemble averaging for the wave probe and pressure transducer data using 600 equally spaced bins for polychromatic waves and 60 for regular waves. Due to the lower number of samples and transients of the free surface through the PIV images a spline fitting was adopted for phase averaging the velocity fields. Splines were fitted on a pixel by pixel basis using the methodology outlined by Fleming *et al.* (2012b) with the splines being sampled at 600 equally spaced intervals for polychromatic waves and 60 equally spaced intervals for regular waves.

The power (P_{PTO}) consumed by the orifice plate (simulated PTO) is calculated using the product of pressure differential and the volumetric flow rate as shown in Equation 2.4:

$$\begin{aligned} \nabla &= \frac{dH_{chamber}}{dt} \times l \\ P_{PTO} &= \Delta p \times \nabla \end{aligned} \tag{2.4}$$

where P_{PTO} is the PTO output per unit width, Δp is the pressure differential between the chamber and the atmosphere, l is the chamber length, ∇ is the volumetric flow rate per unit width and $H_{chamber}$ is the mean water elevation within the chamber. The air is considered to be incompressible.

From Equation 2.4 given the small time interval, small errors in the measurement of the mean height of the water elevation can result in large errors in calculation of power after differentiation. For the first series of experiments utilising the expanded wave probe array within the chamber a surface was fitted to the elevations recorded at each of the wave probes using Gaussian process prediction, as shown in Figure 2.6. The Gaussian prediction utilised a constant regression model with a squared exponential correlation model (Pedregosa *et al.*, 2011). As the model was in a head seas condition it was expected that the elevation within the chamber would be symmetrical. Probes mirrored in the centreline, 1 & 9 and 7 & 10, supported this finding with a mean squared difference in elevation of 0.5 and 0.2 mm respectively. Based on this finding, data from wave probes was mirrored before creating the surface on both sides of the centreline. In the locations where two wave probes were co-located results were averaged prior to mirroring. Uncertainty analysis of the surface fitting method (including wave probe data) gave an uncertainty of 1.09 mm in mean elevation within the OWC chamber using a 95% confidence interval.

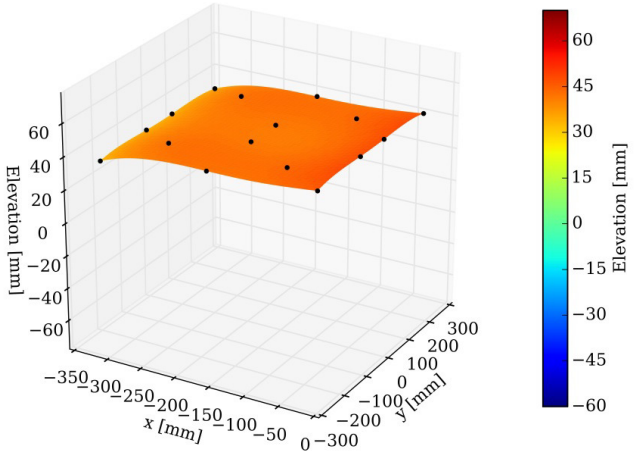

Figure 2.6: Resulting fitted surface within the chamber for the first series of experiments when phase=0.00.

The findings from the first series of experiments showed little variation (see Section 2.3) in the water elevation transversely resulting in a reduced wave probe array. For

this series it was assumed that the transverse elevation was constant across the device. A spline was fitted to the wave probe water elevation and used to determine the mean height within the chamber.

The energy flux per unit width (EF), or instantaneous wave power was determined using the method outlined by Isberg *et al.* (2009). This method uses potential theory to determine the instantaneous wave power using the wave elevation, measured in this case using the incident wave probe. By utilising integrals of the wave elevation time series to generate the wave energy flux at one point in the surface it can be applied to any wave profile including irregular waves. With the power output P_{PTO} and energy flux (EF) the capture width of the device is calculated using Equation 2.5. The capture width describes the proportion of power that is captured by the device from the wave.

$$CW = \frac{\overline{P_{PTO}}}{\overline{EF}} \tag{2.5}$$

One way to quantify the operation of an OWC from velocity fields is to perform an energy balance (Fleming *et al.*, 2012a). An energy balance requires the calculation of a number of parameters within the velocity field of the device. The boundary for the energy balance was arbitrarily chosen to be that shown by the dashed boundary in Figure 2.12, the main requirement being that the boundary is consistent for all wave fields. The total kinetic energy (E_{k_T}) contained within a two-dimensional velocity field per unit width is shown in Equation 2.6:

$$E_{k_T} = \frac{1}{2}\rho_w dx dz \sum_{x,z} V^2_{(x,z)} \tag{2.6}$$

where E_{k_T} is the total kinetic energy within the velocity field per unit width, ρ_w is the water density, dx is the pixel width, dz is the pixel height and $V_{x,z}$ is the velocity vector (Graw *et al.*, 2000). This method assumes the velocity in the y direction is zero.

The two-dimensional vorticity is calculated from the velocity fields using Equation 2.7:

$$\vec{\omega} = \frac{1}{2}\left(\frac{\partial v}{\partial x} - \frac{\partial u}{\partial z}\right) \tag{2.7}$$

where u and v is the velocity in the x and z direction respectively and $\partial v/\partial x$ and $\partial u/\partial z$ are the strains calculated from the velocity field (Graw *et al.*, 2000).

2.3 Results and Discussion

All results presented in this section have been phase averaged using the techniques demonstrated in Section 2.2.2.

Referring to Equation 2.4; the most important factor in the accurate prediction of the power produced by the device is the water elevation within the chamber. Figure 2.7 shows the mean elevation within the chamber based on the fitted surface and the elevation of the incoming wave for the polychromatic wave from the first series of experiments. Initially it is clear that there is a phase difference between the elevation of the incoming wave and that within the chamber. This can be explained by two causes, the first is the placement of the incident wave probe adjacent to the front wall of the chamber as opposed to the centre of the chamber. The other is due to the intrinsic damping effects present within the operation of the device such as air compression and radiation waves within the chamber. Also shown is the devices ability to generate a greater elevation within the chamber than that of the incoming wave.

This effect is partially due to resonance, which can be explained by representing the OWC as a spring-mass-damper system. In this example the spring represents the chamber elevation returning to the static water level, the mass represents the mass and added mass of the water body and damping is caused by forces opposing the change in chamber elevation. This includes the air pressure within the chamber which is controlled by the orifice. By changing any of these properties the natural frequency of the system can be altered. When the incoming wave frequency is close to the natural frequency of the device the reactive energy, or energy opposing the water bodies motion is reduced which can result in higher elevation within the chamber than the incoming wave.

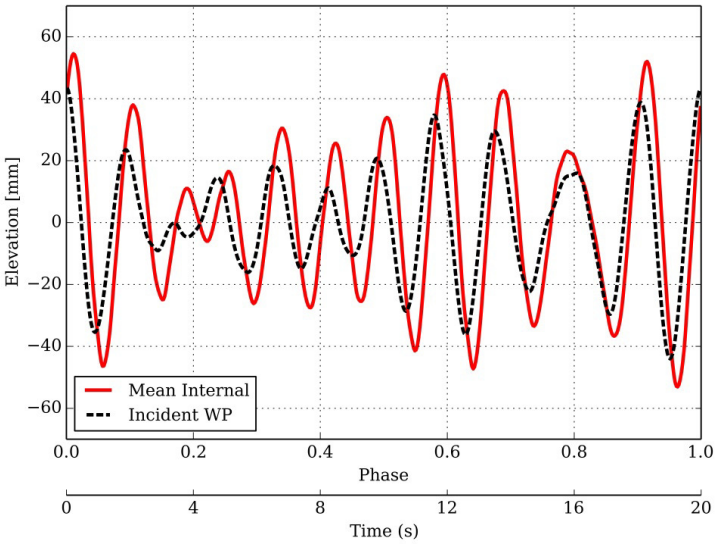

Figure 2.7: Incident wave probe elevation (black, dashed) and mean chamber elevation (red) for the polychromatic wave testing in the first series of experiments

To evaluate the difference between utilising a single wave probe and an array the devices power output was compared using the two methods. Wave probe no. 5 was selected as it was the most central of the array and compared to the surface generated in Section 2.2.2.

The volume flux (Figure 2.8) shows that while the two methods show a similar trend using a single wave probe oscillates above and below the fitted surface with the average difference between the two methods across a full period being 0.006 m^3/s, 44.5% of the average absolute flux. However the average flux of the two methods shows much less difference between the two methods with 0.014 m^3/s and 0.013 m^3/s for the surface and single probe respectively, an error of only 5.9%. When this is converted to power it shows a further reduced impact with an averaged power of 1.55 and 1.52 W/m, an error of only 1.8%.

The large differences in results are due to the single wave probes inability to capture sloshing as this method assumes the elevation within the chamber is flat. A single wave probe can be used to calculate the devices average output, but for any additional analysis such as the calculation of peak power a wave probe array is required to capture the effect of sloshing.

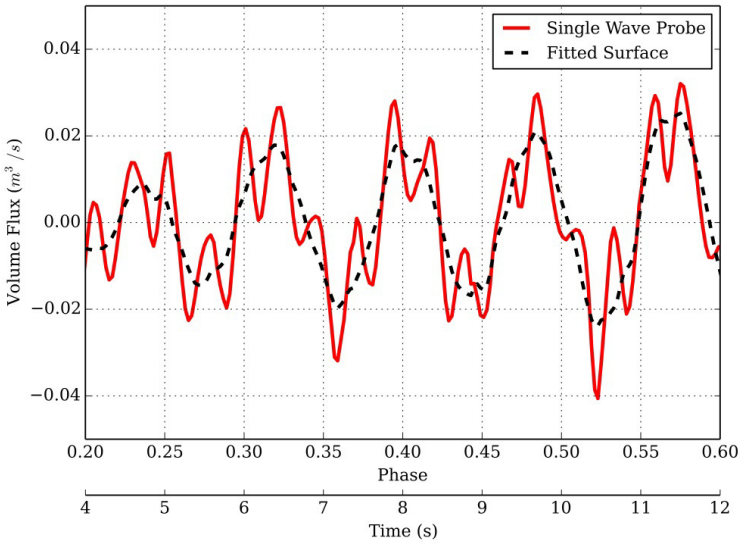

Figure 2.8: Volume flux through the orifice for the polychromatic wave from the first series of experiments comparing the surface fitting method with the use of a single wave probe (wave probe no. 5)

Many numerical models utilise linear superposition to develop predictions (Gervelas *et al.*, 2011; Suzuki *et al.*, 2003). As the polychromatic wave was generated using the linear superposition of three regular waves it was important to examine whether the response of the device in a polychromatic wave could also be predicted with the results from regular waves. Linear theory was used to develop two methods for replicating the 90 mm high polychromatic wave from the first series of experiments with results from regular waves were examined; the first used the summation of the results from the three nominal 30 mm regular wave components, the second used the averaged results from three nominal 90 mm regular wave components. Both methods can be used to simulate the incoming wave. Results from the phase-averaged regular waves were given the phase offset required to match that found in the polychromatic wave and repeated in the same manner used to create the polychromatic wave. Where required the wave component heights were adjusted linearly to match exactly those in the polychromatic wave to improve accuracy.

The resulting mean chamber elevation, using the fitted surface, from each method and the polychromatic wave is shown in Figure 2.9. It can be seen that neither method can accurately predict the elevation of the chamber over the entire period of the polychromatic wave. The averaging method is effective at predicting the elevation when high peaks and low troughs are experienced, while the summation method is more effective for smaller peaks and troughs. A number of possibilities could lead to this occurring

including non-linearity in the devices operation caused by the damping effects explored earlier. This shows that the polychromatic wave cannot be accurately predicted using results from regular waves and that non-linear effects must be incorporated into models to ensure accuracy.

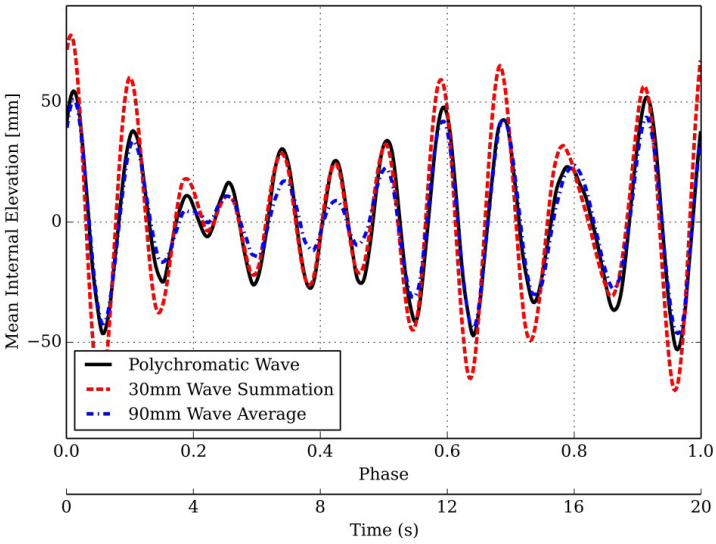

Figure 2.9: Comparison of the internal elevation of the chamber for the polychromatic wave and two prediction methods using regular waves

The efficiency or capture width is of great importance when evaluating a devices performance. The orifice damping coefficient will have a large impact upon performance of an oscillating water column. Matching the orifice's damping coefficient and the sea state will result in improved performance. While the results presented in this chapter only use a single orifice size, comparisons between regular and polychromatic waves are not expected to vary with different orifice sizes. Table 2.2 shows the wave power, device power and capture width of the device for the waves tested in the second series of experiments. In regular waves it can be seen that the capture width is minimally affected by wave height with little variation in capture width for the three wave heights at a frequency of 0.50 Hz. In contrast, for waves of a similar height with differing frequencies the capture width varies between 0.27 and 0.77, for a 0.45 and 0.60 Hz wave respectively. The capture width for the polychromatic wave was greater than two of the three regular wave components it is based on.

Table 2.2: Energy flux, PTO output and capture width for the waves in the second series of experiments

f_i [Hz]	h_i [mm]	$\overline{EF}$ $[W/m]$	$\overline{P_{PTO}}$ $[W/m]$	$\frac{\overline{P_{PTO}}}{\overline{EF}}$
Regular Waves				
0.45	75.7	12.15	3.31	0.27
0.50	45.3	3.92	2.03	0.52
0.50	56.0	5.99	3.17	0.53
0.50	78.4	11.73	6.06	0.52
0.55	74.7	9.71	6.83	0.70
0.60	74.7	8.90	6.85	0.77
Polychromatic Wave				
As specified in Table 2.1		2.71	1.74	0.64

Figure 2.10 shows the comparison between the instantaneous power in the wave and the output of the device for a polychromatic wave. In general, after taking into account the phase difference between the incoming wave elevation and the elevation within the chamber due to factors discussed earlier, there is a clear relationship between the two with greater incoming power resulting in greater output. However, during some stages the response of the device is different to what would be expected. At approximately $t = 4$ seconds we can observe a high amount of power in the wave with close to zero output from the device due to a high amount of reactive energy lost to the device. In addition between $t = 10$ and 15 seconds we can see the output of the device exceeds the incoming wave power due to a reduction in the amount of reactive energy lost to the device. While it has been observed that the device can have a capture width greater than unity, in this case we see examples where the output is in some cases almost twice that of the preceding peak in wave energy. This indicates energy can be stored within the device over a period greater than a single peak and trough through energy stores such as water column heave and sloshing. This energy cannot be dispersed within a single inflow and outflow condition and can have a large effect on the devices operation. Due to the repetitive nature of regular waves these effects cannot be observed during regular wave tests.

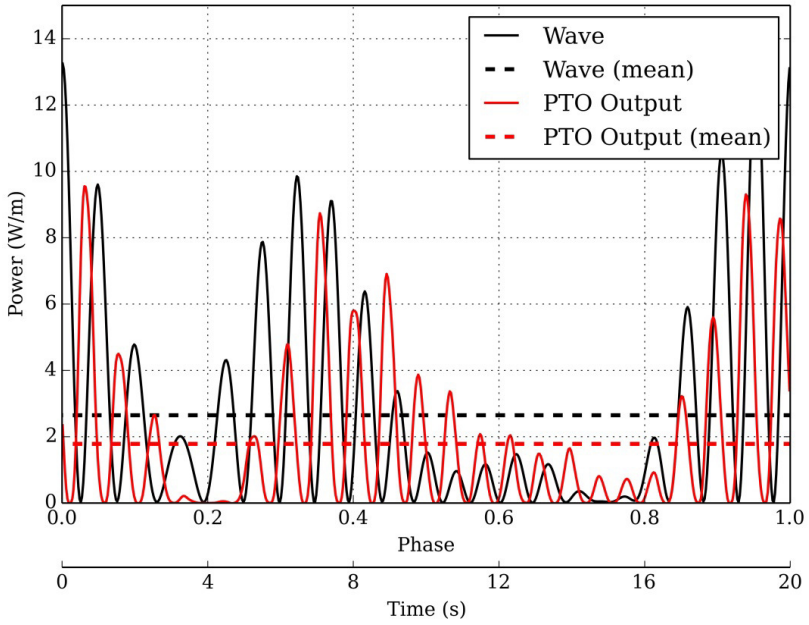

Figure 2.10: Instantaneous wave power (black) and device power (red) for the polychromatic wave in the second series of experiments

One of the energy stores which can have an impact on the devices operation is sloshing. The expanded wave probe array in the first series of experiments provided for a detailed measurement of the sloshing within the chamber. In the head seas condition investigated a majority of the energy within the wave is within the longitudinal plane; however the devices sidewalls may cause changes within the device resulting in transverse flow. The sloshing amplitude was defined as the distance between the highest and lowest elevation within the chamber. To differentiate between transverse and longitudinal sloshing the surface was initially averaged in one dimension to reduce the surface to a 2D representation. Figure 2.11 shows the magnitude of sloshing for a period of the polychromatic wave. This shows that for the head seas condition sloshing is only prevalent in the longitudinal direction, with minimal sloshing transversely. Variation in the sloshing magnitude is due to the intermediate period between the slosh impacting on each wall. For an accurate calculation of the chamber water elevation it is important that sloshing in the longitudinal direction can be measured and taken into account.

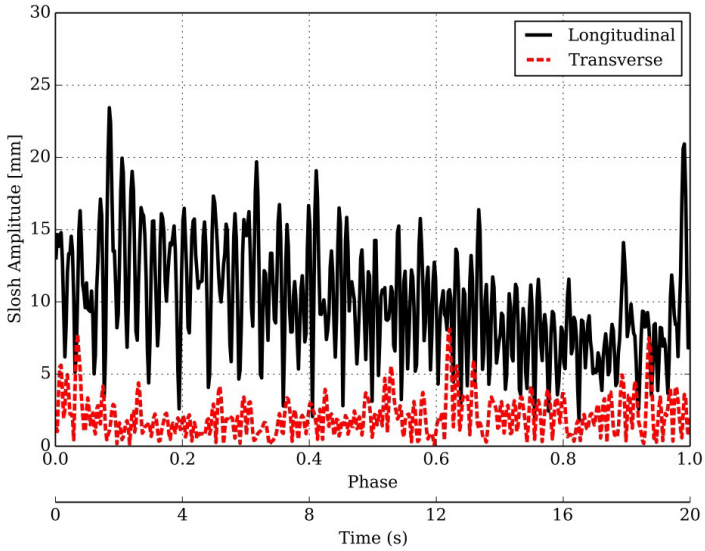

Figure 2.11: Sloshing magnitude within the chamber in both the longitudinal and transverse directions for the polychromatic wave in the first series of experiments

Phase-averaged velocity fields were generated for each of the waves in the second series of experiments. An example of the velocity field during inflow for the OWC is shown below in Figure 2.12. This demonstrates a number of the properties of the flow that have previously been shown to occur with regular waves (Fleming *et al.*, 2011), namely a large vortex at the lower lip and smaller vortices at the upper lip and entry to the chamber. These vortices are caused by the rapid change in geometry which leads to separation of the flow. The creation of vortices should be avoided if possible as energy within a vortex is not available to the PTO.

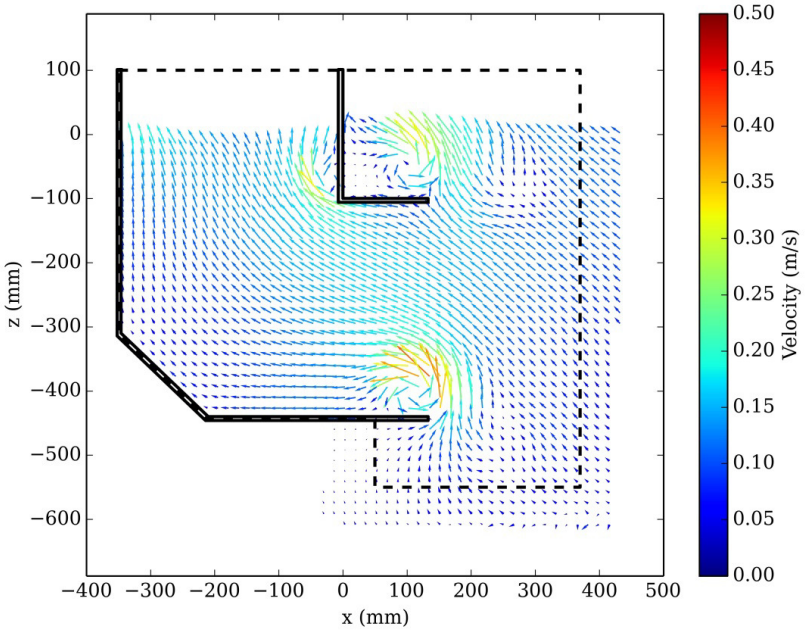

Figure 2.12: Phase-averaged velocity field and the area of interest (dashed) for the OWC for the polychromatic wave when phase=0.98 used in the second series of experiments. 1 in 25 vectors are shown for clarity

In a phase-averaged velocity field, uncertainty can be caused by a number of factors such as variability in flow velocity in areas of turbulence and limitations in the velocity measurement. The uncertainty in velocity measurement was calculated using the method outlined in the ITTC Recommended Procedures and Guidelines (ITTC, 2009) and was found to be 0.00457m/s. Figure 2.13 shows the resulting total mean uncertainty incorporating both uncertainty in the measurement and in flow repeatability within the velocity field for a full period of the polychromatic wave. This highlights the randomness that occurs in flow within vortices and the subsequent difficulty in determining an average flow using phase averaging in these regions. The mean uncertainty within the field is compared between polychromatic and regular waves in Table 2.3. This indicates that for these test conditions the methodology successfully applied previously to regular waves can also be applied to polychromatic waves.

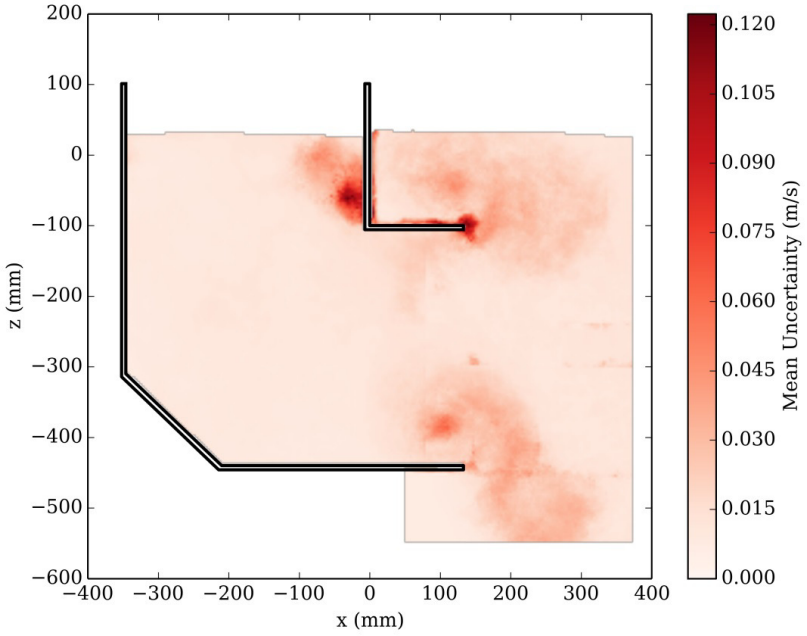

Figure 2.13: Mean uncertainty within the velocity field over a period of the polychromatic wave in the second series of experiments

Table 2.3: Uncertainty in the velocity field for regular and polychromatic waves in the second series of experiments

f_i [Hz]	h_i [mm]	Mean Uncertainty $[m/s]$
Regular Waves		
0.45	75.7	0.015
0.50	45.3	0.019
0.50	56.0	0.023
0.50	78.4	0.023
0.55	74.7	0.031
0.60	74.7	0.023
Polychromatic Wave		
As Specified in Table 2.1		0.015

Secondary properties of the velocity fields such as the kinetic energy (Figure 2.14) and vorticity (Figure 2.15) allow greater understanding of the behaviour of the device by quantifying some properties of the flow. These figures show the greatest concentration of kinetic energy occurs within vortices and as such present a large inefficiency in the operation of the underwater geometry.

An accurate calculation of the kinetic energy lost within vortices is generated by determining the proportion of the total kinetic energy contained within vortices compared with that in the field. For this study areas in which the vorticity exceeded 4 rad/s were defined as being within a vortex. These regions are indicated by the black contours in Figure 2.15.

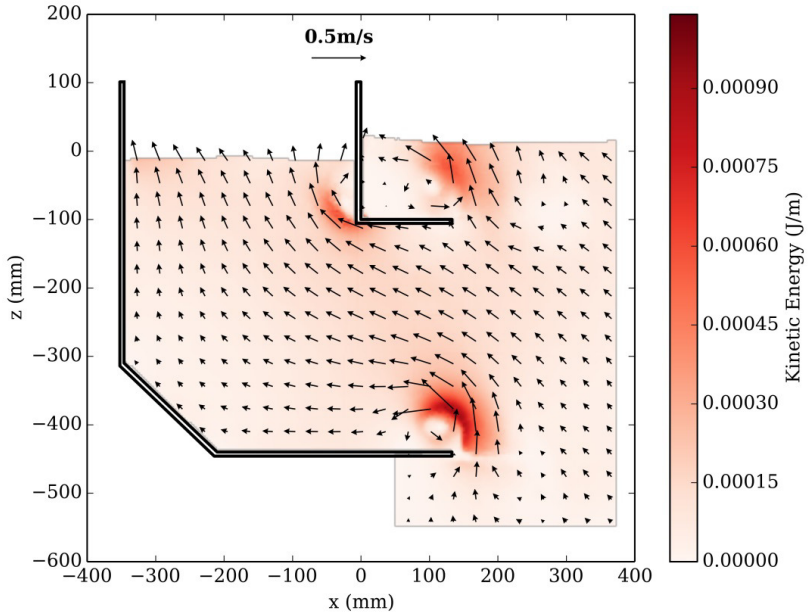

Figure 2.14: Kinetic energy within the flow for the velocity field presented in Figure 2.12

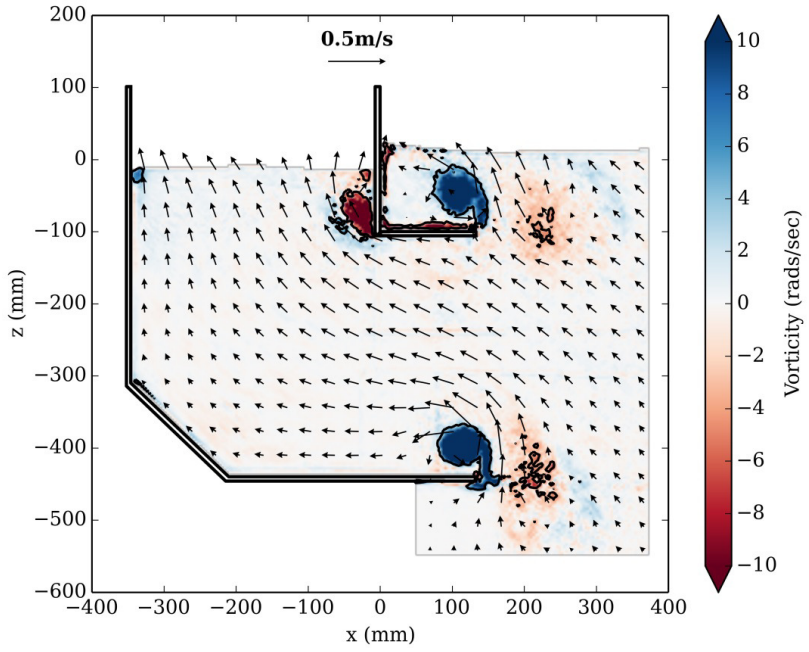

Figure 2.15: Vorticity within the flow for the velocity field presented in Figure 2.12. Black contours highlight areas in which the vorticity is greater than 4 rads/s

Figure 2.16 shows the total kinetic energy and that contained within vortices within the area of interest for a period of the polychromatic wave. The total kinetic energy shows a number of clear and well defined peaks and troughs; each of these corresponds to either an inflow or outflow condition. In contrast the amount of kinetic energy within vortices shows a much smoother profile. This indicates that the energy contained within the vortices takes a period greater than a single inflow and outflow condition to dissipate. This effect would not be captured in regular waves as the repetitive nature of the testing would not allow the energy to dissipate or leave the system.

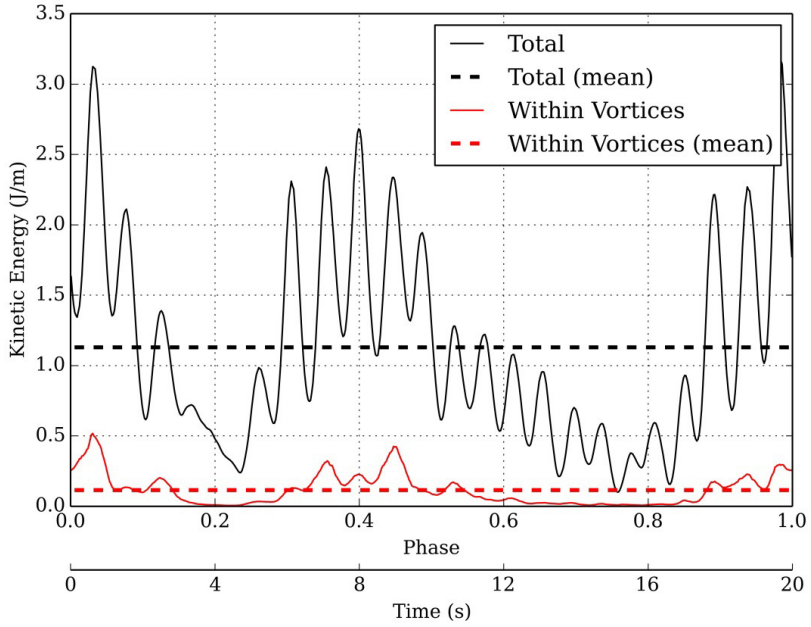

Figure 2.16: Total kinetic energy (black) and kinetic energy lost within vortices (red) for a period of the polychromatic wave in the second series of experiments

The proportion of kinetic energy contained within vortices was compared for the polychromatic and regular waves in Table 2.4. The table shows the mean total kinetic energy E_{k_T}, the mean kinetic energy within vortices E_{k_ω} and the proportion of total kinetic energy contained within vortices. There was little variation in the proportion of energy within vortices for the regular waves with all results falling between 0.13 and 0.16. The polychromatic wave showed a reduction of approximately 20 to 40% with a result of 0.10. This reduction shows how the repetitive nature of the regular waves do not allow energy within vortices to disperse as it would in the more random polychromatic wave. This may lead to incorrect assumptions being made if testing is only conducted in regular waves.

Table 2.4: Distribution of average kinetic energy both within and outside of vortices for the waves in the second series of experiments

f_i [Hz]	h_i [mm]	$\overline{E_{k_T}}$ $[J/m]$	$\overline{E_{k_\omega}}$ $[J/m]$	$\frac{\overline{E_{k_T}}}{\overline{E_{k_\omega}}}$
Regular Waves				
0.45	75.7	2.34	0.30	0.13
0.50	45.3	1.56	0.21	0.14
0.50	56.0	2.12	0.30	0.14
0.50	78.4	3.51	0.48	0.14
0.55	74.7	3.55	0.57	0.16
0.60	74.7	3.40	0.55	0.16
Polychromatic Wave				
As Specified in Table 2.1		1.13	0.12	0.10

2.4 Conclusions

Polychromatic waves are shown to provide a valuable intermediate step between regular waves and irregular wave spectra for the experimental analysis of wave energy converters. They provide a wave which allows regular wave analysis methodologies to be applied to a wave which was more random and therefore closer to the realistic sea state the device will experience. Phase-averaging was shown to be an effective method for the analysis of polychromatic waves for both PIV and non-PIV data and for this series of experiments showed a similar level of uncertainty to that performed in regular waves.

Although the polychromatic waves used in this study were generated through the superposition of regular waves, the devices response could not be accurately predicted through the superposition of results from individual tests in regular waves. Comparison between the incoming wave power and device output showed energy captured within the device was not dispersed within a single inflow or outflow condition and is retained within the devices various energy stores. As a regular wave only captures a single inflow and outflow condition this effect cannot be captured in regular waves.

Accurate measurement of the water elevation in the chamber is essential to determine the devices power output. It is shown that determination of this water surface elevation using a single wave probe will lead to inaccuracies in the calculation of volume flux through the turbine due to sloshing within the chamber. Over a full wave profile it was

shown that these inaccuracies can be averaged which reduces their impact on power calculations however measuring other properties of the volume flux are likely to result in much larger errors if a single probe is utilised. It is therefore recommended that an array of wave probes be placed within the chamber to ensure that this effect is captured.

An energy balance of an OWC shows that energy contained within vortices cannot be transferred to the PTO and is therefore considered to be indicative of inefficiencies in the design of the underwater geometry. The proportion of kinetic energy contained within vortices for regular and polychromatic waves was compared using phase-averaged PIV velocity fields. Testing in polychromatic waves showed a marked decrease of approximately 20 to 40% in the proportion of energy contained within vortices. The repetitive nature of regular waves does not allow energy within the vortices to be dispersed as is the case with the more random polychromatic wave, giving a misrepresentative result when testing with regular waves.

In the future, the selection of components of the polychromatic wave could be made to simulate a specific sea state by utilising many more frequencies and determining the wave height at each frequency from hindcast data. This would allow the creation of a pseudo-irregular spectrum to test while maintaining the defined period of the polychromatic wave.

When testing and evaluating wave energy devices it is important that the test provides a realistic representation of the conditions the device will experience in its operation. Polychromatic waves have been shown to capture a number of effects that cannot be captured using regular waves while still applying the methodology used for regular waves and should be considered when designing a test program to evaluate the performance of a WEC.

Chapter 3

A PIV investigation of OWC operation in regular, polychromatic and irregular waves

This chapter has been submitted for publication in *Renewable Energy*, and at the time of writing is under review. The citation for the research article is:

Mitchell Ferguson, T., Penesis, I., Macfarlane, G. and Fleming, A. (2015) "A PIV investigation of OWC operation in regular, polychromatic and irregular waves", *Renewable Energy*, [Under Review]

Abstract

Model scale testing plays an essential role in the development and evaluation of wave energy converters (WEC) and is generally performed in either regular or irregular waves. Regular waves provide a simple and repetitive test that focus on discrete wave frequencies whilst irregular waves are a spectrum containing many wave frequencies similar to the realistic sea state a WEC will experience. A less used intermediate wave type between regular and irregular waves is a polychromatic wave which overlaps properties of both. Earlier work has demonstrated that evaluating device performance only in regular waves can be misleading due to significant harmonic effects that are not present in a realistic sea state.

This paper presents methodology for data processing and results from experiments using particle image velocimetry (PIV) to capture the velocity fields in and around a generic forward-facing bent-duct oscillating water column (OWC) in the time domain. Details of processes to synchronise and merge data from multiple runs of an irregular wave spectrum into a single complete run are provided. Two methods for the merging of data are presented for data sources with high and low sampling rates.

An energy balance was used to compare the operation of the OWC in regular, polychromatic and irregular waves. The novel application of normalised histograms revealed numerous differences in the devices operation including the frequency and size of vortices and the amount of kinetic energy present in the various energy stores within the device. It was shown that in the irregular wave there was a linear relationship between the total kinetic energy within the field of interest and the amount of energy contained within vortices. Polychromatic waves successfully represented the power output of the device in irregular waves but more investigation is required to evaluate whether they can represent the impact of vortices on the devices operation. Techniques developed in this paper enable the evaluation of WEC design changes using PIV in the time domain, and therefore irregular waves, giving designers the opportunity to evaluate device performance in a realistic sea state.

3.1 Introduction

Capturing wave energy and the efficient conversion of it to a useful energy source can provide a significant opportunity to diversify our energy supply and reduce reliance on fossil fuels. There are a number of wave energy converter (WEC) designs which have shown this ability, one of which is the oscillating water column (OWC) (Falcão,

2010). To further the development of OWC design and progress towards economic viability further research needs to be undertaken to gather a detailed understanding of the devices operation and to identify opportunities to maximise its efficiency.

The testing of full scale prototypes is both expensive due to construction and installation costs and time consuming, as devices need to be on location for an extended period to gather data in a wide range of conditions. Model scale testing provides an alternative that is significantly cheaper and also allows testing in highly controlled conditions, which provide high quality and repeatable data. The use of scaled models also allows numerous data gathering techniques such as flow visualisation that are impractical to apply at full scale.

Particle image velocimetry (PIV) is an experimental technique which allows the calculation of velocity fields without any interference with the flow itself. PIV is performed by initially seeding the fluid with neutrally buoyant particles, which are subsequently illuminated using a light sheet generated using a high powered laser. Particles follow the movement of the water and a camera is used to capture two images at a small time interval. Images are then subdivided into interrogation windows and the fluid velocity at each of these windows is calculated using cross-correlation (LaVision GmbH, 2010). PIV has been used to analyse a wide range of flow fields involving waves including investigations into ship wake in regular waves (Longo *et al.*, 2007) and investigations into breaking waves (Techet, 2005).

Model scale testing is generally performed in a wave basin or flume where waves are artificially generated. These waves generally fall into one of two major categories; regular (Morris-Thomas *et al.*, 2007; Wang *et al.*, 2002) and irregular (Folley *et al.*, 2010; Gervelas *et al.*, 2011). Regular waves consist of a sinusoidal wave with a single height and frequency and are used to gather data on the device at one very specific condition. Irregular waves consist of a wave spectrum containing a range of heights and frequencies and provide conditions much closer to those a device may experience in real-world conditions. A number of different spectrums have been developed based on hind cast wave data to represent various ocean wave conditions. The JONSWAP spectrum represents wave conditions with a reduced fetch and is commonly used to test wave energy devices (Hasselmann *et al.*, 1973). As an irregular wave does not repeat like regular waves, techniques such as phase averaging cannot be applied to analyse data.

In Chapter 2 it was shown that an intermediate wave type, a polychromatic wave, can offer some properties of both regular and irregular waves. This wave type features multiple frequency components similar to an irregular wave, yet by restricting the

wave to a finite number of components, the wave can have a relatively short repeating interval similar to regular wave. Having a repeating interval of manageable size allows the devices performance to be analysed using well established methods developed for regular waves such as phase averaging. Importantly this wave offers a wave profile with a variety of peak and trough heights which reduces the impact of unrealistic harmonic effects on an OWCs operation.

PIV has previously been successfully used to analyse the operation of OWCs in regular waves (Fleming *et al.*, 2011, 2012b; Graw *et al.*, 2000). These studies adopted phase averaging to analyse velocity fields within and around OWCs. As a method for the analysis of OWC velocity fields Fleming *et al.* (2012a) developed an energy balance. This study used PIV velocity fields to identify and quantify energy sources, stores and sinks that are present during OWC operation. Energy stores within the device included water column heave and slosh, chamber air pressure differential and the generation of vortices. A key finding of the study highlighted that energy contained within vortices was not available to the power take-off (PTO), and therefore was a significant inefficiency in the operation of the device. Thus far this analysis has only been applied to an OWC in regular and polychromatic waves as shown in Chapter 2.

This paper presents and demonstrates a procedure and data processing methodology to obtain the velocity fields of an OWC in irregular waves. The paper explores the difference in OWC operation in regular, polychromatic and irregular waves through the use of components of energy balance is explored, in particular looking at the presence of vortices which occur during the operation of the device. Data is presented using histograms to show the distribution of key results relating to the operation of the OWC. To the authors knowledge, this is the first study to apply PIV to the study of any type of WEC in irregular waves.

3.2 Methodology

3.2.1 Experimental Setup

Experiments were performed in the Australian Maritime Colleges Towing Tank. This facility has a length of 100 m, width of 3.5 m and depth of 1.5 m and a single hydraulically powered paddle-type wave maker (Australian Maritime College, 2015). A sloped beach at the end of the tank reduced reflections.

A 1:30 scale model of a generic forward facing bent duct OWC with constant cross section (shown in Figure 3.1) was positioned centrally within the tank and secured

rigidly to the carriage above with the chamber opening directly facing the wave maker in the head seas condition. The model was constructed of 6 mm clear acrylic and had an internal width of 506 mm. The draught of the device allowed a distance of 1060 mm between the lower lip and the bottom of the tank. An orifice with diameter of 50.8 mm simulated the PTO and was located centrally in the roof of the chamber. The orifice size was selected to give the device the desired damped natural frequency of approximately 0.55 Hz (10 second period at full scale). This damping method was selected due to both its simplicity and ability to represent the non-linear pressure-flow relationship of an impulse turbine (Folley *et al.*, 2002).

Water elevation was measured using an array of twin-wire capacitance type wave probes placed both within and in front of the device in the same configuration shown in Chapter 2. The incoming wave elevation was measured using an additional wave probe, the incident wave probe, located adjacent to the front of the chamber and offset approximately 300 mm from the side of the tank and 450 mm from the centreline of the OWC. This distance was considered sufficient to minimise the impact of the OWC on the measured incident waves.

The air pressure differential within the chamber was measured using two Endevco Model 8510B-2 pressure transducers, with the signal conditioned using an Endevco 136 Voltage amplifier. These were placed at the top of the chamber approximately halfway between the orifice and the sidewalls on either side of the device. Data from the wave probes and pressure transducers was captured using a National Instruments PCI-6254-M DAQ card at a rate of 500 Hz.

In Chapter 4, 2D PIV is used to capture velocity fields within the same OWC geometry and it is shown that the majority of the flow occurs in the longitudinal plane. A similar approach was adopted for the present study where underwater optics were used in conjunction with a 120 mJ Nd-Yag laser to project a light sheet in a longitudinal plane along the centreline of the model (Figure 3.2). The water in the vicinity of the device was seeded with neutrally buoyant fluorescing particles of between 36 and 75 μm diameter. A single sCMOS camera (2560 x 2150 pixels) captured image pairs at a rate of 15 Hz with an inter-frame time of 10 ms from outside of the tank and perpendicular to the light sheet. Three fields of view were required to capture the full field of interest with the required resolution, lighting and without excessive obstruction of the field by the model (Figure 3.1).

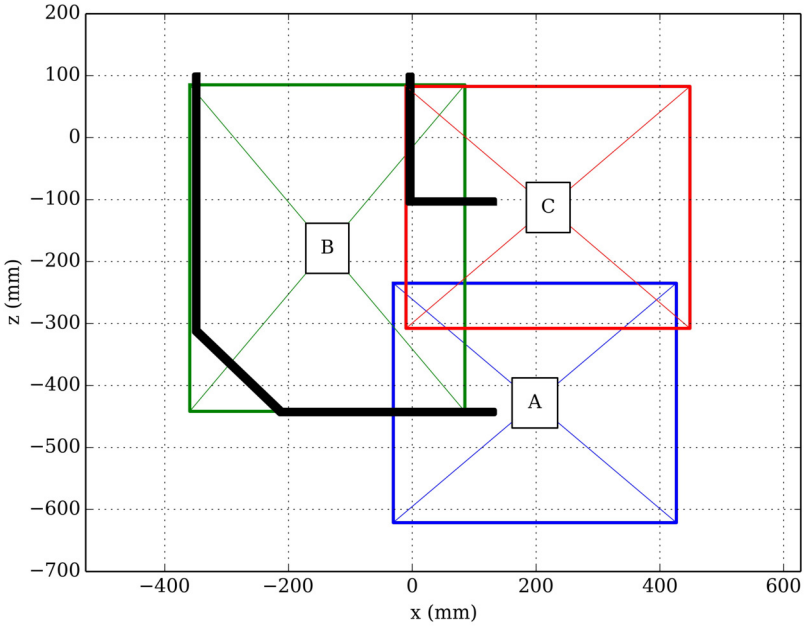

Figure 3.1: Cross section of the forward facing bent duct OWC (black) used in the experiments and the three fields of view captured using the PIV equipment (A, B, C)

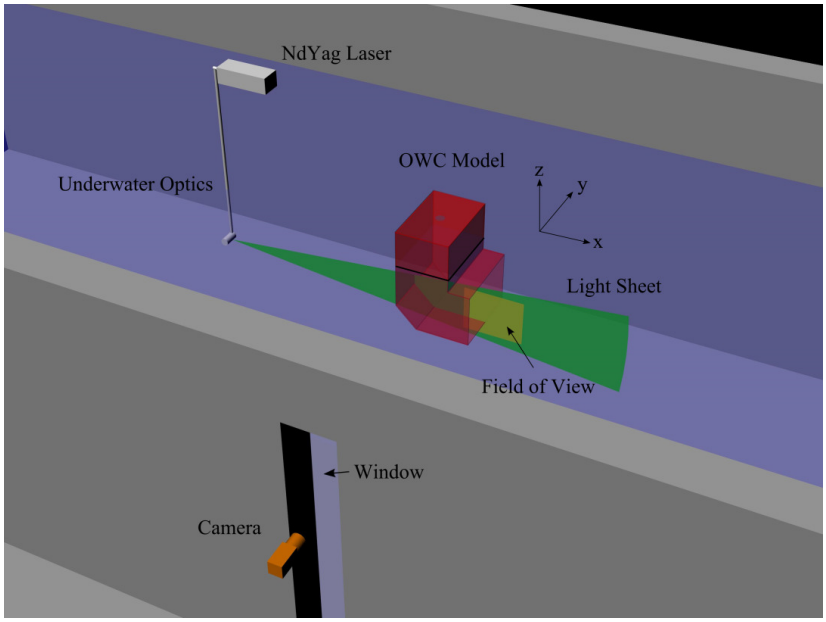

Figure 3.2: Setup of the PIV capture equipment used in the experiments

LaVision GmbH software package DaVis 8 (LaVision GmbH, 2010) was used to capture, analyse and process images and create velocity fields. Images were masked above the waterline using the method described by Fleming *et al.* (2012b) and in areas where the device intersected with the field to avoid the creation of vectors in locations without water. Vector processing was performed using cross-correlation using a multi-pass method.

3.2.2 Wave Types

Experiments were performed using a series of regular waves, a polychromatic wave and an irregular wave spectrum. Regular wave heights and frequencies were selected to provide a representative sample of waves which the device is expected to experience in operation. The polychromatic wave utilised three component frequencies with an even distribution in height. Polychromatic waves can be generated by superimposing regular waves of different frequencies which will result in a wave profile with a variety of peak and trough heights as shown in Figure 3.3. Providing the frequencies selected are compatible the polychromatic wave will have a relatively short period. More information on the use of polychromatic waves can be found in Chapter 2.

Waves were measured at the device using the incident wave probe and their heights and frequencies were calculated by fitting a series of sinusoidal functions to the phase averaged wave profile (Jones *et al.*, 2001-). The method finds the variables in Equation 3.1:

$$\sum_{i=0}^{n} \frac{h_i}{2} \cos 2\pi f_i t + \phi_i \tag{3.1}$$

where n is the number of wave components, h_i is the component height, f_i is the component frequency and ϕ_i is the component phase to find the constants (f,h,ϕ) shown in Table 3.1 and 3.2. Each regular and polychromatic wave run was limited to a length of 60 seconds to avoid reflections from the beach. Runs for each field of view investigated were repeated. The profile of the polychromatic wave is shown in Figure 3.3.

Table 3.1: Heights and frequencies of the components of the polychromatic wave

Desired Frequency [Hz]	Desired Height [mm]	f_i [Hz]	h_i [mm]
0.45	75	0.45	75.7
0.50	45	0.50	45.3
0.50	55	0.50	56.0
0.50	75	0.60	78.4
0.55	75	0.55	74.7
0.60	75	0.60	74.7

Table 3.2: Heights and frequencies of the components of the polychromatic wave

n_i	Desired Frequency [Hz]	Desired Height [mm]	f_i [Hz]	h_i [mm]	ϕ_i [rads]
0	0.45	23	0.45	19	0.08
1	0.50	23	0.50	24	-0.51
2	0.50	23	0.60	23	0.44

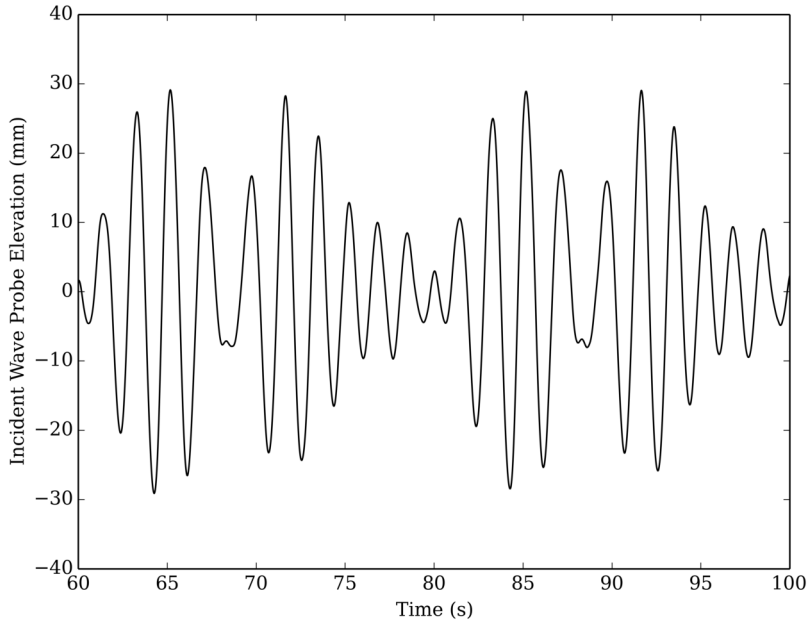

Figure 3.3: Wave profile for two repeating periods of the polychromatic wave, highlighting the variation in peak and trough heights

The irregular wave adopted for this investigation was based on a JONSWAP spectrum with a significant wave height of 70 mm and modal frequency of 0.50 Hz. To successfully integrate the different fields of view (Figure 3.1) into a single velocity field, the wave was generated from the same seed, meaning the wave maker generated the same wave profile for each recorded run. The smoothed spectrum for the measured wave can be seen in Figure 3.4.

The available equipment limited the total number of image pairs captured in each run to 1900, or approximately 125 seconds. Therefore for each of the three fields of view images were captured using three recording periods (Figure 3.5), allowing for a small overlap between each period ensuring a continuous length of approximately 345 seconds or 31.5 minutes at full scale using Froude scaling. Non-PIV data was recorded for the full length of every run.

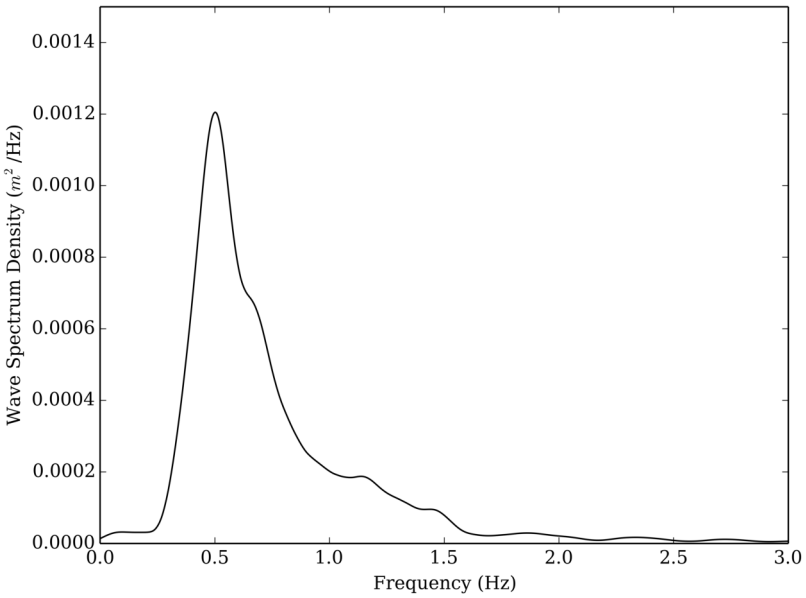

Figure 3.4: Spectral density of the irregular wave

3.2.3 Data Processing

To assess the devices performance it was required to integrate data from each individual run into a single continuous set of data.

Time synchronisation is the process of expressing data recorded for each run in terms of a common time. To determine the relationship between the recorded time for each run and the common time for all runs a single temporal shift is applied to all data for the individual run. The size of this shift is determined using the elevation data from the incident wave probe. Using a single run as a base, each run is compared with the base and the optimal shift is determined using a Nelder-Mead simplex minimisation algorithm (Jones *et al.*, 2001-) to find the shift which results in the smallest average difference in wave elevation between the base and the shifted run (Figure 3.6). This method limits the resolution of the shift to a half of single data point, or a resolution of 0.001 s for the 500 Hz sampling rate adopted here.

Once all runs were synchronised wave probe and pressure transducer data was averaged to generate a single common set of data for the full data length. To reduce the effect of the base selection the process is repeated using the newly calculated elevation as the base. The resulting elevation for the irregular wave is shown in Figure 3.5. An uncertainty analysis combining the uncertainty in measurement and the averaging method was performed. The results are summarised in Table 3.3 with a 95% confidence interval.

Table 3.3: Mean uncertainty of wave probe and pressure transducer data with a 95% confidence interval

Data Source	Uncertainty	Units
Incident WP	1.8	mm
WP 1	2.7	mm
WP 2	2.4	mm
WP 3	2.8	mm
WP 4	2.4	mm
WP 5	2.6	mm
WP 6	4.1	mm
WP 7	3.3	mm
WP 8	2.8	mm
WP 9	3.0	mm
Pressure 1	7	Pa
Pressure 2	11	Pa

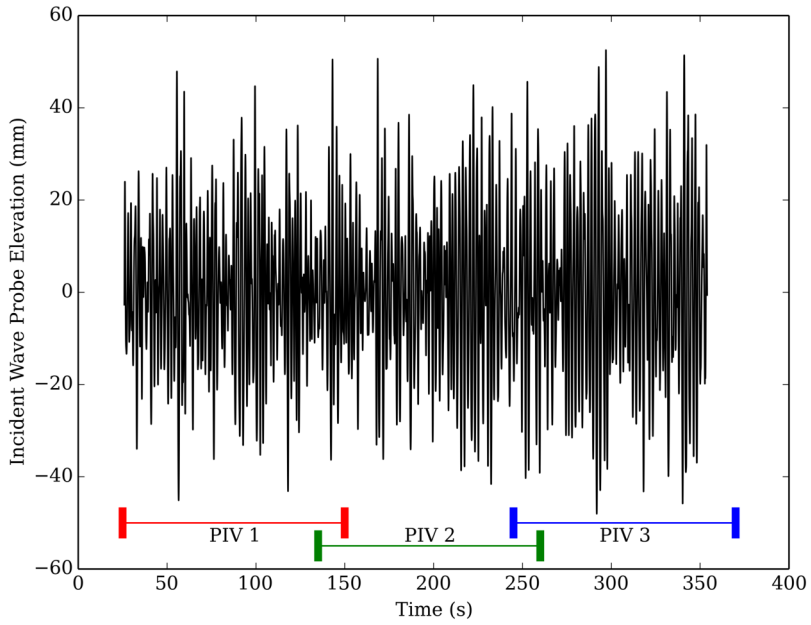

Figure 3.5: The resulting wave elevation for the irregular wave and the three PIV recording periods

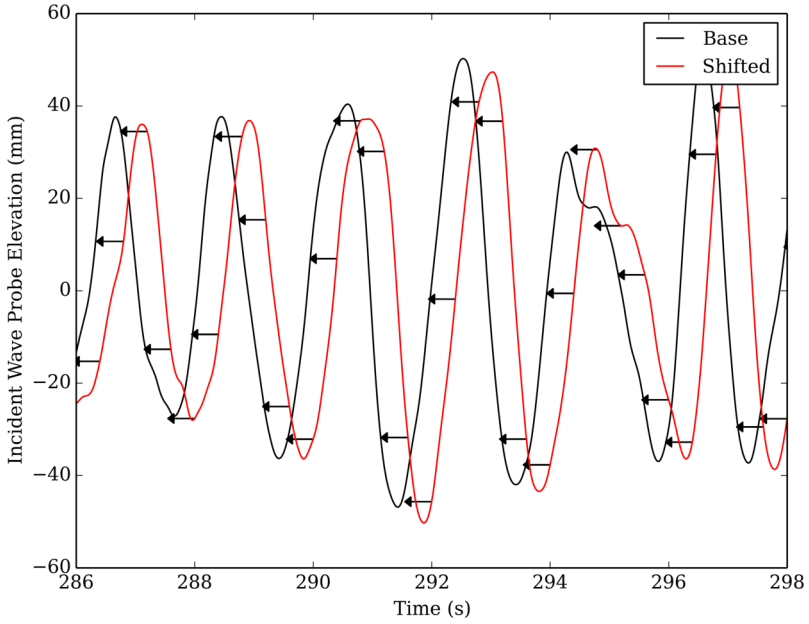

Figure 3.6: Wave elevation for two runs with the irregular wave prior to synchronisation, arrows indicate the temporal shift of 0.45 seconds to be applied

Velocity fields present additional challenges as the data has both temporal and spatial properties. To average this data, velocity fields with different starting times and fields of view have to be combined. Initially it is required to express all the velocities gathered on a common time frame. The lower sampling rate of the velocity fields generated by PIV means that the averaging methodology must be modified to account for the extra time between data points meaning two points may not be sufficiently similar for direct averaging to be applied.

The first stage for synchronising differing runs into a common time frame using the incident wave probe elevation remains the same as that used for wave probe and pressure transducers. Once the data is expressed in a common timeframe the velocity field data is processed using a pixel by pixel approach. The x and z components of the velocity were processed independently.

To account for the lower sampling rate a spline was fitted to the velocity component data for each run using Scipys splprep function to fit a third order B-spline using a smoothing value of 5 x 10^{-5} (Jones *et al.*, 2001-) (each data point was weighted evenly). This setup was sufficient for the vast majority of splines created however in some rare cases where fitting to regions with few continuous data points the smoothing value was increased or a linear spline was used.

As the free surface was present within some fields of view, some pixels analysed have periods where there is no fluid and therefore no velocity. To represent this, the spline

was only generated where the time between two recorded velocities exceeded 0.0667 seconds (time between two data points with a 15 Hz sampling rate).

Each run was processed independently. An attempt to simultaneously fit the spline to data from multiple runs proved unsuccessful because in some cases this created large oscillations in the spline, usually when two data points with differing magnitudes were recorded at a similar time after the temporal shift. The fitted spline was subsequently evaluated for all experimental runs at common times at a sampling rate of 20 Hz (Figure 3.7).

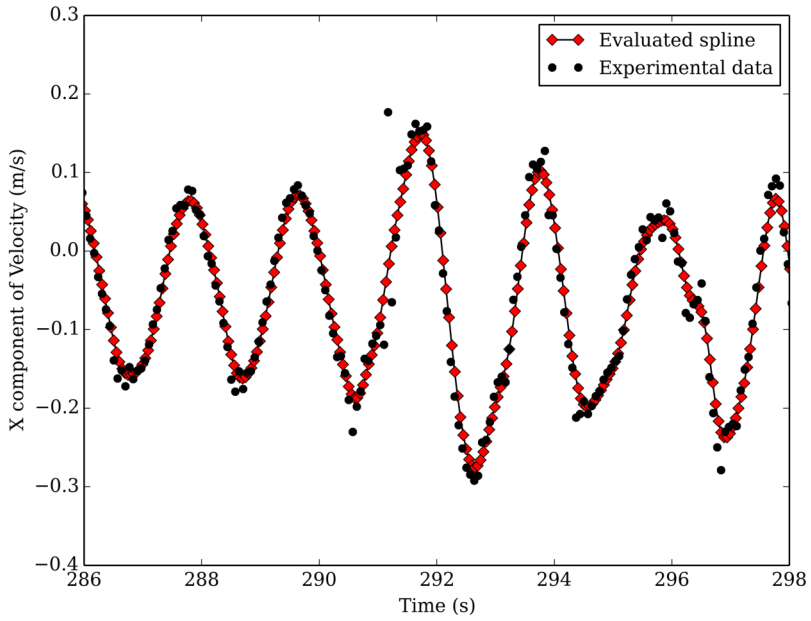

Figure 3.7: Experimental velocity field data from a single run and the evaluated spline fitted for a single run

Once all velocity fields were evaluated at a common time each run was merged using the velocity field mosaic procedure outlined by Fleming *et al.* (2012b). This method uses interpolation to merge velocity fields with differing fields of view by resizing and merging fields using a weighted average. Merges were performed temporally where there was a common field of view and spatially for differing fields of view.

Due to computer memory limitations runs were merged in the following order using the velocity fields developed in the previous step in subsequent merge:

1. Runs with a common starting time and common field of view (temporal merge)
2. Runs with a common field of view (temporal merge)
3. All runs (temporal and spatial merge)

This process results in velocity fields covering the entire field of interest for the full recorded duration resampled at a rate of 20 Hz. This procedure was applied to the regular, polychromatic and irregular waves. The duration of regular and polychromatic wave data was investigated and limited to ensure the data set finished at an integer number of periods to avoid biasing results.

3.3 Calculations

The power consumed by the orifice plate (simulated PTO, P_{PTO}) is calculated using the product of pressure differential and the volumetric flow rate as shown in Equation 3.2:

$$\begin{aligned} \nabla &= \frac{dH_{chamber}}{dt} \times l \\ P_{PTO} &= \Delta p \times \nabla \end{aligned} \tag{3.2}$$

where P_{PTO} is the PTO output per unit width, Δp is the pressure differential between the chamber and the atmosphere, l is the chamber length, ∇ is the volumetric flow rate and $H_{chamber}$ is the mean water elevation within the chamber. The air is considered to be incompressible.

The total kinetic energy (E_{k_T}) contained within a two-dimensional velocity field per unit width is shown in Equation 3.3:

$$E_{k_T} = \frac{1}{2}\rho_w dx dz \sum_{x,z} V^2_{(x,z)} \tag{3.3}$$

where E_{k_T} is the total kinetic energy within the velocity field per unit width, ρ_W is the water density, dx is the pixel width, dz is the pixel height and $V_{(x,z)}$ is the velocity vector (Graw *et al.*, 2000). This method assumes the velocity in the y direction is zero.

The two-dimensional vorticity is calculated from the velocity fields using Equation 3.4:

$$\vec{\omega} = \frac{1}{2}\left(\frac{\partial v}{\partial x} - \frac{\partial u}{\partial z}\right) \tag{3.4}$$

where dv/dx and du/dz are the strains calculated from the velocity field (Graw *et al.*, 2000).

3.4 Results and Discussion

All results presented in this section have been calculated from data prepared using the methods described in Section 2.2: Data Processing.

Figure 3.8 gives an example of the merged velocity field produced during inflow from an experiment in irregular waves. The major features present in the velocity field show little difference to those for an OWC in regular waves (Fleming *et al.*, 2011). As with most OWCs (Graw *et al.*, 2000), this model produces large vortices where sharp changes occur in the geometry, in this case at the lower lip and the front wall of the chamber and a constant flow through the chamber. Whilst testing in regular waves can identify these phenomena, quantifying the magnitude of their effect on the device in a realistic sea state is difficult due to the presence of harmonic effects related to the repetitive flows found in regular waves. Hence, testing in irregular waves gives a more accurate assessment of their impact upon the device in a realistic sea state.

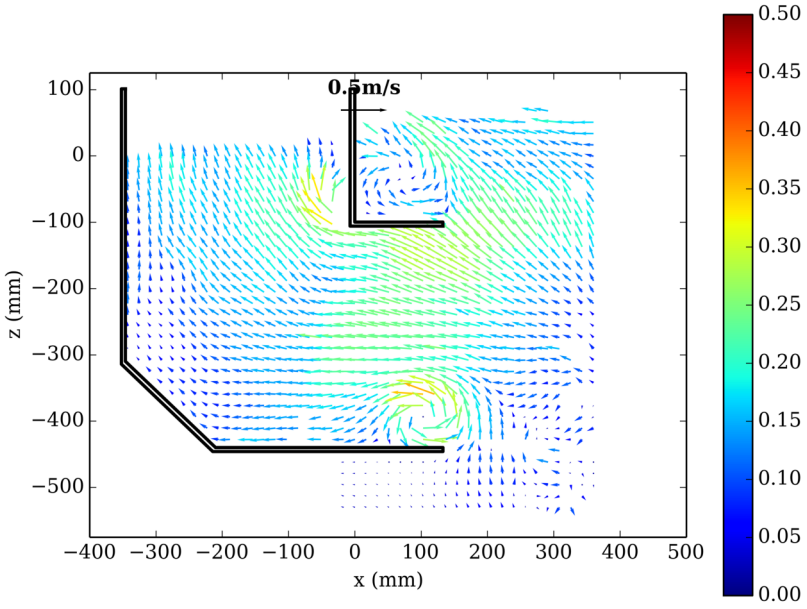

Figure 3.8: Example of a velocity field for the irregular wave

To verify the methodology used the uncertainty of the velocity field was calculated. The uncertainty comprises two components; the uncertainty in the velocity measurement and uncertainty in fitting the spline which can also be attributed to flow repeatability. Higher uncertainty is expected in regions where there are higher velocities, poor quality vectors, or turbulence. The uncertainty in the spline fitting was determined by finding the error between the calculated velocity using the spline fitting method and the measured velocity from PIV.

The uncertainty for the velocity field is shown in Figure 3.9 and reflects this as higher uncertainty is experienced in regions at which vortices occur and near the free surface. There is also a region of high uncertainty extending forward from the bottom lip of the chamber where poor lighting, and subsequently poor quality vectors were produced due to blockage of the light sheet by the model (at z ≈ -450 mm). While high uncertainty is present in the region above the top lip, this region has little impact on the devices performance and can be tolerated. An uncertainty analysis was performed using the procedure outlined by the International Towing Tank Conferences Recommended Procedures and Guidelines (ITTC, 2009). The average uncertainty with a 95% confidence interval for the velocity field of the irregular wave was 0.037 m/s.

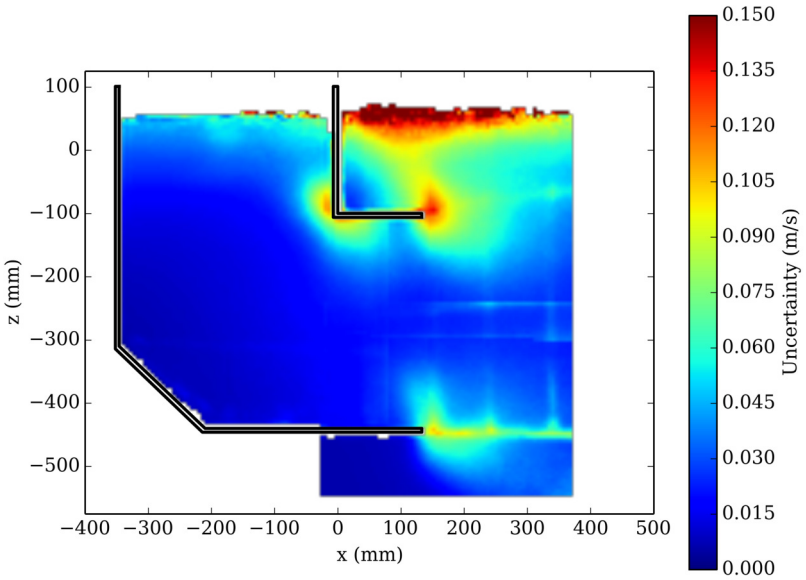

Figure 3.9: Average uncertainty in the velocity field for the irregular wave

To compare the OWC devices operation in differing wave types histograms have been used. Histograms give a graphical representation of the distribution of the data gathered from the time-domain analysis and are created by dividing the magnitude of signal into a number of equally spaced bins. If a value is present more often the histogram will represent this with a greater value. To compare data from signals of differing lengths histograms can be normalised to make the area under the bins equal to one using Matplotlibs *pyplot.hist* algorithm (Hunter, 2007). This means that the height of each bin is independent of both the number of bins used and the length of the sample. This paper compares the polychromatic and irregular waves to a regular wave with a height of 45 mm and frequency of 0.50 Hz as it has closest mean power to the polychromatic and irregular waves. While the magnitude of the signals from different regular waves varied the trends in the distribution remained the same.

Fundamental to the analysis of OWCs is the power generated by the device. The power consumed by the orifice (modelling the PTO) is calculated using a combination of the air pressure differential between the chamber and atmosphere (Figure 3.10) and the flow rate through the orifice (Figure 3.11).

The distribution of pressure within the OWC chamber for the regular wave is presented in Figure 3.10(a) where it can be seen that three peaks occur at; zero, maximum ($\approx$ 120 Pa) and minimum pressure ($\approx$ -160 Pa). These peaks are generated at times when the pressure differential is transitioning between growing and shrinking, or vice versa. The magnitude of negative pressure is greater than that for positive pressure but the device spends a similar proportion of time between positive and negative pressure, this phenomenon was found to be common for all of the regular wave heights and frequencies investigated. The pressure distribution for the irregular wave (Figure 3.10(c)) differs as it only contains a single peak at zero pressure differential; however it also shows an increase in pressure during periods of negative pressure differential. In the irregular wave the peak pressure occurs at a range of different values and therefore the distribution shows a smoothed tapered profile. The polychromatic wave (Figure 3.10(b)) shows a similar distribution to the irregular wave with a peak at zero pressure and a tapering profile. As the polychromatic wave has a repeating wave profile the distribution is not as smooth as the irregular wave.

The other component required to calculate the devices power output is the flow rate through the orifice. Flow was calculated assuming incompressibility using data gathered by wave probes to estimate the average free surface elevation within the chamber and is represented by the histograms in Figure 3.11. The distribution of flow rate for regular waves (Figure 3.11(a)) has many properties similar to that of the air pressure such as the peaks at the maximum and minimum value, however there is no peak at zero flow. As expected, the flow for the irregular wave (Figure 3.11(c)) has a much smoother distribution yet a similar range. An even distribution occurs between -0.03 $m^3/s/m$ and 0.03 $m^3/s/m$, this is likely due to the slow depletion of energy stored within the water column within the chamber during periods of little wave power. This effect is not present in regular waves as there are no significant periods with little instantaneous wave power. The distribution for the polychromatic wave (Figure 3.11(b)) is again similar to that of the irregular wave and does not have the peaks at the maximum and minimum values that are present in the regular wave distribution. Once again the profile is not as smooth as the irregular wave due to the repeating wave profile.

The resulting power from the regular wave (Figure 3.12(a)) has a relatively flat distribution which is due to the constant change in chamber elevation that occurs in a

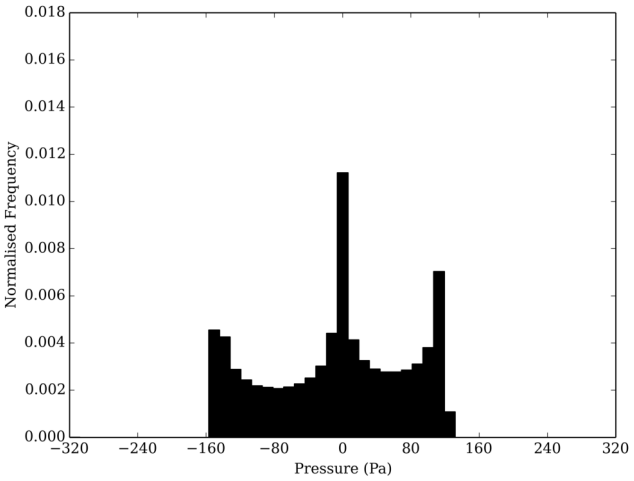

(a)

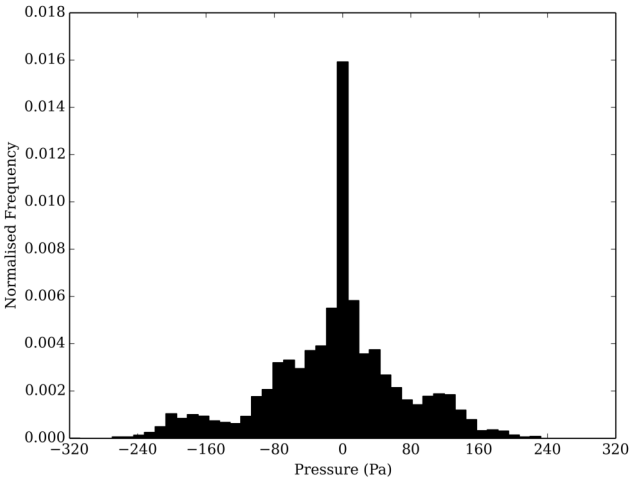

(b)

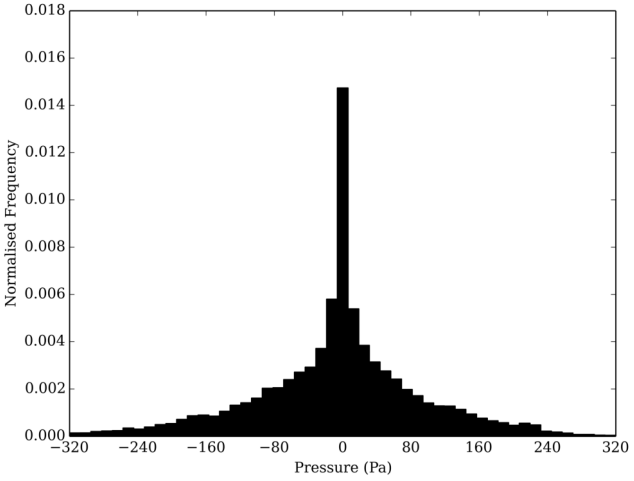

(c)

Figure 3.10: Normalised histograms for the pressure differential between the chamber and atmosphere for (a) a regular wave with a height of 45.3 mm and frequency of 0.50 Hz, (b) the polychromatic wave and (c) the irregular wave

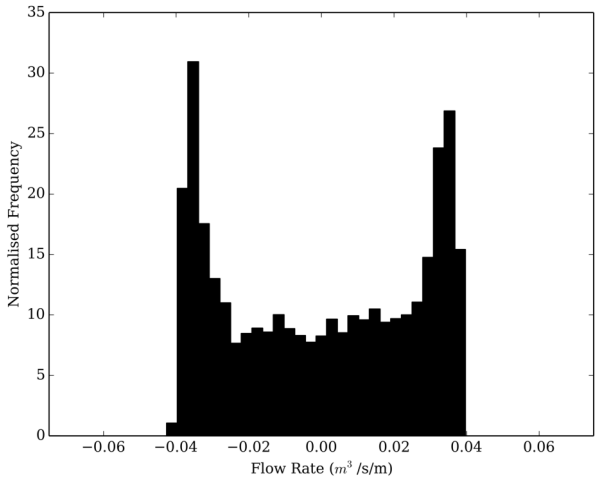

(a)

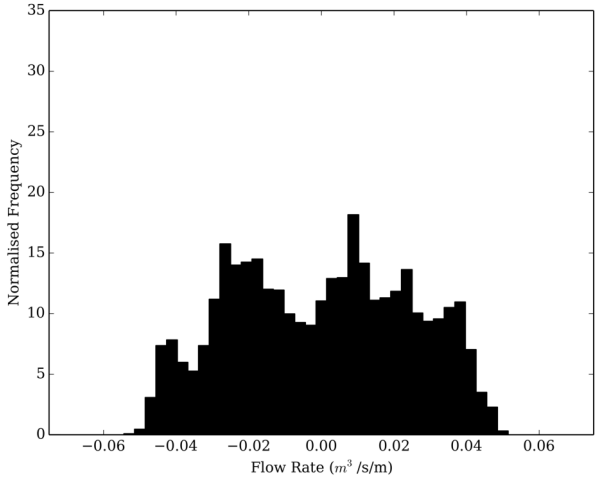

(b)

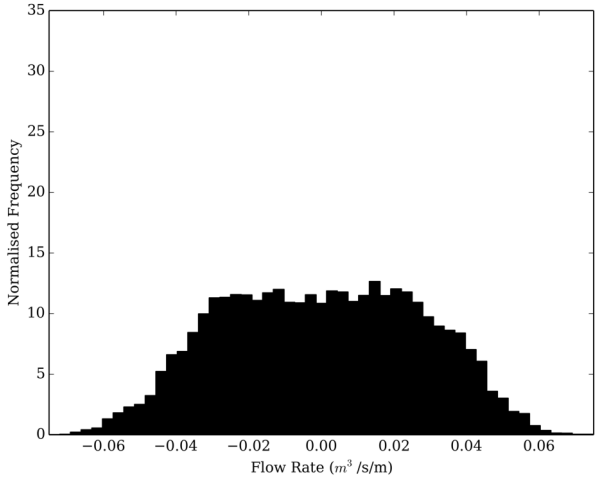

(c)

Figure 3.11: Normalised histograms of the orifice flow rate for (a) a regular wave with a height of 45.3 mm and frequency of 0.50 Hz, (b) the polychromatic wave and (c) the irregular wave

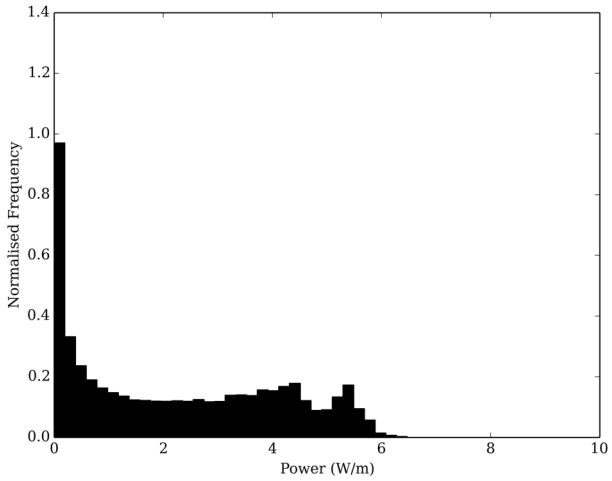

(a)

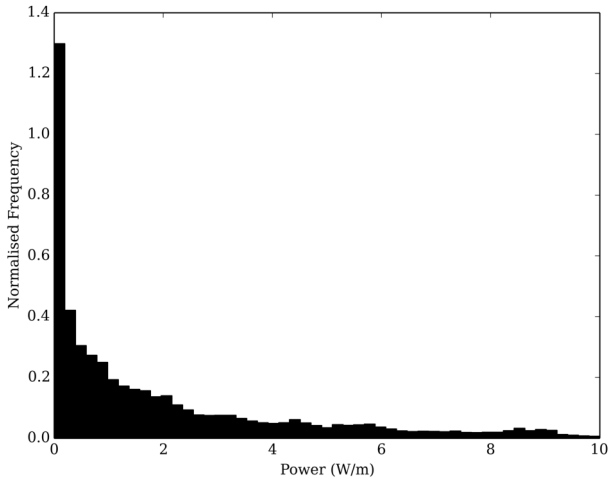

(b)

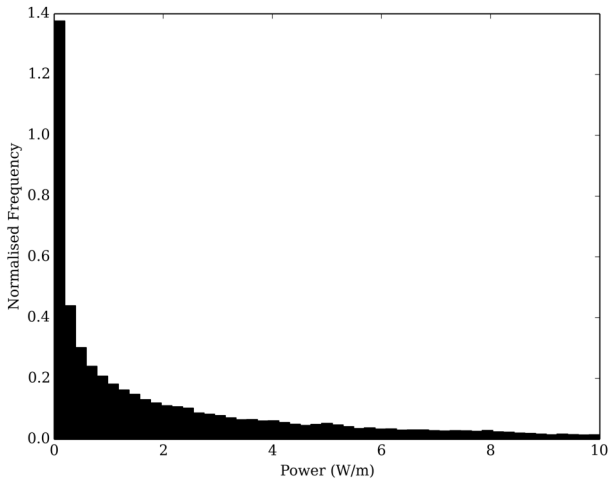

(c)

Figure 3.12: Normalised histograms of the power dissipated by the orifice for (a) a regular wave with a height of 45.3 mm and frequency of 0.50 Hz, (b) the polychromatic wave and (c) the irregular wave

regular wave. Two bumps in the distribution are present near the maximum power generated and correspond with the peak power output during for the inflow ($\approx$ 4.5 W/m) and outflow ($\approx$ 5.5 W/m). The large peak at zero power occurs at the transition between inflow and outflow when there is zero air flow through the orifice. The distribution for the irregular wave (Figure 3.12(c)) also has a peak at zero and shows a rapid reduction for higher powers and also has a much greater range than that of the regular waves. In the polychromatic wave (Figure 3.12(b)) the power has a very similar distribution to that of the irregular wave. This suggests that a polychromatic wave can give better representation into how the device will respond in realistic seas.

An important factor when evaluating a WEC design is the devices capture width or efficiency. Table 3.3 gives the mean wave power ($\overline{EF}$), mean PTO output ($\overline{P_{PTO}}$) and capture width ($\overline{P_{PTO}}/\overline{EF}$) for the three wave types investigated. Wave frequency has a major effect on capture width, as can be seen from the various regular wave frequencies investigated; however wave height also has an impact as evidenced by the capture width reducing as wave height increases with a constant frequency of 0.50 Hz. This is likely due to the increase in non-linear effects such as vortex creation. The irregular wave has a significant wave height of 70 mm and modal frequency of 0.50 Hz and has an average power that sits between that of the 45.3 and 56.0 mm regular waves of the same frequency. Accordingly the capture width also fits between that of these two regular waves, indicating that while the device may have a different operation in regular waves, when comparing the overall efficiency the average response may be the same.

Table 3.4: Energy Flux, PTO output and capture width for the three wave types

f_i [Hz]	h_i [mm]	$\overline{EF}$ $[W/m]$	$\overline{P_{PTO}}$ $[W/m]$	$\frac{\overline{P_{PTO}}}{\overline{EF}}$
Regular Waves				
0.45	75.7	12.19	3.56	0.29
0.50	45.3	3.57	2.16	0.61
0.50	56.0	6.00	3.39	0.57
0.50	78.4	11.76	6.39	0.54
0.55	74.7	9.71	7.23	0.74
0.60	74.7	8.90	7.34	0.82
Polychromatic		2.71	1.87	0.69
Irregular		4.39	2.62	0.59

The energy balance developed for an OWC by Fleming *et al.* (2012a) provides details of various energy stores and sinks that are present during the operation of an OWC. A number of processes are represented in the total kinetic energy within the field of interest including bulk flow, vortices and slosh (Fleming *et al.*, 2012a).

For the regular waves (Figure 3.13(a)) the total energy varies over a narrow band between 0.6 and 2.25 J/m and has two defined regions. The region between 1.5 and 2.25 J/m consists of only outflow, while the region between 0.6 and 1.5 J/m represents periods of both inflow and outflow. Importantly during the regular wave there is always kinetic energy present within the field of interest.

In comparison, the distribution for the irregular wave (Figure 3.13(c)) has a smoother profile with a much wider range of values than the regular wave. Despite the irregular wave having a high average wave power the modal kinetic energy occurs at approximately 0.7 J/m, close to the minimum observed in the regular wave. This is likely to be caused by the distribution of energy from the wave, as the regular wave provides consistent power to the device, whilst the irregular wave has long periods of low power offset by small periods of large power. The distribution for the polychromatic wave (Figure 3.13(b)) is similar to that of the irregular wave but fails to show periods where the total kinetic energy exceeds 3.25 J/m. This indicates that while the polychromatic wave can represent a standard set of conditions it cannot capture extreme events within its relatively short period.

One finding from the energy balance performed is that energy contained within vortices is no longer available to the PTO and is therefore indicative of inefficiency in the design of the underwater geometry. In this case we consider flow to be within a vortex when the vorticity is greater than 4 rad/s. In the regular wave (Figure 3.14(a)) there is always energy contained within a vortex which remains relatively stable with a majority of the distribution between 0.1 and 0.2 J/m. This suggests that in the highly repetitive regular waves energy contained within vortices does not leave the system and instead continues to impact the device. While this could indicate simultaneous creation and dissipation of vortices this is unlikely due to the cyclical inflow and outflow conditions meaning that vortex creation would occur during periods of low flow velocities.

In contrast, for the irregular wave (Figure 3.14(c)) the energy within the vortices peaks close to zero and shows a much smoother profile. Based on this, testing in regular waves will misrepresent the size and frequency of vortices occurring during the devices operation, thus potentially providing misleading results on the efficiency of the device. In this case the polychromatic wave (Figure 3.14(b)) varies significantly from both regular and irregular waves as it experiences a peak at zero, indicating there is

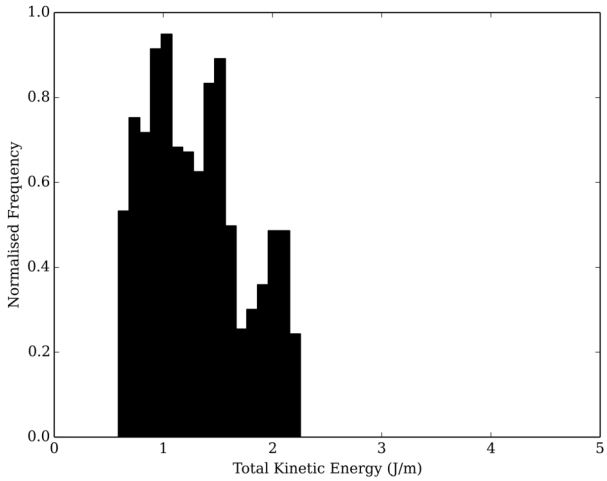

(a)

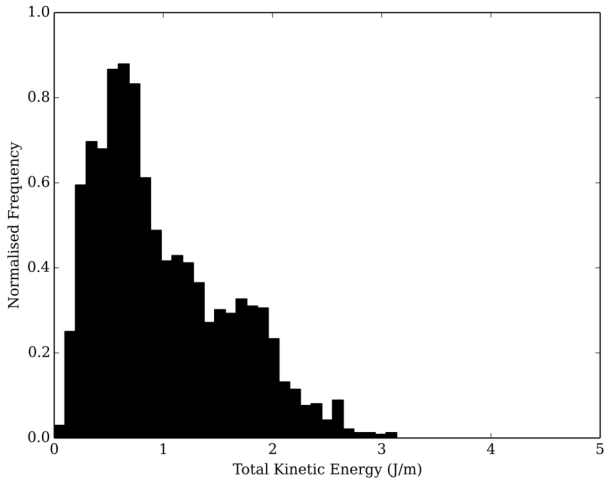

(b)

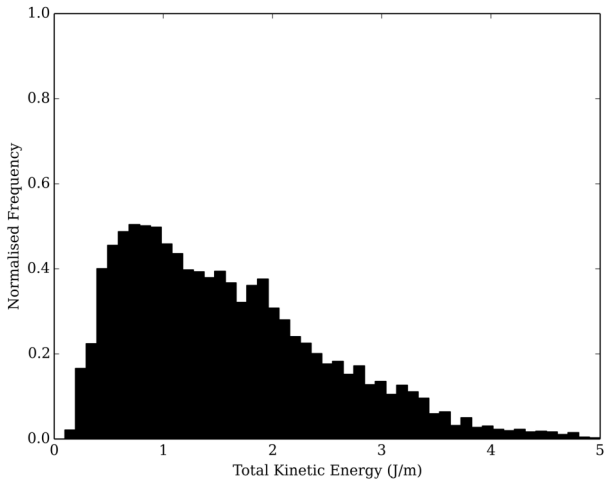

(c)

Figure 3.13: Normalised histograms of the total kinetic energy contained within the field of interest for (a) a regular wave with a height of 45.3 mm and frequency of 0.50 Hz, (b) the polychromatic wave and (c) the irregular wave

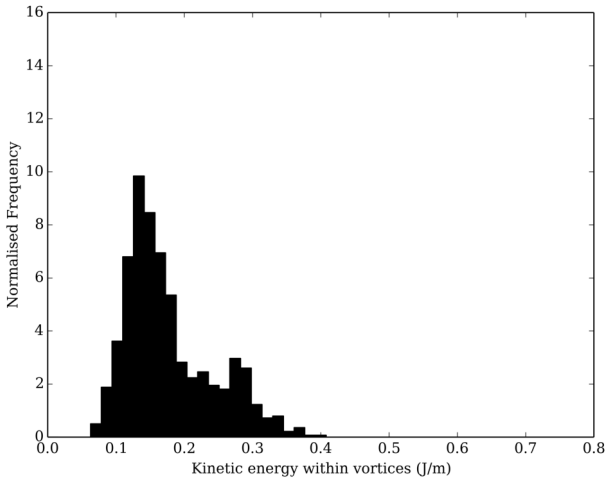

(a)

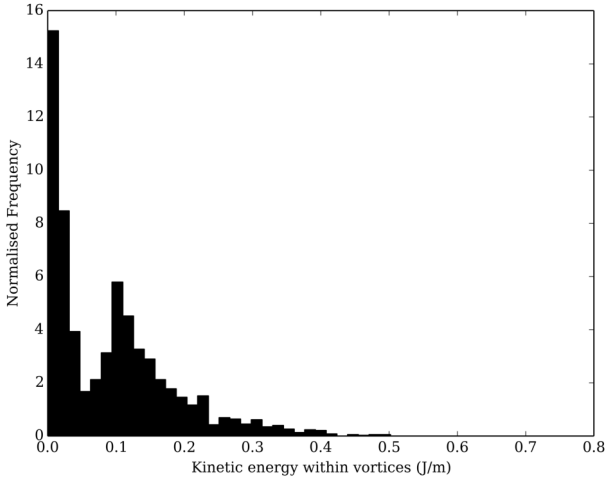

(b)

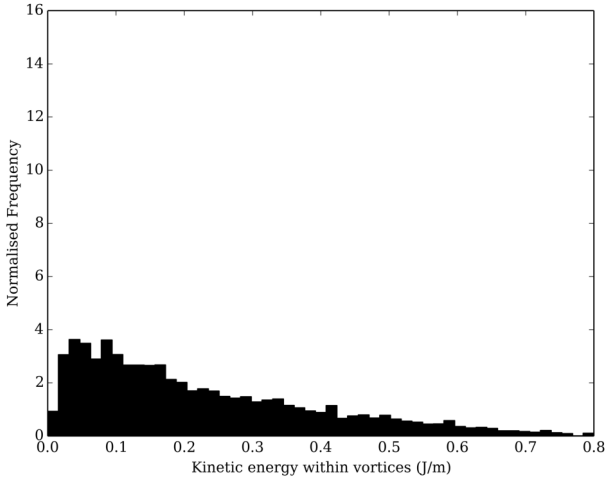

(c)

Figure 3.14: Normalised histograms of the total kinetic energy contained within vortices within the field of interest for (a) a regular wave with a height of 45.3 mm and frequency of 0.50 Hz, (b) the polychromatic wave and (c) the irregular wave

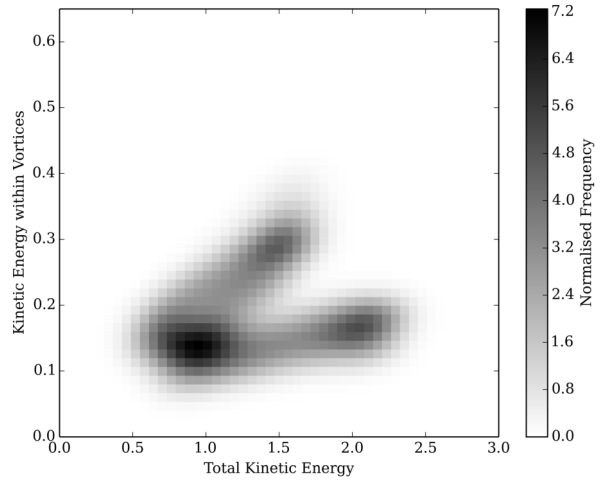

(a)

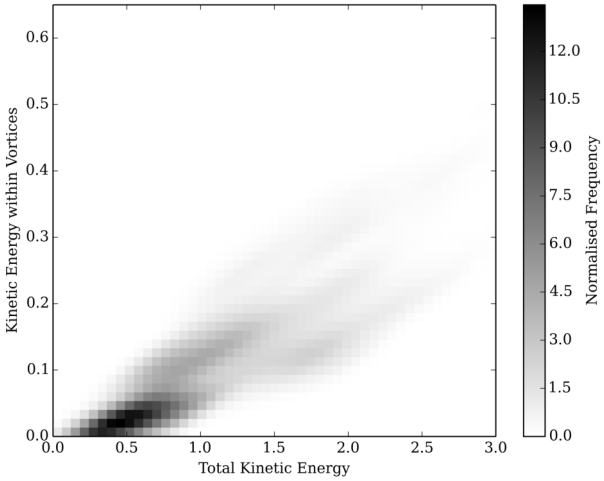

(b)

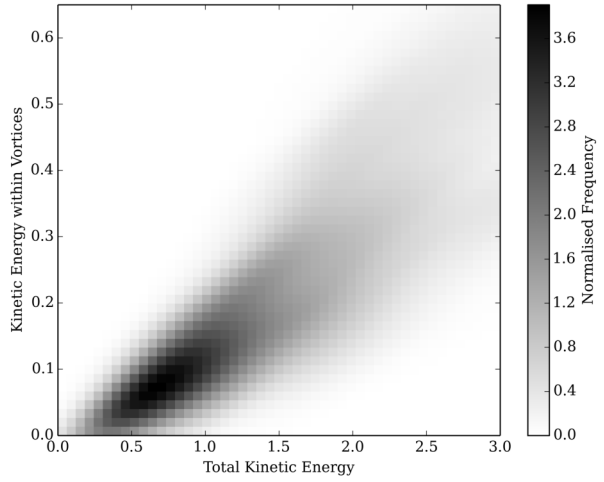

(c)

Figure 3.15: Smoothed, normalised two dimensional histograms showing the relationship between the total amount of kinetic energy and the amount of kinetic energy contained within vortices for (a) a regular wave with a height of 45.3 mm and frequency of 0.50 Hz, (b) the polychromatic wave and (c) the irregular wave

a large amount of time where there is a negligible amount of energy lost to vortices. This effect is likely due to a period in the polychromatic wave where there is only a small amount of energy entering the system from the waves.

To further investigate this, the 2D histograms provided in Figure 3.15 compare the total kinetic energy contained within vortices (for the field of view investigated). In the regular wave (Figure 3.15(a)) two distinct branches can be seen, corresponding to the inflow (top) and outflow (bottom) conditions. It can be seen that more energy is contained within vortices during inflow. This is due to vortex transport as the major vortex formed at the lower lip during inflow is ejected from the field of interest at the start of the outflow condition. It can also be seen that there is greater kinetic energy in outflow condition than the inflow condition. In contrast, the irregular wave (Figure 3.15(c)) does not distinguish between the inflow and outflow conditions and instead shows a linear relationship between the amount of kinetic energy within vortices and the total kinetic energy. Interestingly the linear relationship does not originate from the origin indicating that significant vortices require a certain level of energy within the system before they form which leads to non-linearity in the devices response. Alternatively the relationship may be quadratic which may link to Morison's equation, further investigations with a wider range of irregular waves and geometries should be used to further investigate this effect.

The polychromatic wave (Figure 3.15(b)) has two main features; the first is an area of high frequency between total kinetic energy of 0 and 1 J/m. This feature is similar to the irregular wave in its distribution however it is flatter indicating more kinetic energy is required to generate vortices in the polychromatic wave. This is likely to correspond to the period in which there is little power being delivered by the wave. The second feature is the multiple branches, each of these will correspond to a distinct inflow or outflow condition during the polychromatic wave profile. These distinct branches occur due to the more repetitive nature of the polychromatic wave compared to the irregular wave.

In future use of polychromatic waves, it may be more practical to use more than three frequency components whilst maintaining the finite period and give each component a height corresponding with the energy within a relevant irregular wave spectrum. This should allow a better comparison between irregular and polychromatic waves to be performed.

3.5 Conclusions

A novel series of physical experiments have been performed to investigate the operation of an OWC type wave energy device in three very different types of waves by quantifying the fluid flow within the devices chamber using PIV. The wave conditions include; a series of regular sinusoidal waves covering a range of wave heights and frequencies; a polychromatic wave consisting of three wave frequencies that create a defined repeating interval, and; a standard irregular wave spectra. Providing steps are taken to ensure that the wave profile for each wave type remains consistent, synchronisation of data gathered from multiple experimental runs can be performed using temporal shift. The magnitude of this shift can be determined using an algorithm to minimise the average difference in wave elevation at the incident wave probe.

For data sources with a high sampling rate, such as wave probes and pressure transducers, averaging can be performed using point-by-point averaging. However for data sources with a lower sampling rate, such as PIV generated velocity fields, spline fitting is likely to be required to perform an adequate fit. To get the best results splines should be fitted and evaluated to each run individually before merging.

Histograms have been shown to be useful when investigating time-series data such as that generated by irregular waves. Normalising the histogram allows data from very different sources to be compared. While normalising was used in this study, non-normalised histograms should prove to be especially useful when performing a comparative optimisation study as the devices performance could be compared in more detail than simply utilising averages.

Polychromatic waves offer many advantages over the use of regular waves. When investigating the power output of an OWC the polychromatic wave was able to generate a similar distribution for the orifice flow rate, pressure and power generated by the device as that in an irregular wave. The use of an energy balance showed similarities between the polychromatic wave and the irregular wave for the total kinetic energy within the field of interest but significantly different results for the amount of energy contained within vortices.

A comparison relating the amount of energy contained within vortices with the total kinetic energy showed the importance of testing in a more realistic wave type than regular waves. As the regular wave showed two clear branches relating to the inflow and outflow conditions, while the irregular wave showed an even and linear relationship for these two properties. The polychromatic wave showed a similar distribution to the irregular wave but more variety in the wave profile may be required to make a true

comparison to the irregular wave. It was shown that a minimal amount of energy was required for significant vortices to be formed, indicating non-linearity in the devices response.

Future investigations are required to investigate more complex polychromatic waves which have a greater number of frequency components than the three used within this investigation while maintaining a manageable repeating period. Component wave heights should be determined using a relevant wave spectrum to generate a wave profile that has a similar energy to an irregular wave spectra. A comparison between this wave and an irregular wave would allow a more detailed analysis on the use of polychromatic waves as a substitute for irregular waves.

To gain the most realistic assessment of the operation and performance of a WEC it is important to test in a sea state which is more complex, and realistic, than regular waves. Polychromatic waves provide an intermediate step between a regular and irregular wave and can be used for the investigation of the devices power output but a more detailed study is required to determine if they can be substituted for irregular waves when investigating vortices within the device.

Chapter 4

PIV investigation of 3-dimensional flow within an oscillating water column

The work presented in this chapter has been published as a refereed journal paper was published in the *International Journal of Marine Energy*. The citation for this journal paper is:

Mitchell Ferguson, T., G. Macfarlane, A. Fleming, and I. Penesis (2015). "PIV investigation of 3-dimensional flow within an oscillating water column", *International Journal of Marine Energy* **11**, pp. 120-131.

Abstract

A comprehensive understanding of the flow within an oscillating water column (OWC) is essential to improving the efficiency of the underwater geometry of this type of wave energy converter. This study aims to investigate the impact of the sidewalls on the flow and the changes in flow across the device. Scale model experiments were performed on a forward facing bent duct OWC to generate two-dimensional (2D) particle image velocimetry (PIV) velocity fields at four longitudinal planes across the width of the device. These fields showed there was substantial variation in the flow at the different planes, with a transfer of flow from the central planes during inflow towards the sidewalls during outflow, in addition to the outer planes spending a greater proportion of time in outflow and vice versa. This identified locations at which there is an even distribution between inflow and outflow. Divergence of the velocity fields was calculated to identify non-2D aspects to the flow revealing a vortex forming on the inner lip of the sidewall demonstrating the devices ability to utilise the volume outside of the extents of the sidewalls to generate power. This study has shown there are significant three-dimensional aspects to the flow within and around the device which must be considered when designing the underwater geometry.

4.1 Introduction

The key to furthering the development and commercialisation of wave energy converters (WEC) is to improve the ratio of power output to cost (Behrens *et al.*, 2012). One method for achieving this is to improve the efficiency of the device, which will result in higher average power output. An area in which there is the potential for efficiency gains is the underwater geometry. With improved understanding of how energy is converted from waves into the oscillation of the free surface within the chamber the design can be optimised to reduce losses and therefore increase efficiency and output.

Physical model scale testing is used for the detailed investigation of a devices operation in a controlled environment without the cost associated with full scale testing. Particle image velocimetry (PIV) is an advanced experimental technique for the determination of velocity fields within a plane without interference with the flow. Velocity fields allow the quantitative analysis of the flow within and around the device. Previous studies have used PIV to capture velocity fields at the devices centreline to investigate the flow in and around an OWC which has included the identification of large vortices (Graw *et al.*, 2000) and the generation of an energy balance (Fleming *et al.*, 2012a). Fleming et al. applied phase averaging techniques to OWC velocity fields to reduce uncertainty

and generate an averaged flow across a period of a regular wave (Fleming *et al.*, 2011, 2012b).

It is widely understood that it is possible for an OWC to have a capture width or efficiency in converting wave energy which is greater than unity (Cruz (ed.), 2008). This is due to the devices ability to capture energy from outside of the nominal width of the device by wave diffraction. Due to this the flow in the vicinity of the sidewalls is of particular significance to the devices overall performance and efficiency.

As WEC research progresses from the testing of individual devices to commercial scale arrays, interaction between devices will become an important factor in the overall performance of the array (Behrens *et al.*, 2012). To understand and predict this interaction, the flow within the device cannot be considered to be two-dimensional (2D), and changes in the flow around the device must be understood.

This paper presents an experimental analysis of flow within an OWC, focussing on the impact of the sidewalls on the flow within the device. Phase-averaged 2D PIV velocity fields within and around a model scale generic forward facing bent duct OWC were generated at four longitudinal planes across the devices face. The results show variation in the flow at different planes for both individual elements such as vortices, and overall changes within the flow. The velocity fields divergence identified a number of aspects of the flow that occurred outside the longitudinal planes investigated. Recommendations are made for the design of the device to improve efficiency, particularly in the vicinity of the sidewalls.

4.2 Methodology

4.2.1 Experimental Setup

Experiments were conducted in the Australian Maritime Colleges Towing Tank which has a length of 100 m, width of 3.5 m and depth of 1.5 m (Australian Maritime College, 2015). Waves were generated using a single hydraulically powered paddle type wave maker. A 1:30 scale model of a generic OWC with a cross section shown in Figure 2b was positioned centrally within the tank and was rigidly supported from above. There was a distance of 1080 mm between the tank bottom and lower lip of the model and a distance of approximately 1500 mm between the sidewalls and tank sides. The model was constructed of clear 6 mm thick acrylic and an internal chamber width of 506 mm; the leading edges were square. The power take off (PTO) was simulated with a diameter 50.8 mm orifice, which provides a similar pressure-flow relationship as an

impulse turbine (Folley *et al.*, 2002). The ratio between the chamber surface area and the orifice area was 65.

An array of capacitance type wave probes monitored by Churchill wave probe monitors was positioned both within and in front of the chamber to measure the water elevation as shown in Chapter 2. An additional wave probe was positioned adjacent to the front wall of the chamber (approximately 350 mm from the side wall of the tank) to acquire a record of the incident waves. Data from this probe provided the datum for the phase relationship between the incident waves and those within and around the device. It was assumed that this wave probe was sufficiently removed from the OWC model to minimise its influence on the recorded wave profile. Two Endevco Model 8510B-2 pressure transducers conditioned by an Endevco 136 Voltage amplifier were placed within the top of the chamber to measure the pressure differential between the chamber and the atmosphere. Data from the wave probe monitors and pressure transducers was recorded using a National Instruments PCI-6254-M DAQ card at a rate of 500 Hz. The PIV setup consisted of a dual cavity 120 mJ Nd-Yag laser with underwater optics to project a longitudinal light sheet (Figure 4.1).

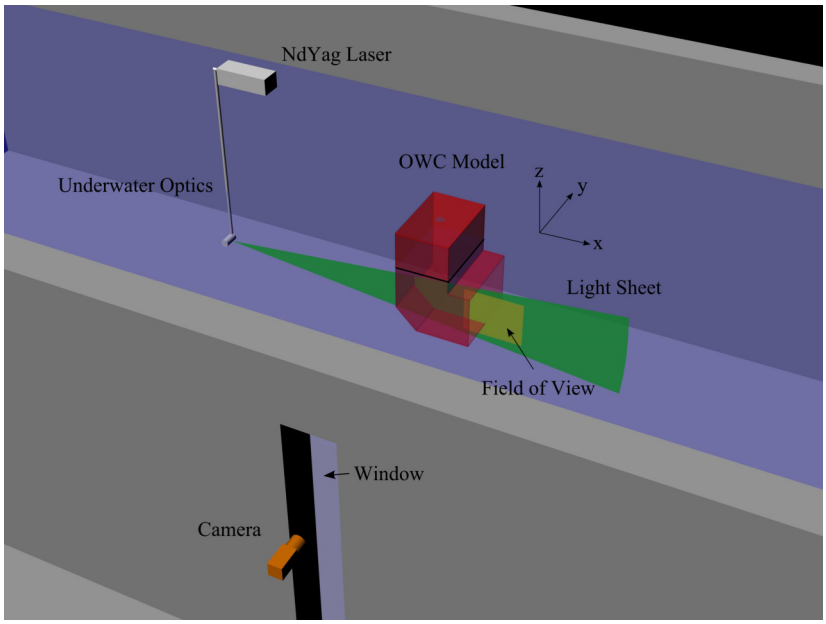

Figure 4.1: PIV setup for the capture of velocity fields

As the majority of the flow occurs in the longitudinal plane (Fleming *et al.*, 2011), four locations parallel with the longitudinal centreline of the model were investigated (see Figure 4.2(a)). In Chapter 2 it is shown that in the head seas condition the elevation of the water surface within the chamber is symmetrical, as such only planes on a single side of the device were investigated. Planes in the $-y$ side of the device were selected

to reduce the distance between the field of interest and the PIV camera. The position of the planes was assigned a non-dimensionalised value (W) where W= 0.00 is the OWC centreline and W = 1.00 is the inside of the sidewall. The water was seeded with neutrally buoyant fluorescing particles of between 36 and 75 μm diameter, as described by Fleming *et al.* (2012b). A sCMOS double frame camera (16 bit, 2560x2150 pixels) was positioned outside of the tank and captured images through an acrylic window. Image pairs were captured at a rate of 15 Hz with an inter frame time of 10ms.

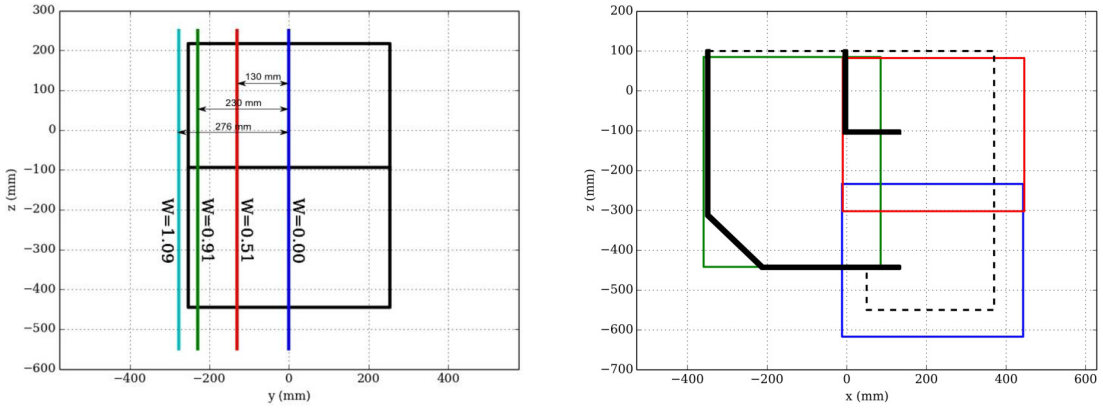

(a) (b)

Figure 4.2: (a) Location of the four planes investigated from the front view of the OWC geometry. (b) The region of interest (dashed) surrounding the side view of the OWC geometry and an example of the camera positions used

The region of interest surrounding the device is shown in Figure 4.2(b) by the dashed black line. To capture the flow within the region with the required resolution the camera was required to be positioned at multiple locations. Three locations were generally required to capture vectors with sufficient vector density; a portrait alignment capturing the interior of the chamber (green) and two landscape alignments (red, blue) capturing the region in front of the device. For the plane outside of the chamber (W = 1.09), only the area in the vicinity of the chamber outlet was captured.

LaVision GmbH software package DaVis 8 (LaVision GmbH, 2010) was used to capture, analyse and process image pairs to create velocity fields. Prior to vector calculation images were masked above the waterline and in areas where the geometry of the device intersected with the image plane using the method described by Fleming *et al.* (2012b) to avoid creation of spurious vectors. Vector processing was performed using a multiple pass method with two initial passes with a square 64x64 pixel interrogation window, followed by a single pass with a square 32x32 pixel interrogation window. This resulted in a spatial resolution of between 2.5 and 3.5 mm depending on the particular field of view being investigated. All experiments on the OWC device were in regular

waves where the nominal height and frequency were selected to represent the range of conditions the device is expected to experience (Table 4.1). The measured height was calculated using the method outlined in Chapter 2.

Table 4.1: Frequency and height of the regular waves

Frequency [Hz]	Nominal Height [mm]	Average Measured Height [mm]
0.45	75	78
0.50	45	45
0.50	55	56
0.50	75	77
0.55	75	75
0.60	75	76

To eliminate the impact of wave reflections from the end of the tank testing each run was limited to a duration of 60 seconds. Each combination of camera location and wave was completed twice giving a total of 120 seconds or 1800 image pairs.

4.2.2 Data Processing

Phase Averaging

Phase averaging is a technique for the averaging of periodic signals, such as those generated by waves, which has been used extensively when analysing PIV flow fields of oscillating water columns (Fleming *et al.*, 2011). This uses the cyclical nature of the wave period to overlay data onto a single period and is performed in two stages; phase assignment and averaging.

Phase assignment is the process of determining the location of each data point with each over a non-dimensionalised period of the wave. This is identified by fitting a sinusoidal function to the incident wave probe elevation which is used to determine the start and end of each period of the regular wave as demonstrated in Chapter 2. Phase values are then assigned linearly between the start of the period (phase = 0) and the end of the period (phase = 1) as seen in Figure 4.3.

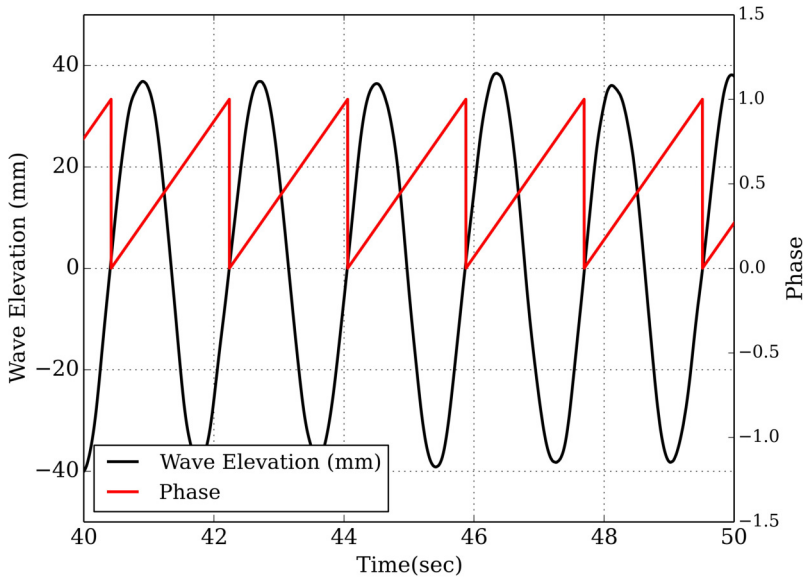

Figure 4.3: Phase assignment of a regular wave with height of 75 mm and frequency of 0.55 Hz

As the sampling rate for the PIV velocity fields varies drastically from that used for wave probe and pressure transducer data, a different averaging methodology is applied for each data type, as shown in Table 4.2. Ensemble averaging is performed on wave probe and pressure transducer data; this involves sorting the phase assigned data into 60 equally spaced bins (Fleming *et al.*, 2011). The data in each bin is then averaged. An example of the wave elevation at the incident wave probe is shown in Figure 4.4. The average uncertainty for the incident wave elevation is 0.45 mm.

Due to the lower sampling rate of the PIV system, velocity fields are averaged by fitting splines. For each pixel the velocity in the x and z direction is sorted by phase. A cubic spline is then fitted to each set of data, which is then evaluated at 60 evenly spaced times (Fleming *et al.*, 2012b). The mean uncertainty of the velocity field varied between 0.025 and 0.011 m/s depending on the plane investigated.

Table 4.2: Phase averaging methodology for different signals

Signal	Sampling Rate	Phase Assignment	Averaging Methodology
Wave probe Pressure transducer	500 Hz 500 Hz	Incident wave probe data fitted to sinusoidal signal	Ensemble averaging using 60 equally spaced bins (Fleming *et al.*, 2011)
Velocity fields	15 Hz		Fitted spline evaluated at 60 evenly spaced times (Fleming *et al.*, 2012b)

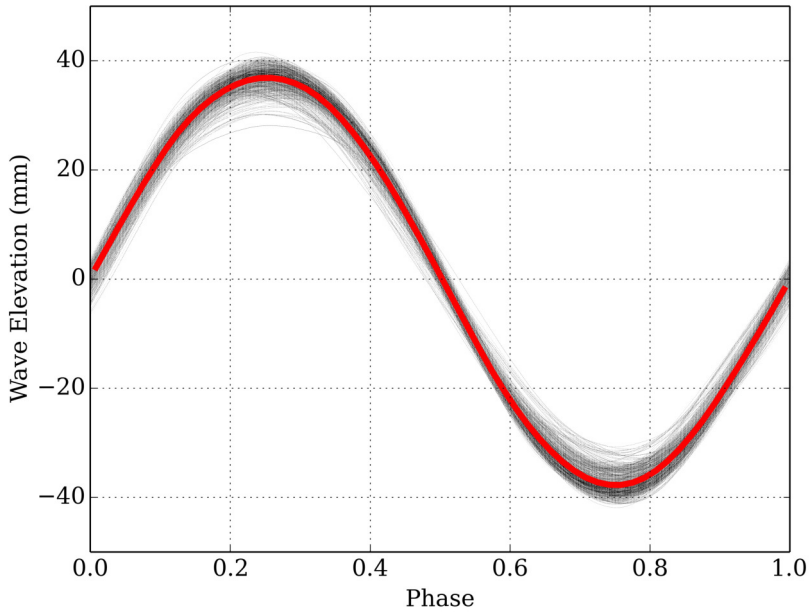

Figure 4.4: Phase averaged data for the incident wave probe (black) and phase averaged result (red) for a regular wave with height of 75 mm and frequency of 0.55 Hz showing result of phase averaging. The average uncertainty for the incident wave elevation is 0.45 mm

4.3 Results and Discussion

Phase-averaged PIV velocity fields were generated for each wave at each of the four planes investigated. A number of characteristics of the flow can be observed including identification of features such as vortices. The operation of the device can be divided into two main conditions: (1) inflow; where the water level within the chamber is rising, and (2) outflow; where the water level within the chamber is falling. In a purely 2D flow without the presence of sidewalls we would expect there to be minimal difference in the velocity fields of each plane. Instead, it was found that there were significant changes in flow across the device. This was caused by a mechanism in which there was increased flow velocity at the centre of the device during inflow, which was subsequently redistributed towards the sidewalls during outflow resulting in greater outflow velocities at the sidewalls. This section will outline these findings and possible reasons behind this phenomenon.

Figure 4.5 provides an example of velocity fields for an inflow (left) and outflow (right) condition for a single regular wave of a height of 75 mm and frequency of 0.55 Hz for each of the planes investigated. A number of differences were observed at the different planes; some of these were distinct features such as vortices forming on the inside of the sidewall or at the lower lip, whilst others indicated changes in the overall quantity of flow occurring at different planes within the two flow conditions.

One of the features which have been identified as being prevalent and important in the efficiency of the device in similar geometries is the lower lip vortex (Graw *et al.*, 2000). This occurs due to separation as the flow passes the bottom lip during inflow and can be seen in Figure 5 (a), (c) and (e). There is clear interference between the flow at the sidewall and the lower lip vortex in Figure 5 (e).

The flow in the vicinity of the sidewall (Figures 4.5 (e), (f), (g) and (h)) shows significant out of plane flows indicated by discontinuity within the velocity field. Figure 5e shows significant out of plane flows at the inlet caused by flow passing the inner lip during inflow. However once past the region of the inlet there is little change in the flow compared with the other planes (Figures 5 (a), (c)). During outflow (Figures 4.5 (f), (h)) we can see evidence of more out of plane flow however in this case it occurs outside of the chamber. Further investigation of the out of plane flow will occur later within this article.

While individual features of the flow change, there are also differences in the total quantity of flow. Comparing the flow during inflow in the rear of the chamber in Figures 4.5 (a), (c) and (e), there is a decrease in the velocity compared with that at

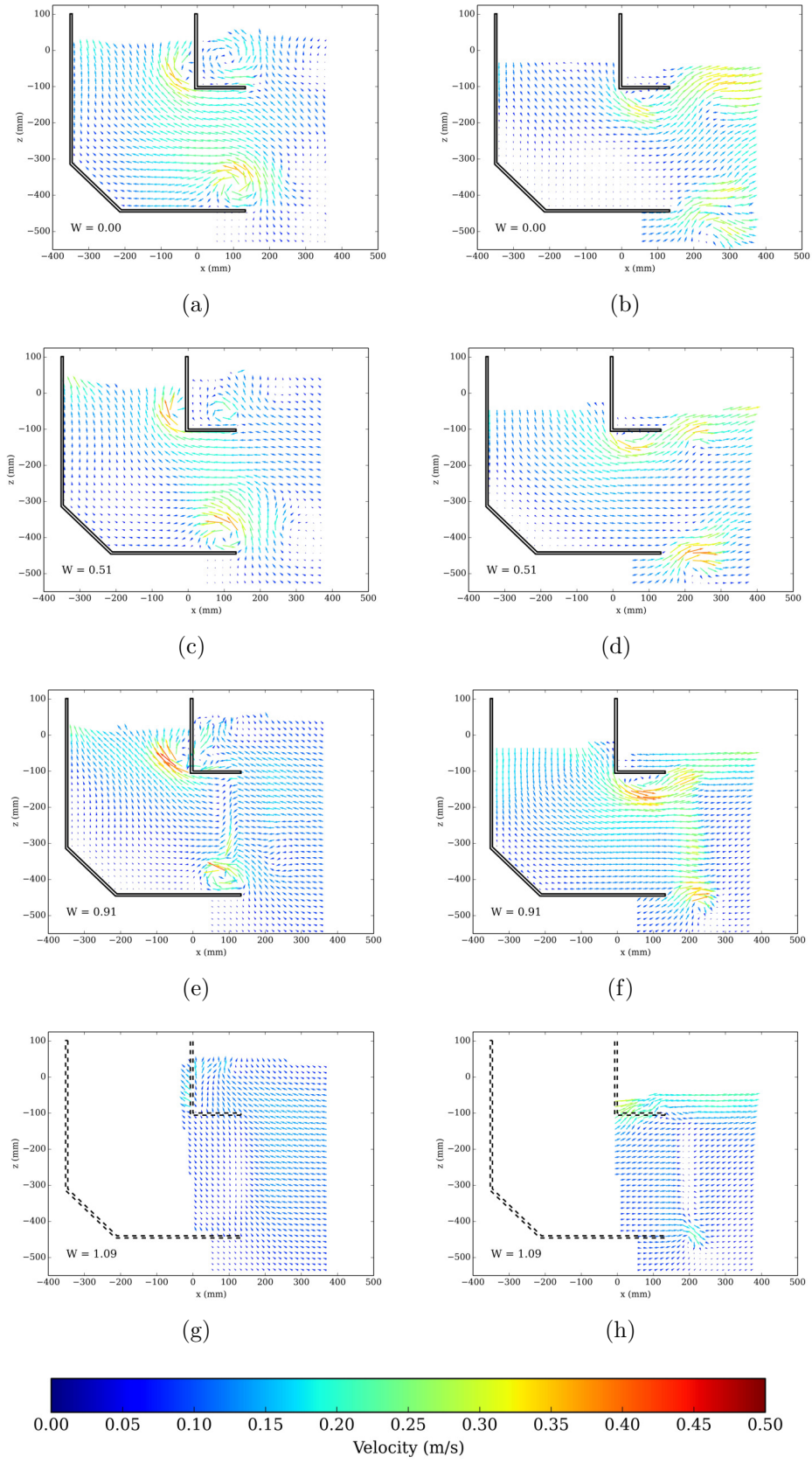

Figure 4.5: Velocity fields for inflow (left, phase = 0.18) and outflow (right, phase = 0.68) conditions in a regular wave with height of 75 mm and frequency of 0.55 Hz showing the change in flow that occurs across the chamber. Only one in 36 vectors are shown for clarity

the centreline. Continuing to look at the rear of the chamber during outflow (Figures 4.5 (b), (d) and (f)) the opposite occurs as there is higher velocity flow at the sidewalls during outflow. This suggests there may be a transfer in flow from the centre of the chamber during inflow towards the sidewalls during outflow.

To quantify the shift in flow from the centreline towards the sidewalls the average velocity within the chamber is calculated. Figure 4.6 shows localised maxima during periods of greatest flow for both inflow (phase = 0.15 approx.) and outflow (phase = 0.60 approx.) and localised minima at the locations during transition between the two conditions (approximately phase = 0.40 and phase = 0.90 approx.). During inflow there is greater velocity flow within the central plane, whilst during outflow there is greater velocity flow at the sidewall. This quantifies the observations from Figure 4.5 and supports the finding that the quantity of flow changes substantially at different planes during the two conditions.

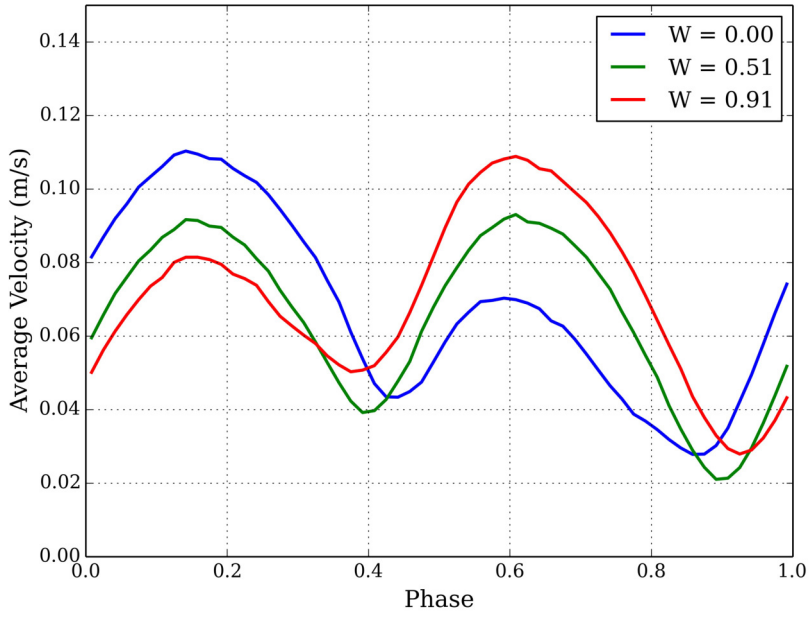

Figure 4.6: Change in average velocity within the chamber for the three planes within the chamber in a regular wave with a height of 75 mm and frequency of 0.55 Hz showing the transition in flow from the centreline during inflow towards the sidewalls during outflow

By identifying the peaks and troughs in the average velocity we can identify the point at which the flow transitions between four key points: maximum inflow, transition from inflow to outflow, maximum outflow and transition from outflow to inflow. This allows the length of time the flow is for each plane to be determined. The average values for all of the waves investigated is shown in Figure 4.7.

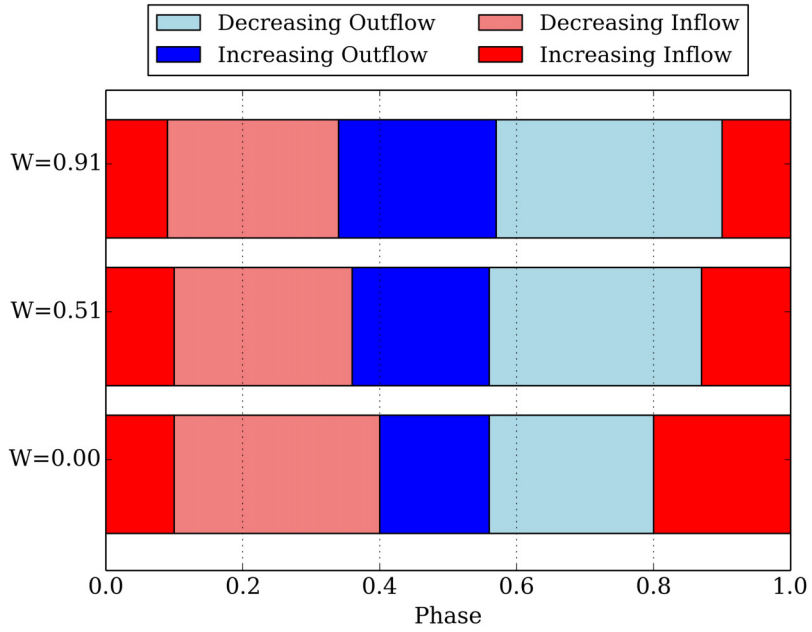

Figure 4.7: Average proportion of time spent in each of the conditions outlined at each plane showing a decrease in the time spent in the inflow condition at the sidewall

This data shows that the point of maximum velocity for both the inflow and outflow conditions does not vary substantially. However transition between conditions shows significant variation. The average transition from inflow to outflow occurs earlier at the sidewall (phase = 0.34) than the centreline (phase = 0.40), whilst the average transition from outflow to inflow occurs later at the sidewall (phase = 0.90) compared with the centreline (phase = 0.80). The flow at the sidewalls spends a greater proportion (average 56%) of time in the outflow condition, whilst the centreline spends a greater proportion (average 60%) in the inflow condition.

The combination of the change in average velocity and the change in transition between inflow and outflow conditions can be explained by the presence of cross plane flow within the chamber. During inflow there is greater velocity at the centreline, as the flow reaches the peak this begins to equalise as the greater flow at the centreline is redistributed across the width of the column. This effect is increased during outflow as there is a reduced resistance to outflow at the sidewalls. The overall effect is increased flow at the centreline during inflow being redistributed to the outer planes during outflow.

Using the transition points identified in Figure 4.7 the flow at each plane can be split into two distinct conditions; inflow and outflow. The average velocity during each of these conditions is used to determine how the flow is distributed between these two conditions. Figure 4.8 shows a comparison of the average velocity contained within

the inflow condition with the average velocity for a full period for each of the three internal planes investigated. Values greater than 1 indicates higher average velocity in the inflow, and values lower than 1 indicate higher average velocity in the outflow. As can be seen, a similar trend occurs as at all combinations of incident wave height and frequency.

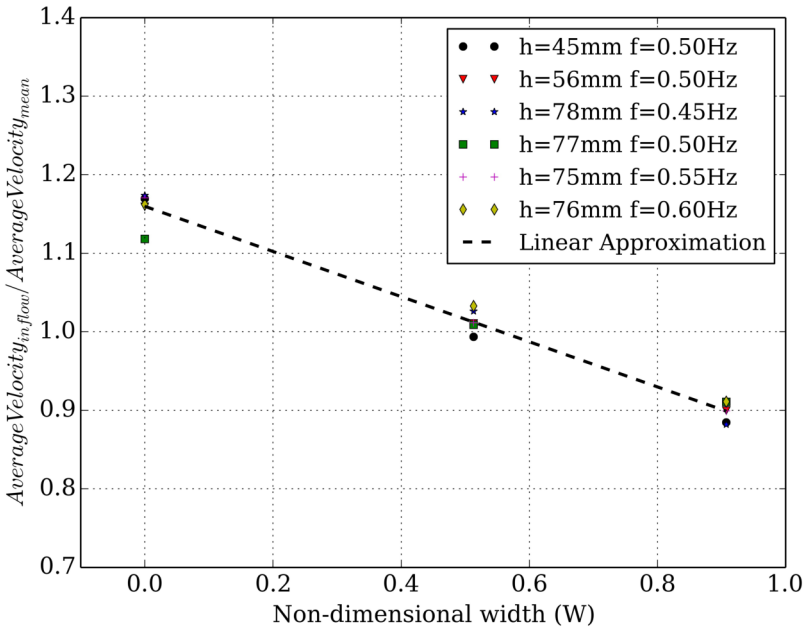

Figure 4.8: Proportion of the average velocity contained within the inflow condition at each of the planes and waves investigated. Inflow and outflow conditions were defined using the minimum average velocity (Figure 4.6)

Figure 4.8 also allows the identification of a critical location when performing experiments on OWCs. Previous studies have generally only considered a single location to evaluate device performance, usually at the centreline plane (Graw *et al.*, 2000). The results presented here indicate that data acquired at the centreline plane will not provide the best representation of the flow across the entire device. Therefore, when planning experiments where only a single plane is being investigated then it is important to considered the most appropriate lateral location, which is where the average velocity in the inflow and outflow condition is equal. For the model used in this study it is recommended that experiments be performed at a non-dimensional width of 0.55.

An additional property that can be calculated from a 2D velocity field is divergence. Divergence represents the flow entering or leaving the 2D flow field and can be calculated using Equation 4.1:

$$div\mathbf{V} = \frac{dV_x}{dx} + \frac{dV_z}{dz} \tag{4.1}$$

where **V** is the velocity field, V_x and V_z are the local velocity components, dx is the pixel width and dz is the pixel height.

Whilst divergence can show flow entering and leaving the 2D plane it cannot capture flow passing through the 2D plane. Positive values indicate flow entering the plane and negative values indicate flow leaving the plane, whilst a value of zero indicates there is no flow entering or leaving the plane. This calculation allows the visualisation of some 3D aspects of the flow without requiring a 3D PIV setup.

Figure 4.9 shows the divergence field for the centreline plane (W = 0.00) and the plane located at a non-dimensional width of 0.51. During inflow a major flow feature at these planes is the lower lip vortex. It is clear from looking at divergence that the vortex is not a purely 2D phenomenon, but has flow entering and leaving each plane. The W = 0.51 plane (Figure 4.9(b)) shows a large flow leaving the plane via the vortex, whilst the centreline plane (Figure 4.9(a)) shows flow entering the plane at the corresponding location. The transfer of flow via the lower lip vortex is therefore one mechanism by which flow is transferred from the outer planes to the centre during inflow.

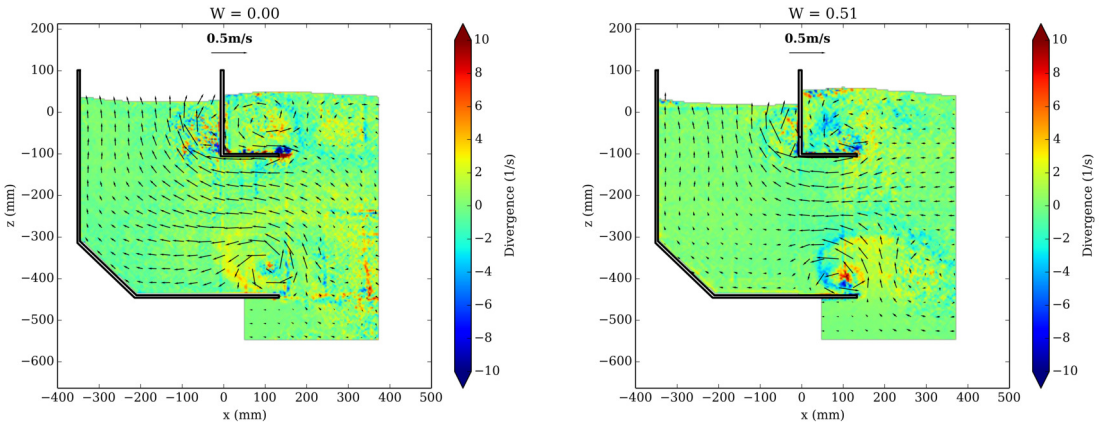

(a) (b)

Figure 4.9: Divergence field for two planes in a regular wave with a height of 77 mm and frequency of 0.50 Hz during the inflow condition at phase = 0.23 where positive values indicate flow entering the field and negative values indicate flow leaving the field demonstrating the transportation of flow via the lower lip vortex

Flow at the leading edge of the sidewalls is affected by both the flow within the chamber and the incoming wave on the outside of the chamber. Figure 4.10 shows the divergence of the flow in the vicinity of the sidewall. Flow on the inside of the sidewall (Figure 4.10(a)) shows an interesting pattern where there is a region of flow entering and rapidly leaving the plane just within the chamber. This likely indicates the presence of vortex rotating around the positive z axis. A small anomaly in Figure 4.10(a) occurs

at z = 230 mm (approx.) where small errors in the velocity field are caused by the stitching between two fields of view. This does not have an effect on results outside of this location.

The cause of this can be seen in the plane on the outside of the sidewall (Figure 4.10(b)). This shows flow leaving the plane from in front of the sidewall. As flow enters the chamber from outside the sidewall it passes the sharp edge of the sidewall causing separation and a vortex to form within the chamber. This is a similar mechanism to that which causes the lower lip vortex. The presence of the vortex within the chamber will reduce the amount of energy within the longitudinal plane within the sidewall as energy is trapped and lost within the vertical vortex, however this will be somewhat offset by the additional energy captured from outside of the sidewall.

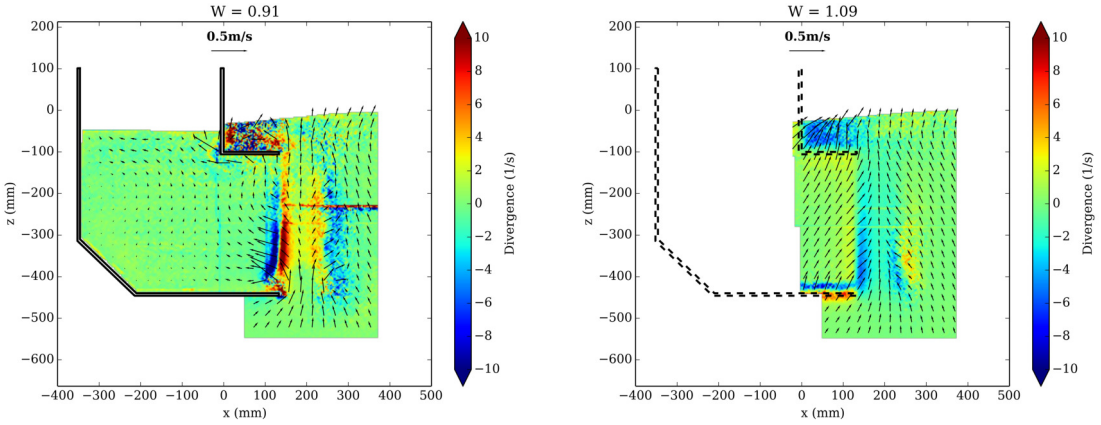

(a) (b)

Figure 4.10: Divergence field for two planes in a regular wave with a height of 77 mm and frequency of 0.50 Hz during the inflow condition at phase = 0.97 demonstrating flow entering the chamber from outside of the sidewalls and forming a vortex within the chamber at the sidewall

Having identified some reasons for the increased flow at the centreline during inflow, it was important to identify reasons for the increased outflow at the sidewalls. Figure 4.11 shows the divergence field for the outer two planes during early stages of the outflow condition. The plane inside of the sidewall (Figure 4.11(a)) shows a large amount of flow leaving it, whilst the plane outside the sidewall (Figure 4.11(b)) shows the vortex which was previously within the chamber (Figure 4.10(a)) being ejected. Importantly this vortex is being ejected into a volume which is outside of the sidewall limits.

By utilising the volume of water outside of the sidewalls during the outflow condition the device has a wider effective width which leads to increased flow as compared to the inflow condition. This provides a mechanism for increasing the efficiency of the

device, which may result in a capture width greater than unity. This is seen as the power output during outflow is greater than during inflow (Fleming *et al.*, 2011; Graw *et al.*, 2000). As this additional effective width occurs outside the sidewalls there is reduced resistance to flow at the outer parts of the chamber. This results in increased flow at the sidewalls during the outflow condition.

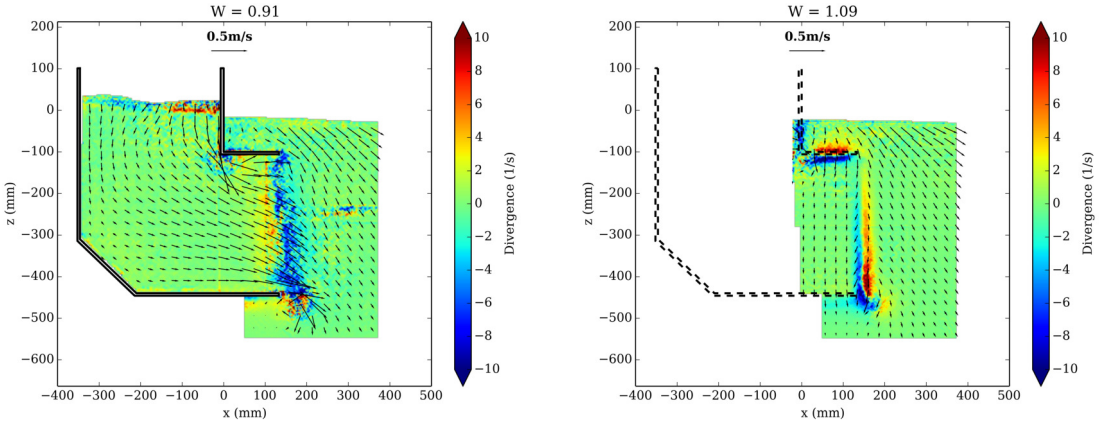

(a) (b)

Figure 4.11: Divergence field for two planes in a regular wave with a height of 77 mm and frequency of 0.50 Hz at the early in the outflow condition at phase = 0.55 demonstrating the expulsion of the sidewall vortex and flow outside of the chamber width

This study has identified significant changes in the flow at different locations across the device. The flow in the vicinity of the sidewalls demonstrates the devices ability to utilise the volume of water outside of its extents to both gather energy on inflow and increase the rate of flow during outflow, therefore increasing the devices capture width. Further design work could lead to greater efficiency gains in this area by reducing the size of the vortex forming within the sidewall lip during inflow resulting in more of this energy is available to the PTO. This may be achieved by introducing an angled or curved lip at the sidewall. As there are substantial differences in the flow at different locations there are also likely to be efficiency gains which could be realised by optimising the centreline for inflow, and the outer areas for outflow.

4.4 Conclusions

Scale model testing was performed to generate phase-averaged 2D PIV velocity fields for four longitudinal planes at different locations across a forward facing bent duct oscillating water column. These fields identified large variation in flow at the planes investigated, in particular flow in the vicinity of the inlet at the sidewalls exhibited large

out of plane velocities. There was also a pattern of higher velocity at the centreline during inflow, and higher velocity during outflow at the outer planes.

The average velocity within each plane showed a transfer in the flow from the centreline during inflow to the outer planes during outflow. The average flow velocity within the chamber identified the transition between inflow and outflow. The transition points varied at the different planes resulting in the outer planes spending a greater proportion of time in outflow (56%) and the central planes spending a greater proportion of time in inflow (60%). This can be explained by increased flow at the centreline during inflow being redistributed to the outer planes during the transition from inflow to outflow. The average velocity during each condition was used to determine the point at which the average velocity for inflow and outflow was equal. For the device under investigation this was found to be at a non-dimensional width of 0.55 (approx.).

When planning experiments where only a single plane is being investigated it is recommended that consideration be given to the most appropriate lateral location. Ideally, this should be where the average velocity in the inflow and outflow conditions are approximately equal, which this study has shown is very unlikely to be at the centreline, but approximately halfway between the centreline and the sidewall of the device.

The velocity fields divergence showed transport of flow from the outside towards the centre via the lower lip vortex during inflow. When investigating flow near the sidewalls it was found that flow was entering the inlet from outside of the sidewalls during inflow resulting in the formation of a vortex at the sidewall inlet. During outflow there was significant flow from the inside of the chamber to the volume outside of the sidewalls. The combination of these effects which restrict the inflow at the sidewall and encourage outflow at the sidewalls are likely to lead to the redistribution of flow from the centreline during inflow to the sidewalls during outflow which has been observed.

The findings from this study show that there are substantial differences in flow at different locations. One area for particular development is the leading edge of the sidewall which could be redesigned to reduce the size of the vortex during inflow and to encourage outflow into areas outside the sidewalls. This work also has implications for the integration of devices into arrays of devices into arrangements where they are directly adjacent such as in breakwaters as it shows the ability of the device to absorb energy from beyond the sidewalls. If devices are placed directly adjacent to one another this effect will be reduced and therefore the efficiency of the individual device will also be reduced.

Chapter 5

Summary, Conclusions and Further Work

5.1 Summary and Conclusions

To become competitive with other energy sources WECs efficiency needs to be improved. Well-designed model scale testing plays a key role in providing designers with the information and knowledge to achieve this. This study aimed to investigate model scale testing of wave energy converters using particle image velocimetry. The study focussed on the use of more complex wave types than regular waves, and acquiring information about the 3D flows that occur within an OWC with an aim to improve test procedures. In this chapter the major findings are presented and recommendations for future areas of research are identified and discussed.

This investigation initially adapted the phase averaging methodology (which had previously only been applied to regular waves (Fleming *et al.*, 2012b)) to a more complex polychromatic wave. In Chapter 2 this approach was adopted to investigate the linearity of the devices response in a polychromatic wave and utilised a wave probe array to study longitudinal and transverse sloshing within the chamber. After successfully applying phase averaging to wave probe and pressure transducer data, the methodology was expanded to PIV generated velocity fields. To further expand the analysis to irregular waves a time domain approach was developed to analyse the velocity fields. This is used to compare the velocity fields of regular, polychromatic and irregular waves in Chapter 3. The other component of the study was to investigate 3D flows that occur during the devices operation. PIV velocity fields were captured at a number of longitudinal planes across the device and the results are presented and discussed in Chapter 4.

The overall purpose of the study was to investigate two key properties of the OWCs behaviour during model scale testing. The first being:

- Can model scale testing in regular waves be used to provide an accurate representation of the expected flow in an irregular/polychromatic sea?

It was determined that there were significant differences in the operation of the device in regular, polychromatic and irregular waves. In particular the devices operation in regular waves is subject to harmonic effects which are not present in the other two wave types. Chapter 2 showed polychromatic waves offered a large improvement in the complexity of waves able to be investigated over regular waves, while still allowing well proven analysis techniques such as phase averaging to be utilised, which is valuable in any comparative study. Chapter 3 showed that irregular waves should be utilised if a quantified performance evaluation is required.

The second question this work set out to explore was:

- Are there significant changes in flow across an OWC and if so what impact will these have on the performance?

The work presented in Chapter 2 found that while there was negligible change in the elevation of the water within the chamber across the device there were still significant 3D flows within and around the device. Of particular importance was the finding in Chapter 4 of the devices ability to utilise the water volume outside of its sidewalls to generate additional power during outflow.

In addition to the previously explored questions this study allowed the use of PIV in model scale testing of wave energy devices to be evaluated. With sufficient data processing, PIV gives highly accurate and detailed velocity fields at a cost of additional complexity in comparison to more traditional instrumentation such as wave probes and pressure transducers. As discussed in more detail in Section 5.3.1, the use of PIV should be carefully considered to ensure the additional complexity is justified for the investigation being undertaken.

5.2 Key Findings

The following section summarises the key findings and limitations of the study.

5.2.1 Phase Averaging Polychromatic Waves

- Phase averaging methodology previously applied to data generated in regular waves can be successfully applied to data generated in polychromatic waves. The application of this methodology generated averaged results for both PIV velocity fields and other data sources with a reduction in uncertainty.
- Limitations: Phase averaging should only be applied if the response of the device has the same period as the polychromatic wave. Prior to performing phase averaging a detailed study should be performed to ensure each period of the wave is sufficiently similar to those previous to ensure phase averaging can be performed.

5.2.2 OWC Operation in Polychromatic Waves

- The use of polychromatic waves in model scale testing of wave energy converters gives the opportunity to investigate the devices operation in a more complex sea state than regular waves, while still being able to use well established data processing methods developed for regular waves. The use of polychromatic waves reduces the impact of unrealistic harmonic effects which are present in regular waves. This is evident as the amount of kinetic energy contained within vortices in polychromatic waves is decreased by 20 to 40% compared with similar regular waves.

- Limitations: This study investigated polychromatic waves with three frequency components of equal height. While this generated a wave profile which was more irregular than a regular wave the average energy flux was much lower than the regular waves it was compared against.

5.2.3 OWC Operation in Irregular Waves

- Irregular waves offer a good approximation of a realistic sea state when performing physical model scale testing however data requires analysis in the time domain. Irregular waves generate a smooth distribution for both the total kinetic energy and kinetic energy contained within vortices. In the irregular wave a linear relationship between the amount of kinetic energy contained within vortices and the total kinetic energy may be shown.

- Limitations: This study only investigated a single wave spectrum and was not able to evaluate changes in device operation as the spectrum is altered. Future studies should investigate the impact of a change in sea state in particular significant wave height as this may highlight the impact of non-linearities in device operation.

5.2.4 Sloshing within the Chamber

- Capturing sloshing within the chamber is important to get an accurate measurement of the water elevation within the chamber. A wave probe array identified sloshing occurring in the longitudinal plane, but not in the transverse plane. Therefore to accurately measure the water chamber elevation a longitudinal array of water surface elevation sensors is recommended. Using a single wave probe over an array results in an average error in the chamber volume flux of $\pm$ 6%.

- Limitations: This study only investigated the head seas condition, while this condition is ideal for the devices operation often this will not be the case. If studying a condition using an oblique or multi-directional wave transverse sloshing may occur and should be investigated further.

5.2.5 3D Effects

- The transition between inflow and outflow conditions occurs at different times across the device. It was found that the outer volume of the chamber spends a greater proportion of time in outflow (56%) and the central volume of the chamber spends a greater proportion of time in inflow (60%).
- The divergence of a 2D velocity field is a valuable tool to use for the identification of 3D flow features such as vortices and the transfer of flow across planes. Using this tool large vortices were identified at the inside lip of the sidewall during inflow.
- The device utilises the volume outside of its sidewalls during outflow. This phenomenon allows the device to have an effective width greater than the extents of its sidewalls and greater power can be generated during outflow than inflow.
- Limitations: The use of divergence allows the identification of flow entering or leaving a field and was valuable for the identification of flow features such as vortices but cannot identify flow passing directly through the field. This study identified the effects of cross flow within the chamber, but a 3D PIV system could be used to identify and quantify the exact process by which the cross flow takes place.

5.3 Experimental Methodology in Model Scale Testing

Model scale testing is widely used to both evaluate and optimise wave energy converters. Experiments can be performed with varying levels of complexity in both the instrumentation and sea states in which the device is exposed to. The following section outlines recommendations for the model scale testing of wave energy devices.

5.3.1 Use of PIV in WEC Experimentation

PIV provides highly accurate and detailed information on the flow within and around wave energy devices; however its use increases the complexity of both the experimental setup and data processing. To justify the additional complexity of the study it is important that the additional data gathered is important for the study being undertaken. The work performed in this study utilised the velocity field data for two main purposes; a comparison of the flow within the device in different wave types and the identification of 3D flows within the device.

While the use of PIV provides a huge amount of data contained within the velocity fields, this can be deceptive as in complex flows it is challenging to develop methods to quantify the totality of the flow. Because of this it is important when designing an experimental program utilising PIV that clear and detailed outcomes are outlined prior to testing and that the use of PIV will achieve these outcomes.

Based on this study PIV would offer valuable data in the following studies:

- Quantitative flow visualisation: Velocity fields allow the identification of flow features which can have a positive or negative impact upon the performance of the underwater geometry of the device. By gaining a detailed understanding of the flow within or around a device the geometry can be altered to maximise the efficiency and improve performance.

- Comparative studies: Comparative studies can be used for many purposes such as evaluation of geometry changes, investigation of response in different wave frequencies or heights or flow at differing planes across a device such as the work performed in this study. By limiting the number of variables between the studies the velocity fields can be used to provide detailed information on the impact of the changes to the flow and can therefore be used to gain a much greater understanding of the devices operation.

- Validation of numerical models: Accurate flow fields can be used to provide detailed information for the validation of numerical models. In particular those utilising CFD can use the velocity fields to identify inaccuracies at specific locations, instead of using averaged data such as chamber air pressure or chamber water surface elevation.

5.3.2 Wave Types in WEC Experimentation

Using the correct wave type for the study being performed is very important to ensuring the findings are relevant to the final design, without using a more complex wave than is required.

Regular waves provide a basic starting step for the investigation of a wave energy device and should be used for proof of concept studies, initial flow visualisation studies, verification of basic numerical models and initial performance prediction. The highly repetitive nature of a regular wave is useful for initial studies but for further analysis unrealistic harmonic effects may be present which can reduce the applicability of findings.

Utilising polychromatic waves as an intermediate stage between regular and irregular wave testing will provide additional information about the devices performance without a significant increase in the complexity of the study required. By reducing the impact of unrealistic harmonic effects, polychromatic waves provide a good wave type for optimisation studies where a comparison of multiple designs can be made in common conditions.

While irregular waves have more complex data analysis requirements, an irregular spectrum provides the best tool for the performance prediction of a device in a realistic sea state. An irregular spectrum also should be used for the identification of rare or extreme events which cannot be replicated using the other wave types.

5.4 Further Work

This work presented in this study could be extended by:

- Further development into the utilisation of polychromatic waves to simulate an irregular spectrum by investigating a polychromatic wave with more frequency components and an energy distribution calculated to exactly match that of an irregular spectrum. Comparisons between a more complicated polychromatic wave and irregular wave spectrum would allow further evaluation of the practicality of adopting polychromatic waves over irregular waves.

- Utilising PIV to further investigate the presence of non-linear effects that occur in the operation of the device. This investigation could use regular or polychromatic waves of differing heights to quantify the linearity of effects such as the lower lip vortex.

- Examining the incorporation of OWCs into a breakwater focussing on the impact this has upon the flow around the side walls. This work should also explore the impact of multiple devices adjacent to one another and the possible reduction in power due to devices inability to utilise the volume outside of its sidewalls identified in Chapter 4.
- Expanding the investigation of 3D flows in the device by utilising 3D PIV to further quantify the effects that were identified in this work, in particular the cross flow within the chamber.
- Exploring the use of non-constant cross sections to maximise output by utilising the changes in the magnitude of flow identified across the device.
- Performing experiments in an oblique seas condition to investigate the impact that has on both the performance of the device and the cross flows within the device.

References

Australian Maritime College (2015). *Towing Tank.* URL: http://www.amc.edu.au/maritime-engineering/towing-tank.

Behrens, S., Hayward, J., Hemer, M., and Osman, P. (2012). "Assessing the wave energy converter potential for Australian coastal regions". *Renewable Energy* **43,** pp. 210–217.

Brito-Melo, A., Neuman, F., and Sarmento, A. J. N. A. (2008). "Full-scale data assessment in OWC Pico plant". *International Journal of Offshore and Polar Engineering* **18**(1), pp. 27–34.

Carnegie Wave Energy (2015). *CETO 6 Images.* URL: http://carnegiewave.com/galleries/ceto-6-images/.

Clément, A., McCullen, P., Falco, A., Fiorentino, A., Gardner, F., Hammarlund, K., Lemonis, G., Lewis, T., Nielsen, K., Petroncini, S., *et al.* (2002). "Wave energy in Europe: current status and perspectives". *Renewable and Sustainable Energy Reviews* **6**(5), pp. 405–431.

Cruz (ed.), J. (2008). *Ocean Wave Energy: Current Status and Future Perspectives.* Springer.

Dizadji, N. and Sajadian, S. E. (2011). "Modeling and optimization of the chamber of OWC system". *Energy* **36**(5), pp. 2360–2366.

El Lababidy, S., Bose, N., Liu, P., Walker, D., and Di Felice, F. (2005). "Experimental analysis of the near wake from a ducted thruster at true and near bollard pull conditions using Stereo Particle Image Velocimetry (SPIV)". *Journal of Offshore Mechanics and Arctic Engineering* **127**(3), pp. 191–196.

Falcão, A. F. d. O. (2010). "Wave energy utilization: A review of the technologies". *Renewable and Sustainable Energy Reviews* **14**(3), pp. 899–918.

Falnes, J. (2007). "A Review of Wave-Energy Extraction". *Marine Structures* **20**(4), pp. 185–201.

Fleming, A. (2012). "Phase-averaged analysis of an oscillating water column wave energy converter". PhD thesis. University of Tasmania.

Fleming, A., Penesis, I., Goldsworthy, L., Macfarlane, G., Bose, N., and Denniss, T. (2011). "Phase averaged flow analysis in an oscillating water column wave energy

converter". *In*: Proceedings of the ASME 2011 30th International Conference on Ocean, Offshore and Arctic Engineering. Rotterdam, The Netherlands.

Fleming, A., Penesis, I., Macfarlane, G., Bose, N., and Denniss, T. (2012a). "Energy balance analysis for an oscillating water column wave energy converter". *Ocean Engineering* **54,** pp. 26–33.

Fleming, A., Penesis, I., Macfarlane, G., Bose, N., and Hunter, S. (2012b). "Phase averaging of the velocity fields in an oscillating water column using splines". *Proceedings of the Institution of Mechanical Engineers, Part M: Journal of Engineering for the Maritime Environment* **226,** pp. 335–345.

Folley, M., Whittaker, T., and Henry, A. (2005). "The performance of a wave energy converter in shallow water". *In*: Proceedings of the 6th European Wave and Tidal Energy Conference. Glasgow, United Kingdom.

Folley, M. and Whittaker, T. (2010). "Spectral modelling of wave energy converters". *Coastal Engineering* **57**(10), pp. 892–897.

Folley, M. and Whittaker, T. (2002). "Identification of non-linear flow characteristics of the LIMPET shoreline OWC". *In*: Proceedings of the 12th International Offshore and Polar Engineering Conference. Kitakyushu, Japan.

Folley, M. and Whittaker, T. (2013). "Validating a spectral-domain model of an OWC using physical model data". *International Journal of Marine Energy* **2,** pp. 1–11.

Forestier, J. M., Holmes, B., Barrett, S., and Lewis, A. W. (2007). "Value and Validation of Small Scale Physical Model Tests of Floating Wave Energy Converters". *In*: Proceedings of the 7th European Wave and Tidal Energy Conference. Porto, Portugal.

Geoscience Australia and ABARE (2010). *Australian Energy Resource Assessment.* Canberra.

Gervelas, R., Trarieux, F., and Patel, M. (2011). "A time-domain simulator for an oscillating water column in irregular waves at model scale". *Ocean Engineering* **38**(8-9), pp. 1007–1013.

Godoy-Diana, R. and Czitrom, S. P. R. (2007). "On the tuning of a wave-energy driven oscillating-water-column seawater pump to polychromatic waves". *Ocean Engineering* **34**(1718), pp. 2374–2384.

Graw, K. U., Schimmels, S., and Lengricht, J. (2000). "Quantifying losses around the lip of an OWC by use of particle image velocimetry (PIV)". *In*: Proceedings of the 4th European Wave Energy Conference. Aalborg University, Denmark.

Gunn, K. and Stock-Williams, C. (2012). "Quantifying the global wave power resource". *Renewable Energy* **44,** pp. 296–304.

Hasselmann, K., Barnett, T., Bouws, E., Carlson, H., Cartwright, D., Enke, K., Ewing, J., Gienapp, H., Hasselmann, D., Kruseman, P., *et al.* (1973). "Measurements of wind-wave growth and swell decay during the Joint North Sea Wave Project (JON-

SWAP)". *Ergnzungsheft zur Deutschen Hydrographischen Zeitschrift Reihe* **A(8)**(12), p. 95.

Heath, T. V. (2012). "A review of oscillating water columns". *Philosophical Transactions of the Royal Society A: Mathematical, Physical and Engineering Sciences* **370**(1959), pp. 235–245.

Holmes, B. (2009). *Tank Testing of Wave Energy Conversion Systems.* European Marine Energy Centre. London, United Kingdom.

Hunter, J. D. (2007). "Matplotlib: A 2D graphics environment". *Computing In Science & Engineering* **9**(3), pp. 90–95.

Intergovernmental Panel on Climate Change (2012). *Renewable Energy Sources and Climate Change Mitigation.* New York, United States of America: Cambridge University Press.

Isberg, J., Eriksson, M., and Leijon, M. (2009). "Transport of energy in polychromatic fluid gravity waves". *Journal of Engineering Mathematics* **64**(1), pp. 15–23.

ITTC (2009). "ITTC Recommended Procedures and Guidelines: Uncertainty Analysis An Example for PIV Measurement". *In*: ITTC - International Towing Tank Conference. Procedure 7.5-01-03-03.

ITTC (2014). "ITTC Recommended Procedures and Guidelines: Wave Energy Converter Model Test Experiments". *In*: ITTC - International Towing Tank Conference. Procedure 7.5-02-07-03.7.

Jones, E., Oliphant, T., Peterson, P., *et al.* (2001-). *SciPy: Open Source Scientific Tools for Python.* URL: http://www.scipy.org/.

Korde, U. A. (1999). "Efficient primary energy conversion in irregular waves". *Ocean Engineering* **26**(7), pp. 625–651.

LaVision GmbH (2010). *Product-Manual for DaVis 8.* Göttingen, Germany: LaVision GmbH.

Liu, Z., Hyun, B.-S., Shi, H., and Hong, K. (2010). "Practical Simulation of Oscillating Water Column Chamber for Wave Energy Conversion". *International Journal of Green Energy* **7**(3), pp. 337–346.

Longo, J., Shao, J., Irvine, M., and Stern, F. (2007). "Phase-averaged PIV for the nominal wake of a surface ship in regular head waves". *Journal of Fluids Engineering* **129**(5), pp. 524–540.

Mankins, J. C. (1995). *Technology readiness levels: a white paper.* NASA.

Mitchell Ferguson, T., Penesis, I., Macfarlane, G., and Fleming, A. (2014a). "Phase-averaged analysis of an oscillating water column in polychromatic waves". *In*: Proceedings of the 2nd Asian Wave and Tidal Energy Conference.

Mitchell Ferguson, T., Penesis, I., Macfarlane, G., and Fleming, A. (2014b). "Phase-averaging of PIV flow fields of an oscillating water column in polychromatic waves". *In*: Proceedings of the 2nd Asian Wave and Tidal Energy Conference.

Molyneux, D., Xu, J., and Bose, N. (2007). "Measurements of Flow Around an Escort Tug Model with a Yaw Angle". *Marine Technology* **46**(3), pp. 140–154.

Morris-Thomas, M. T., Irvin, R. J., and Thiagarajan, K. P. (2007). "An investigation into the hydrodynamic efficiency of an oscillating water column". *Journal of Offshore Mechanics and Arctic Engineering* **129**(4), pp. 273–278.

Morrison, I. G. (1995). "The Hydrodynamic Performance of an Oscillating Water Column Wave Energy Converter". PhD thesis. University of Edinburgh.

Morrison, I. G. and Greated, C. A. (1992). "Oscillating water column modelling". *In*: Proceedings of the 23rd International Conference on Coastal Engineering. **1,** pp. 502–511.

Müller, G. and J.T. Whittaker, T. (1995). "Visualisation of flow conditions inside a shoreline wave power-station". *Ocean Engineering* **22**(6), pp. 629–641.

Muthanna, C., Stansberg, C. T., and Baarholm, R. (2009). "Experimental Study of the Local Wave Velocity Field During a Wave impact Occurrence". *In*: Proceedings of the 28th International Conference on Ocean, Offshore and Arctic Engineering. Honolulu, Hawaii, USA.

Ocean Power Technologies (2015). *APB350 A1 deployed off the coast of New Jersey.* URL: http://www.oceanpowertechnologies.com/media/.

Oceanlinx Ltd (2013a). *Past Projects.* URL: http://www.oceanlinx.com/projects/past-projects.

Oceanlinx Ltd (2013b). *South Australia.* URL: http://www.oceanlinx.com/projects/south-australia.

Olvera, A., Prado, E., and Czitrom, S. (2007). "Parametric resonance in an oscillating water column". *Journal of Engineering Mathematics* **57**(1), pp. 1–21.

Pedregosa, F., Varoquaux, G., Gramfort, A., Michel, V., Thirion, B., Grisel, O., Blondel, M., Prettenhofer, P., Weiss, R, Dubourg, V., *et al.* (2011). "Scikit-learn: machine learning in Python". *Journal of Machine Learning Research* **12,** pp. 2825–2830.

Pelamis Wave Energy Converter (2015). *In: Wikipedia.* URL: https://en.wikipedia.org/wiki/Pelamis_Wave_Energy_Converter.

Raffel, M., Wereley, S., Willert, C., and Kompenhans, J. (2007). *Particle image velocimetry : a practical guide.* Heidelberg, New York: Springer.

Suzuki, M. and Arakawa, C. (2003). "Numerical Methods to Predict Characteristics of Oscillating Water Column for Terminator Type of Wave Energy Converter". *In*: Proceedings of the 13th International Offshore and Polar Engineering Conference. Hawaii, USA.

Takahashi, S., Nakada, H., Ohneda, H., and Shikamori, M. (2011). "Wave power conversion by a prototype wave power extraction caisson in Sakata Port". *Coastal Engineering Proceedings* **1**(23).

Techet, A. H. (2005). "High Speed PIV of Breaking Waves on Both Sides of the Air-Water Interface". *In*: Proceedings of the 6th International Symposium on Particle Image Velocimetry. Pasadena, California, USA.

The Guardian (2008). *Islay set to be prince of tides.* URL: http://www.theguardian.com/environment/2008/apr/06/windpower.scotland.

Thomas, G. (2008). *The theory behind the conversion of ocean wave energy: a review.* Ocean Wave Energy: Current Status and Future Perspectives. Berlin: Springer.

Wang, D. J., Katory, M., and Li, Y. S. (2002). "Analytical and experimental investigation on the hydrodynamic performance of onshore wave-power devices". *Ocean Engineering* **29**(8), pp. 871–885.

Washio, Y., Osawa, H., and Ogata, T. (2001). "The open sea tests of the offshore floating type wave power device Mighty Whale - characteristics of wave energy absorption and power generation". *In*: Proceedings of the MTS/IEEE Oceans 2001. Honolulu, HI.

Wavedragon (2015). *Wavedragon.* URL: http://www.wavedragon.net/.

Webb, I., Seaman, C., and Jackson, G. (2005). *Oscillating Water Column Wave Energy Converter Evaluation Report.* The Carbon Trust.

Appendix A

Phase averaged analysis of a oscillating water column in polychromatic waves

This conference paper wave presented at the 2nd Annual Asian Wave and Tidal Energy Conference in Toyko, Japan. The citation for this paper is:

Mitchell Ferguson, T., Penesis, I., Macfarlane, G. and Fleming, A. (2014) "Phase averaged analysis of an oscillating water column in polychromatic waves", *2nd Annual Asian Wave and Tidal Energy Conference*, Tokyo, Japan, 2014.

This article has been removed for copyright or proprietary reasons.

Appendix B

Phase averaging of PIV flow fields of an oscillating water column in polychromatic waves

This conference paper wave presented at the 2nd Annual Asian Wave and Tidal Energy Conference in Toyko, Japan. The citation for this paper is:

Mitchell Ferguson, T., Penesis, I., Macfarlane, G. and Fleming, A. (2014), "Phase averaging of PIV flow fields of an oscillating water column in polychromatic waves", *2nd Annual Asian Wave and Tidal Energy Conference*, Tokyo, Japan, 2014.

Appendix C

Experimental Setup

This chapter features some selected photographs of the model during testing.

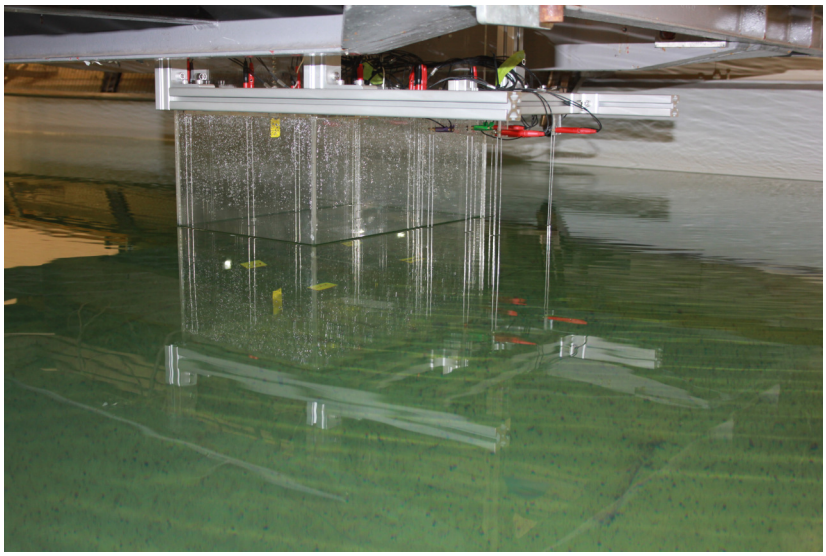

Figure C.1: Clear acrylic OWC model within the tank prior to testing

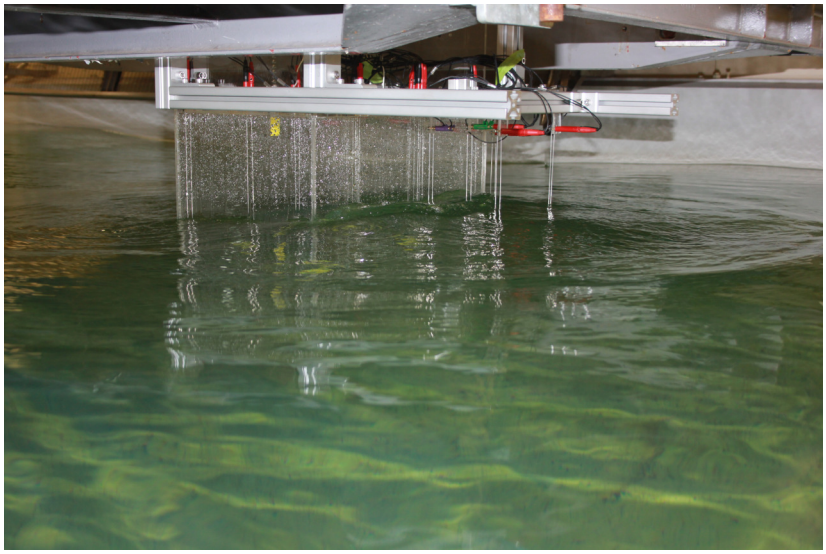

Figure C.2: Clear acrylic OWC model within the tank during the inflow stage

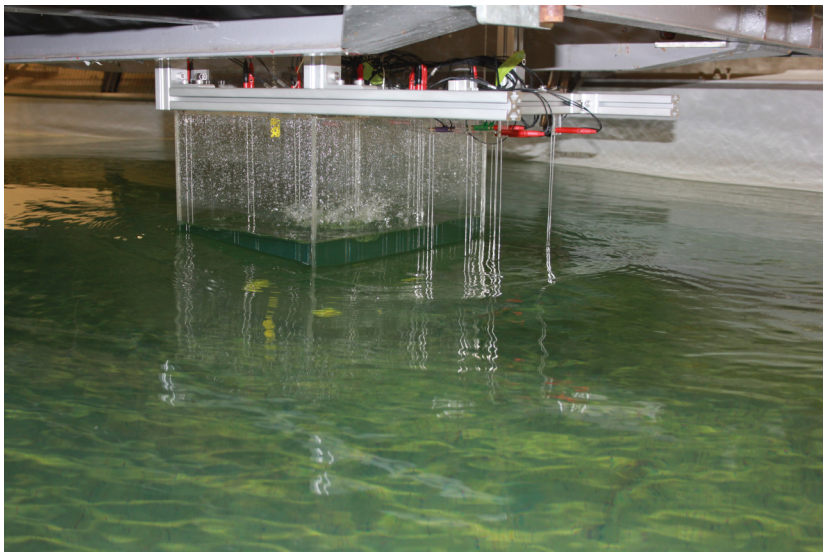

Figure C.3: Clear acrylic OWC model within the tank during the outflow stage

Appendix D

Experimental Raw Data

This section features examples of raw unprocessed data captured from a single run in a 0.07 m 0.55 Hz regular wave.

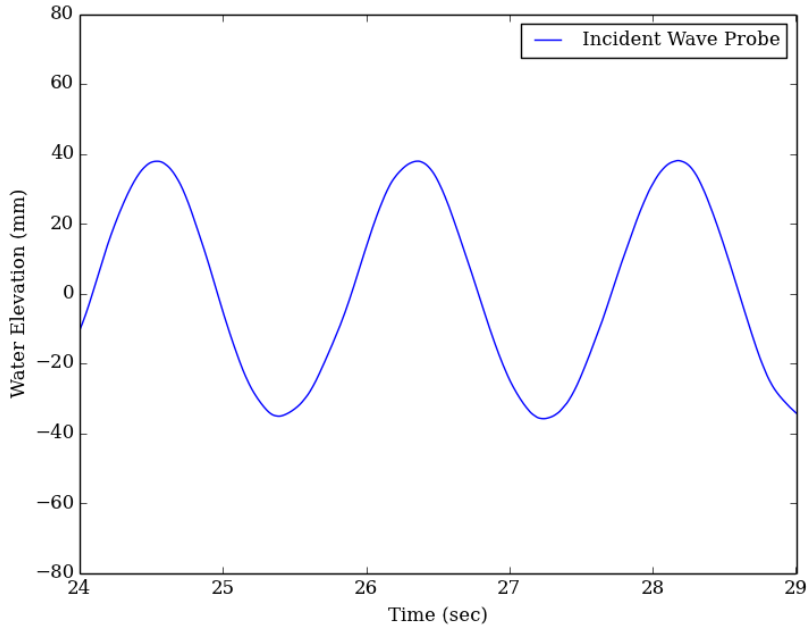

Figure D.1: Raw wave probe data for the incident wave probe from a run with a 0.07 m 0.55 Hz regular wave

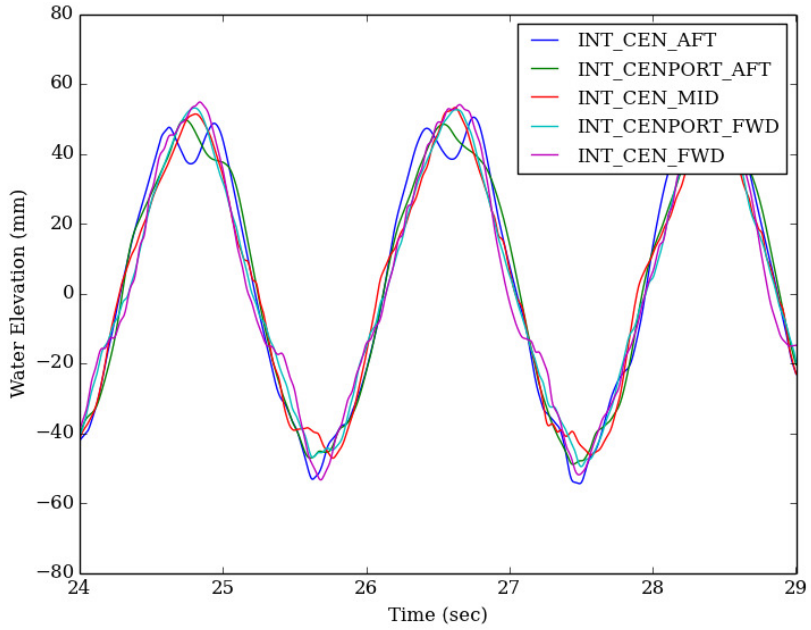

Figure D.2: Raw wave probe data for the internal wave probes from a run with a 0.07 m 0.55 Hz regular wave

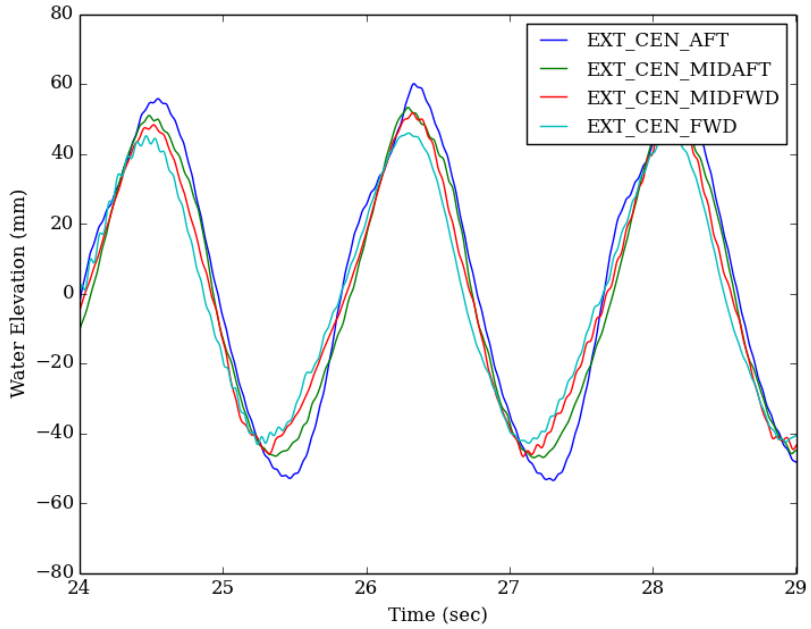

Figure D.3: Raw wave probe data for the external wave probes from a run with a 0.07 m 0.55 Hz regular wave

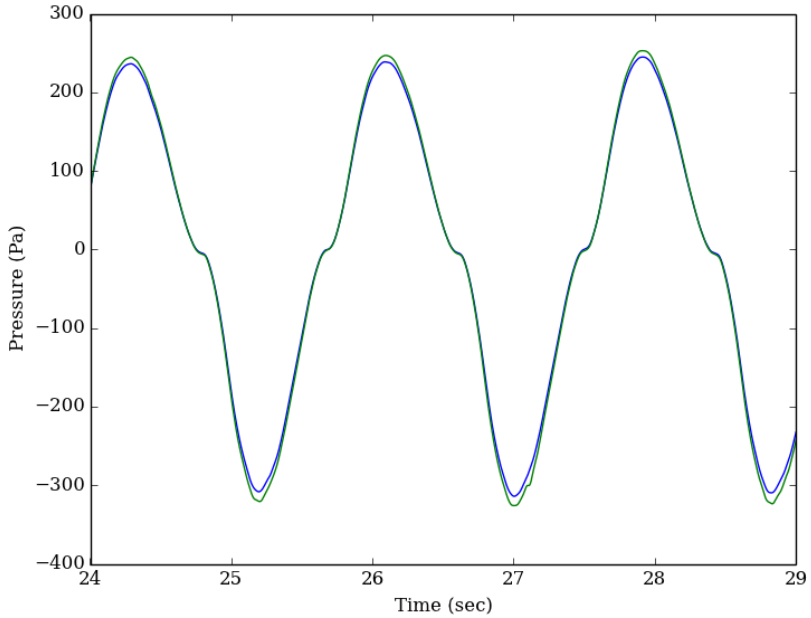

Figure D.4: Raw wave pressure transducer data from a run with a 0.07 m 0.55 Hz regular wave

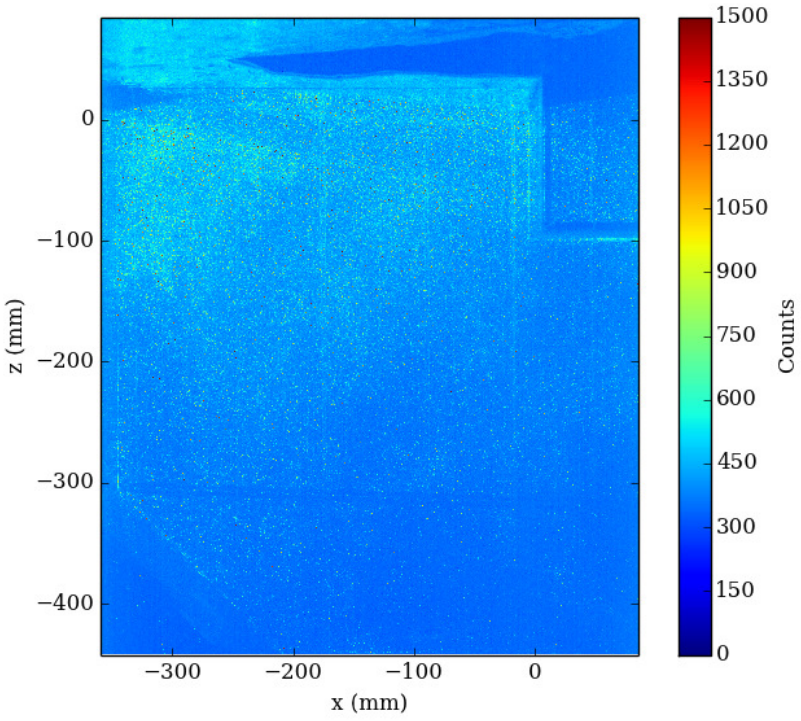

Figure D.5: Unprocessed PIV image for the first frame captured at camera position B from a run with a 0.07 m 0.55 Hz regular wave

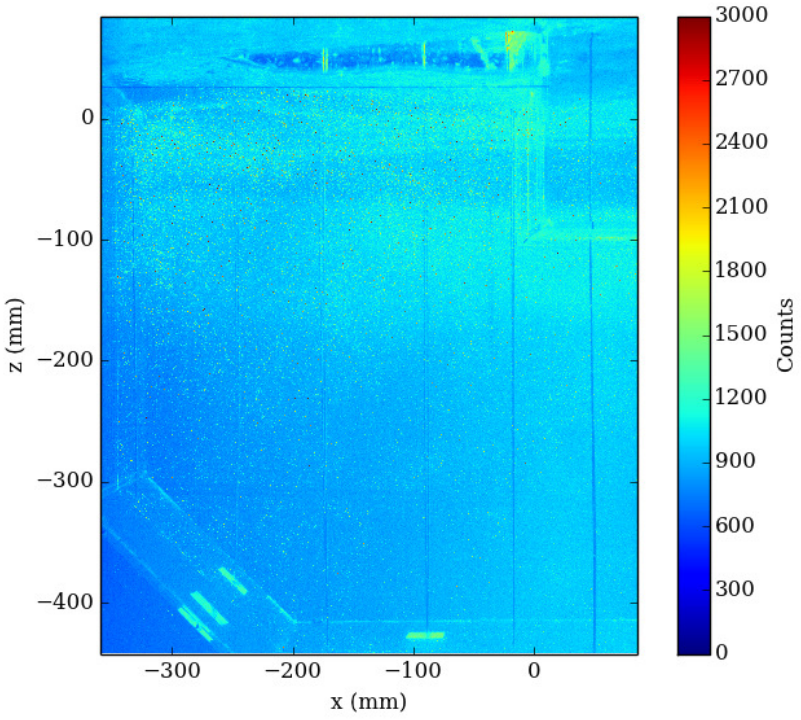

Figure D.6: Unprocessed PIV image for the second frame captured at camera position B from a run with a 0.07 m 0.55 Hz regular wave

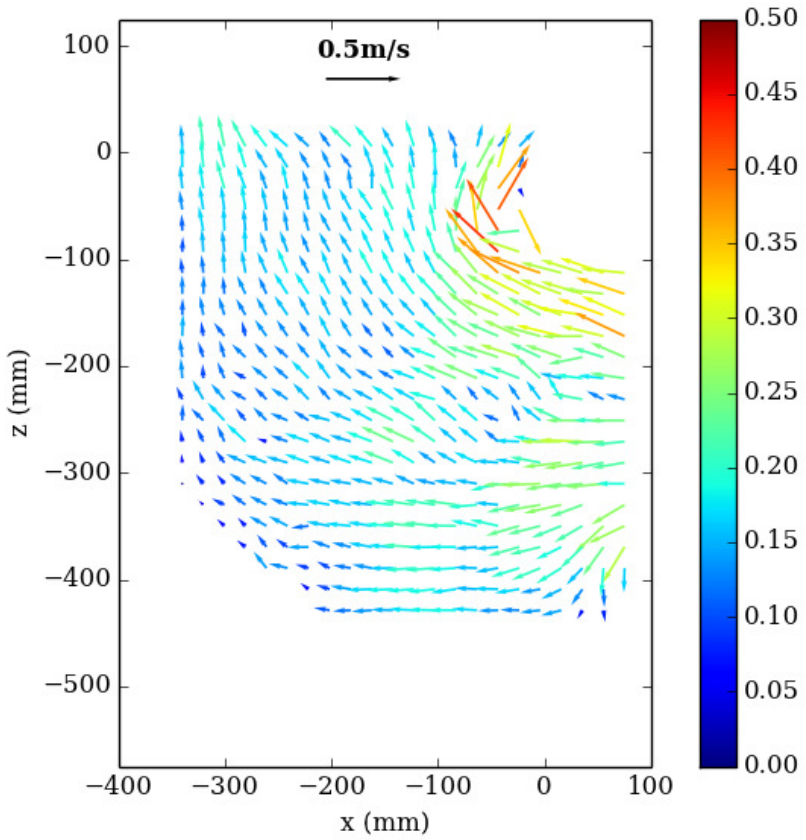

Figure D.7: Raw velocity field generated from the image in Figure D.3 from a run with a 0.07 m 0.55 Hz regular wave